RIVER BANK EROSION IN THE MINNESOTA RIVER VALLEY

A DISSERTATION

SUBMITTED TO THE FACULTY OF THE

UNIVERSITY OF MINNESOTA

BY

ANDREW C KESSLER

IN PARTIAL FULFILLMENT OF THE REQUIERMENTS

FOR THE DEGREE OF

DOCTOR OF PHILOSOPHY

DR. SATISH C GUPTA

DECEMBER 2015

ACKNOWLEDGMENTS

I gratefully acknowledge the assistance that was provided over the years in completing this research by Blue Earth County Environmental Services Staff especially Scott Salisbury and Professor Susan Galatowitsch of Fish, Wildlife and Conservation Biology for their insights about early survey data; Ryan Mattke and the staff at the University of Minnesota, John R. Borchert Map Library for their help with the historical aerial photographs; and Greg Spoden and Pete Boulay of the State Climatologist Office of the Minnesota Department of Natural Resources for sharing the long-term climatic data. In addition, I'd like to acknowledge help from Ashley Grundtner, Melinda Brown, David Thoma, and Kari Wolf with field work and manuscript reviews. The original 2009 Lidar scan was jointly funded by the Minnesota Corn and Soybean Research and Promotion Councils. Remaining research projects were partially supported with funds from the Minnesota Corn Research and Promotion Council. I'd also like to acknowledge the tireless work of my major adviser Dr. Satish Gupta whose guidance made this research possible. Finally, I would like to acknowledge my wife Andrea and our three daughters for supporting me through this endeavor.

ABSTRACT

Sediments remain one of the major causes of water quality impairments in the United States. Although soil erosion from agricultural lands has been viewed as the major source of sediment to rivers and lakes, in many watersheds, river banks are also contributing a significant amount of sediments to surface waters. Currently, limited research has been reported on the methods to quantify and to understand the causes and mechanisms that control river bank erosion. The research reported in this dissertation utilized emerging technologies and novel procedures to investigate (1) historic and modern rates of river bank erosion in the Blue Earth River Basin, a major source of sediment to the Minnesota River and Lake Pepin; (2) methods to delineate seeps (a major mechanism of bank sloughing) on the face of river banks and their impact on bank erosion; and (3) water retention capacity of depressional areas across the prairie pot hole regions of the Greater Blue Earth River Basin. The results of this research indicate that river bank erosion is and has been a major source of sediment in the Greater Blue Earth River Basin even before European immigrants began to settle in Minnesota; the return intensity from light detection and ranging (Lidar) can be used to delineate seepage areas on river banks and this along with lidar generated digital elevation model provides an opportunity to quantify seepage impacts on bank erosion; and the historic storage capacity of a prairie pothole landscape such as the Greater Blue Earth River Basin is relatively small (152 mm) and concentrated only in large depressions. This suggests that restoration of depressional areas will unlikely have a major impact on river flows without additional modifications.

TABLE OF CONTENTS

LIST OF TABLES

LIST OF FIGURES

SYNOPSIS

Excess sediment is one of the major causes of surface waters impairment throughout the United States. Excess suspended sediments negatively impact aquatic organisms, while phosphorus attached to sediment is frequently a driver of eutrophic conditions in lakes and rivers. There are ongoing efforts across the nation to identify sources and the causes of excess sediment loading in surface waters. In Minnesota, Lake Pepin is a prime example of surface water that has been affected by non-point source sediments and associated phosphorus often causing eutrophic conditions and sometime even fish kills. The Greater Blue Earth River Basin (GBERB) had been widely identified as a major source of sediment to the Minnesota River and onto Lake Pepin. In this thesis, I discuss four independent studies that focused on issues related to excess sediment in rivers of South Central Minnesota. The four issues dealt in these studies are: (1) LIDAR quantification of bank erosion, (2) assessment of river bank erosion pre- and post-European settlement, (3) impact of seepage on river bank erosion, and (4) drainage impacts on surficial water retention capacity of a prairie pothole watershed. This synopsis is intended to provide an overview of the four studies discussed in this thesis.

The overarching structure of this research was to first quantify the major source of modern day sediment to the Minnesota River and subsequently to Lake Pepin (*Chapter 2*). Then, this research assessed how the primary source of modern day sediment (i.e. river banks) production may have varied over historic times (*Chapter 3)*. Next, *Chapter 4* evaluated the use of emerging technologies to identify the location of subsurface seeps, a major mechanism that causes river bank sloughing/erosion. Finally, storing water in upland locations has been suggested as a means to reduce river flows and slow bank

erosion in the Minnesota River Basin (MRB). In *Chapter 5*, we quantify the historic water retention capacity of the GBERB and the locations where depressions can hold significant quantity of water. The remainder of this synopsis presents key findings from each of the studies.

LIDAR QUANTIFICATION OF BANK EROSION IN BLUE EARTH COUNTY, MINNESOTA

In this research, airborne Lidar scans collected in 2005 and 2009 were used to estimate sediment and phosphorus contributions from the river banks along the Blue Earth, Le Sueur, Watonwan, Big Cobb, Little Cobb, and Maple Rivers in Blue Earth County, MN. The results of the assessment showed that bank erosion/sloughing in Blue Earth County is the primary source of sediments to rivers in the GBERB, accounting for as much as 63% to 79% of the total suspended loads at the outlets of the Blue Earth and Le Sueur Rivers, respectively. Total volume change in river valleys of Blue Earth County was estimated at 1.71 million m^3 over four years. Most of this volume loss (75%) was a result of tall river banks (>3 m high) sloughing even though they only occupied 33% of the river length. Based on total and soluble phosphorus content of bank materials, phosphorus contributions from river banks erosion accounted for 0.13% to 0.20 % and 40% to 49% of the measured soluble and total phosphorus loads at the mouth of the Blue Earth River and the Le Sueur River, respectively. These results indicate that river banks are the primary source of sediment as well as a significant source of total phosphorus to rivers of the GBERB and then in turn to the Minnesota River and downstream Lake Pepin.

ASSESSMENT OF RIVER BANK EROSION IN SOUTHERN MINNESTOA RIVERS POST EUROPEAN SETTLEMENT

This study quantified the historic rates of river bank erosion in order to investigate whether or not the primary source of modern day sediment in the GBERB have varied since European settlement. Quantification was done by tracing the position of river banks overtime on 1855 Public Land Survey System PLATs and aerial photographs. Rates of erosion over time were then compared to evaluate if significant shifts had occurred. In addition to this characterization, we also used the 2005 and 2009 Blue Earth County airborne Lidar data to evaluate if a subset of bank erosion estimates could be extrapolated across the entire GBERB, a technique that has been commonly applied in fluvial geomorphology studies.

The results showed that bank erosion was episodic, making comparisons of erosion rates from dissimilar time intervals unreliable. For comparable time intervals from 1855-1938 and 1938-2009 or 1938-1971 and 1971-2009, average river bank retreat rates were statistically similar suggesting that bank retreat rates have remained stable since European settlement. However, a greater number of banks slumped from 1971-2009 relative to 1938-1971. This suggested two possibilities: (1) either more river banks are eroding now than in the past or/and (2) the quality of aerial photographs is better in recent times such that it allows for better identification of eroding river banks. Additional analysis also showed that physical characteristics of river banks (face area, inclined surface area, length, slope, height, and aspect) were a poor predictor of total volume loss (r^2=0.01 to 0.36) and thus extrapolation of a subset of bank erosion measurements to the whole basin as has been done in the literature is not appropriate.

QUANTIFYING SEEPAGE CAUSED RIVER BANK EROSION USING LIDAR

In this study, we evaluated emerging technologies of thermal imaging as well as return light intensity from Lidar as a means to locate seepage on the face of river banks. Thermal imaging is based on the principle that seep waters are cooler (in summer) or warmer (in winter) than the face of the river bank. Comparatively, use of light return intensity from Lidar is based on the principle that infrared light is absorbed by water and thus there will be less return light intensity from seep locations. The testing of these technologies was done in the field at two different locations in Blue Earth County (tall river bank) and Carver County (a developing ravine) MN. The results established that Lidar is a suitable alternative to thermal imaging for identifying seepage locations along the face of river banks. We show that Lidar return light intensities as well as elevation change data provides a useful tool for locating seep locations as well as quantifying seepage caused bank sloughing. Measurements with terrestrial Lidar at the Carver Creek ravine showed a significant relationship between Lidar return intensity and soil moisture for various soil layers. A subsequent controlled experiment with latex painted wet and dry soil cores from various ravine layers showed that soil color plays a larger role than the soil moisture in Lidar return intensities. This indicates that in evaluating the use of Lidar to quantify seepage caused bank erosion, one also needs to account for differences in soil color between layers when identifying seep areas.

DRAINAGE IMPACTS ON SURFICIAL WATER RETENTION CAPACITY OF A PRAIRIE POTHOLE WATERSHED

There is a pervasive belief that drainage of depressions in the prairie pothole region of the Upper Midwest has led to substantial increase in river flows and thus

greater bank erosion. As a corollary, it is often stated that surficial water storage in prairie pothole region can reduce river flows and in turn bank erosion. To evaluate this objective, we used Lidar data to estimate the historic surficial water retention capacity of depressions in the GBERB. Lidar estimates showed that the historic depressional storage was 152 mm for GBERB. Furthermore, the majority (53%) of this storage was in large depressions (> 40 ha) which accounted for less than 1% of the number of observed depressions. This suggests that the restoration of most drained areas (which are shallow) would have little impact on the storage capacity of the GBERB and efforts to increase the surficial water holding capacity of the GBERB would be best served in the restoration of large (>40 ha) depressions.

Further, a simple mass balance calculation accounting for change in storage and the difference in annual evapotranspiration between wetlands and the croplands showed that restoration of all depressions in the Minnesota portion of GBERB would provide a maximum of 131 mm additional water retention capacity over and above the modern day capacity. However, this capacity is in large depressions that are not uniformly spread in the basin and water will have to be conveyed to these depressions. Furthermore, this capacity is only available first year when the depressions are empty and for subsequent years this capacity will decrease unless these depressions are emptied each year.

CHAPTER 1: INTRODUCTION

Non-point source pollution (NSP) is one of the largest remaining sources of water quality impairments in the United States. Frequently, sediment and phosphorus are two major constituents that are contributing to surface water impairments. The presence of suspended sediments in rivers and lakes increases turbidity, which limits light penetration and plant growth for aquatic organisms. In addition, suspended sediments have also been shown to have direct deleterious impacts on aquatic organisms (Newcombe and Jensen, 1996). Phosphorus attached to sediment is frequently a driver of eutrophic conditions in surface water bodies. Lake Pepin on the border of Minnesota and Wisconsin and Lake Erie in Ohio are two prime examples of surface waters that have been affected by non-point source sediment and phosphorus. Both these pollutants have contributed to eutrophic conditions in these lakes and even fish kills during some warm summers.

Lake Pepin, a floodplain lake on the Mississippi River about 80 km southeast of St. Paul is fed by the St. Croix, Mississippi, and Minnesota River Basins (Figure 1). Monitoring data from the Metropolitan Council Environmental Services (MCES) has shown that the Minnesota River carries a higher load of suspended sediment than the St. Croix and Mississippi Rivers (Meyer and Schellhaass, 2002). However, there has been disagreement over the degree to which overland sources contribute sediment and phosphorus to these waterways versus near channel sources, such as river bank erosion. Much of the Minnesota River Basin (MRB) has been extensively tile drained with numerous surface and side inlets which serve as a conduit of field sediments to rivers and streams (Thoma et al., 2005a; Ginting et al., 2000).

A study by the Minnesota Pollution Control Agency (MPCA) found that the majority of sediment in the MRB was from overland sources (Payne, 1994). However, more recent studies have indicated that river banks are likely one of the major sources of sediment in the MRB (Gupta and Singh, 1996; Sekely et al., 2002; Thoma et al., 2005; Belmont et al., 2011; Day et al., 2013a) and also a significant source of total phosphorus (Thoma et al., 2005; Grundtner et al., 2014). Recently, suggestions have also been made that there is increased rates of river bank erosion from drainage of depressional lands by tile drainage (Schottler et al., 2014).

New technologies and methods have emerged that can improve our estimates of river bank contributions to suspended sediment loads in various rivers (see Thoma et al, 2005), as well as provide better understanding of mechanisms that are causing river bank failures. Such an improved understanding and quantification can lead to better assessment as how anthropogenic factors are contributing to water quality impairments and what management changes can be adopted to minimize this impact. This dissertation summarizes four studies that investigated the issues of (1) LIDAR quantification of bank erosion, (2) assessment of river bank erosion post European settlement, (3) impact of seepage on river bank erosion, and (4) drainage impacts on surficial water retention capacity of a prairie pothole watershed. This research was undertaken in the context of understanding why the Minnesota River is muddy and why Lake Pepin is filling up at a rapid rate?

QUANTIFICATION OF BANK EROSION

Within the MRB, the Greater Blue Earth River Basin (GBERB) contributes 55% of the sediment load to the Minnesota River at Mankato (Payne, 1994). However, the

GBERB occupies only 21% of the land area of MRB (see Figure 1). This disproportionate contribution of sediments from GBERB relative to other basins in MRB is believed to be due to tall and steep banks that line many of the rivers in the Blue Earth County. In addition, Blue Earth County has the most river miles of any county in Minnesota (http://www.dnr.state.mn.us/watertrails/blueearthriver/more.html) thus presenting prime conditions for large sediment load to rivers in South Central Minnesota. Several researchers have shown that tall and actively eroding river banks in GBERB are the result of continuous down cutting that resulted after the River Warren drained the melt waters of Lake Agassiz some 13,400 BP and stranded these tributaries from its master stream, the Minnesota River (Clayton and Moran, 1982; Matsch, 1983; Gran et al., 2009).

Over the past 15 years, several techniques have been used to estimate the contribution of river banks to sediment load in various rivers of the GBERB. These include, airborne light detection and ranging (Lidar; Thoma et al., 2005), traditional total station survey (Sekely et al., 2002), sediment fingerprinting (Belmont et al., 2011), and terrestrial Lidar scans (Day et al., 2013b). All of these studies have found that a significant portion of modern day sediment in various rivers of the GBERB is derived from river bank erosion.

Sekley et al. (2002) conducted multi-temporal ground surveys on 7 river banks along the Blue Earth River to estimate rates of river bank erosion in the GBERB. These authors then used bank area as a surrogate to extrapolate their results to the entire Blue Earth River showing that 36% to 48% of the sediment in the waterway was from river bank erosion. Using multiple techniques including sediment fingerprinting and terrestrial

Lidar scans from Day et al. (2013b), Belmont et al. (2011) estimated that river bank erosion in the Le Sueur River watershed accounted for 67% of the measured sediment load. Thoma et al. (2005) used multi-temporal airborne Lidar scans over a 56 km of the Blue Earth River, and showed that 23% to 56% of the sediment load at the river's outlet was derived from bank erosion. Thoma et al. (2005) results differed from other studies in that they characterized the full length of the river channel rather than extrapolate measurements from a few banks to the whole river length. The recent increase in airborne Lidar availability (Notebaert et al., 2009; Perroy et al., 2001) provides an opportunity to expand upon the study of Thoma et al. (2005) and characterize bank erosion/sloughing along various rivers in Blue Earth County, MN.

HISTORIC RATES OF BANK EROSION

While substantial effort has been made in characterizing modern day sediment loads in the GBERB and MRB (Sekely et al., 2002; Thoma et al., 2005; Gran et al., 2009; Belmont et al., 2011; Day et al., 2013a), far less effort has been directed towards quantifying bank erosion rates since European immigrants settled in the area and major land use and climatic changes began to occur. Furthermore, the focus of characterization in earlier studies has been on one time period thus failing to capture the potential variability in bank erosion rates over time (Sekely et al., 2002; Thoma et al., 2005), or to compare erosion estimates from dissimilar time periods and then apportion the differences to anthropogenic factors (Belmont et al., 2011; Gran et al., 2009).

In their studies, Belmont et al. (2011) and Gran et al. (2009) compared a modern day 10 year average rate of erosion to a historic average for the Holocene period (> 10,000 years), drawing the conclusion that the modern day average rates of annual

erosion are much greater than the historic normal and the present day rates of erosion have been accelerated by human changes to the landscape. However, studies that have compared rates of river bank erosion from similar time periods have shown it to be episodic (Black et al., 2010; Zaimes et al., 2004), suggesting that comparisons of average erosion rates between dissimilar time periods will lead to erroneous conclusions.

Aerial photographs have frequently been used to estimate rates of bank erosion (Leys and Werritty, 1999; Shields et al., 2000; Hughes et al., 2006; Hooke, 2007; Nicoll and Hickin, 2010; De Rose and Basher, 2011). Within the GBERB, Blue Earth County, Minnesota has multiple years of aerial photographs starting in 1931 thus providing the opportunity to estimate annual river bank erosion rates for similar time periods and then assess how the settlement of European immigrants in the MRB has impacted bank erosion rates.

MECHANISMS OF BANK EROSION

Although techniques have been developed to estimate the magnitudes of river bank erosion (see Sekely et al., 2002; Thoma et al., 2005; Gran et al., 2009; Belmont et al., 2011; Day et al., 2013a), there is still a debate on the mechanisms of river bank erosion especially the mechanisms related to mass failure; the major contributor of sediment load.

Seepage, referred to here as shallow interflow exiting the face of a river bank, has recently gained attention as a significant mechanism of river bank erosion and mass wasting (Fox et al., 2007; Wilson et al., 2007; Chu-Agor et al., 2008; Chu-Agor et al., 2009; Lindow et al., 2009; Midgley et al., 2013). In field investigations, Midgley et al. (2013) showed that seepage was capable of destabilizing river banks eventually leading

to mass wasting. Lindow et al. (2009) observed similar results in laboratory experiments. However, there are limited tools available for identifying where seepage exists on the face of river banks (especially in areas that are not easily accessible) and how it impacts bank stability.

Currently, ground based thermal imaging has been used to remotely identify the location of seepage along the face of river banks (Deitchman and Loheide, 2009; Pfister et al., 2010). However, ambient air temperature can mask points where seepage exits river banks (Deitchman and Loheide, 2009; Pfister et al., 2010). Alternatively, laser reflectance with its sensitivity to variations in soil moisture (Narayana et al., 1993) can be an excellent tool to identify seepage locations. Brennan and Webster (2006) showed that Lidar could be used to differentiate saturated from dry soils. Since airborne and terrestrial laser technologies are readily available, this provides an opportunity to test if Lidar can be used to identify locations where seepage exits the face of river banks as well as to evaluate the impacts of seepage on river bank stability.

QUANTIFYING DEPRESSIONAL STORAGE

As river bank erosion has gained recognition as a major source of sediment to rivers in the Minnesota River Basin (Sekely et al., 2002; Thoma et al., 2005; Belmont et al., 2011), it has been suggested that changes in hydrology (tile drainage) has increased discharge flow rates in rivers and has thus led to higher modern day rates of river banks erosion (Belmont et al., 2011; Schottler et al., 2014). However, recent analysis of river flows and precipitation has shown that increased river flows in the Upper Midwestern United States are mainly due to increased precipitation and not due to installation of tile

drainage or changed cropping system (Gupta et al., 2015). Irrespective of the underlying cause of river flow increases, managing water storage in depressions could provide a means to mitigate increased river flows and thus lower its impact both in river bank undercutting as well as in sediment carrying capacity. However, the potential for water storage in depressions within the MRB and GBERB has yet to be quantified.

Historically, the lack of high resolution topographic data, such as Lidar, has hindered efforts to quantify the capacity of depressions to retain water across a landscape. With the increased availability of Lidar, data studies have begun to develop techniques for quantify water retention in existing wetlands (Liu and Wang, 2008; Huang et al., 2011; Shook and Pomeroy, 2011; Shaw et al., 2012). For example, Huang et al. (2011) developed a flood water regulation index for existing wetlands by estimating the depth of runoff they could retain for storm events in Stutsman County, North Dakota. While techniques have been developed to quantify water retention from existing wetlands, many wetlands in the MRB and GBERB have been drained (Dahl, 2006). Additional work is needed to quantify the retention capacity of drained depressions to better understand their potential for mitigating hydrologic alterations driven by climate and/or land use changes.

THESIS STRUCTURE OVERVIEW

The thesis has been organized into four chapters (Chapters 2-5), each of which are independent studies focused around one of the central themes on the source, magnitude, mechanistic causes, and potential solutions to river bank erosion in the MRB. Each of Chapters 2 through 5 is structured as self-contained papers which include an Introduction, Methods, Results, Conclusions, and References. Except chapter 4, all other chapters have been published in various journals. Chapter 2 was published in the Journal of

Environmental Quality, Chapter 3 in Geomorphology, and Chapter 5 in the Journal of the American Water Resources Association. References were kept separate for each chapter. Chapter 6 provides overall conclusions of the thesis.

REFERENCES

Belmont, P., K.B. Gran, S.P. Schottler, P.R. Wilcock, S.S. Day, C. Jennings, J.W. Lauer, E. Viparelli, J.K. Willenbring, D.R. Engstrom, and G. Parker. 2011. Large shift in source of fine sediment in the Upper Mississippi River. Environmental Science and Technology. 45:8804-8810.

Black, E., C.E. Renshaw, F.J. Magilligan, J.M. Kaste, W.B. Dade, and J.D. Landis. 2010. Determining lateral migration rates of meandering rivers using fallout radionuclides. Geomorphology. 123:364-369.

Brennan, R., and T.L. Webster. 2006. Object-oriented land cover classification of Lidar-derived surfaces. Canadian Journal of Remote Sensing. 32:162-172.

Chu-Agor, M.L., G.A. Fox, and G.V. Wilson. 2009. Empirical sediment transport function predicting seepage erosion undercutting for cohesive bank failure prediction. Journal of Hydrology. 377:155-164.

Chu-Agor, M.L., G.A. Fox, R.M. Cancienee, and G.V. Wilson. 2008. Seepage caused tension failures and erosion undercutting of hillslopes. Journal of Hydrology. 359:247-259. DOI: 10.1016/j.jhydrol.2008.07.005

Dahl, T.E. 2006. Status and trends of wetlands in the conterminous United States 1998 to 2004. U.S. Department of the Interior, Fish and Wildlife Service, Washington, D.C.

Day, S.S., K.B. Gran, P. Belmont, and T. Wawrzyniec. 2013a. Measuring bluff erosion part 2: pairing aerial photographs and terrestrial laser scanning to create a watershed scale sediment budget. Earth Surface Processes and Landforms. DOI:10.1002/esp.3359.

Day, S.S., K.B. Gran, P. Belmont, and T. Wawrzyniec. 2013b. Measuring bluff erosion Part 1: Terrestrial laser scanning methods for change detection. Earth Surface Processes and Landforms. DOI:10.1002/esp.3353.

De Rose, R.C., and L.R. Basher. 2011. Measurement of river bank and cliff erosion from sequential Lidar and historical aerial photography. Geomorphology. 126:132-147.

Deitchman, R.S., and S.P. Loheide II. 2009. Ground-based thermal imaging of groundwater flow processes at the seepage face. Geophysical Research Letters. 36:L14401, DOI: 10.1029/2009GL038103.

Devauchelle, O., A.P. Petroff, H.F. Seybold, and D.H. Rotherman. 2012. Ramification of stream networks. Proceedings of the National Academy of Sciences. 109:20832-30836.

Fox, G.A., G.V. Wilson, A. Simon, E.J. Langendoen, O. Akay, and J.W. Fuchs. 2007. Measuring streambank erosion due to ground water seepage: correlation to bank pore water pressure, precipitation and stream stage. Earth Surface Processes and Landforms. 32:1558-1573, DOI: 10.1002/esp.1490.

Ginting, D., J.F. Moncrief, and S.C. Gupta. 2000. Runoff, solids, and contaminant losses into surface tile inlets draining lacustrine depressions. J. Environ. Qual. 29:551–560.

Gran, K., P. Belmont, S. Day, C. Jennings, A. Johnson, L. Perg, and P. Wilcox. 2009. Geomorphic evolution of the Le Sueur River, Minnesota, USA, and implications for current sediment loading. The Geological Society of America. Special Paper 451.

Grundtner, A.L., S.C. Gupta, P.R. Bloom. 2014. River bank materials as a source and as carriers of phosphorus to Lake Pepin. Journal of Environmental Quality 43:1991-2001.

Gupta, S.C., and U.B. Singh, 1996. A review of non-point source pollution models: Implications for the Minnesota River Basin. A report submitted to the Minnesota Department of Agriculture. p77.

Gupta, S.C., A.C. Kessler, M.K. Brown, and F. Zvomuya. 2015. Climate and agricultural land use change impacts on streamflow in the upper Midwestern United States. Water Resources Research. DOI:10.1002/2015WRO17323.

Hooke, J.M. 2007. Spatial variability, mechanism and propagation of change in an active meandering river. Geomorphology. 84:277-296.

Huang, S., C. Young, M. Feng, K. Heidemann, M. Cushing, D.M. Mushet, and S. Liu, 2011. Demonstration of a conceptual model for using Lidar to improve the estimation of floodwater mitigation potential of Prairie Pothole Region wetlands. Journal of Hydrology. 405:417-426.

Hughes, M.L., P.F. McDowell, and W.A. Marcus, 2006. Accuracy assessment of georectified aerial photographs: implications for measuring lateral channel movement in GIS. Geomorphology. 74:1-16.

Leys, K.F., and A. Werritty. 1999. River channel planform change: software for historical analysis. Geomorphology. 29:107-120.

Lindow, N., G.A. Fox, and R.O. Evans. 2009. Seepage erosion in layered stream bank material. Earth Surface Processes and Landforms. 34:1693-1701, DOI: 10.1002/esp.1974.

Liu, H. and L. Wang, 2008. Mapping detention basins and deriving their spatial attributes from airborne Lidar data for hydrological applications. Hydrological Processes. 22:2358-2369.

Midgley, T.L., G.A. Fox, G.V. Wilson, D.M. Heeren, E.J. Langendoen, and A. Simon. 2013. Seepage-induced streambank erosion and instability: in situ constant-head experiments. Journal of Hydrologic Engineering. 18:1200-1210, DOI: 10.1061/(ASCE)He.1943-5584.0000685.

Payne, G.A. 1994. Sources and transport of sediment, nutrients and oxygen demanding substances in the Minnesota River Basin, 1989-92. USGS Water Resources Investigations Report. 93-4232.

Pfister, L., J.J. McDonnell, C. Hissler, and L. Hoffmann 2010. Ground-based thermal imagery as a simple, practical tool for mapping saturate area connectivity and dynamics. Hydrological Processes. 24:3123-3132, DOI: 10.1002/hyp.7840.

Meyer, M.L. and S.M. Schellhaass. 2002. Sources of phosphorus, chlorophyll, and sediment to the Mississippi River upstream of Lake Pepin: 1976-1996. A report for environmental studies of phosphorus. Metropolitan Council Environmental Services.

Newcombe, C.P., and J.O.T. Jensen. 1996. Channel suspended sediment and fisheries: a synthesis for quantitative assessment of risk and impact. North American Journal of Fisheries Management. 16:693-727.

Nicoll, T.J., and E.J. Hickin,. 2010. Planform geometry and channel migration of confined meandering river on the Canadian prairies. Geomorphology. 116, 37-47.

Schottler, S.P., J. Ulrich, P. Belmont, R. Moore, J.W. Lauer, D.R. Engstrom, and J.E. Almendinger. 2014. Twentieth century agricultural drainage creates more erosive rivers. Hydrological Process. 28:1951-1961, DOI: 10.1002/hyp.9738.

Sekely, A.C., D.J. Mulla and D.W. Bauer. 2002. Streambank slumping and its contribution to the phosphorus and suspended sediment load of the Blue Earth River, Minnesota. Journal of Soil and Water Conservation. 57:243-250.

Shaw, D.A., G. Vanderkamp, F.M. Conly, A. P. Pietroniro, and L. Martz. 2011. The fill-spill hydrology of prairie wetland complexes during drought and deluge. Hydrological Processes. DOI: 10.1002/hyp.8390.

Shields, F.D. Jr., A. Simon, and L.J. Steffen. 2000. Reservoir effects on downstream river channel migration. Environmental Conservation. 27 54-66.

Shook, K.R. and J.W. Pomeroy. 2011. Memory effects of depression storage in Northern Prairie hydrology. Hydrological Processes. 25:3890-3898.

Thoma, D.P., S.C. Gupta, M.E. Bauer, and C.E. Kirchoff. 2005. Airborne laser scanning for riverbank erosion assessment. Remote Sensing of Environment. 95:943-501.

Wilson, G.V., R. Periketi, G.A. Fox, S. Dabney, D. Shields, R.F. Cullum. 2007. Soil properties controlling seepage erosion contributions to river bank failure. Earth Surface Processes and Landforms. 32:447–459.

Zaimes, G.N., R.C. Schultz, and T.M. Isenhart. 2004. Stream bank erosion adjacent to riparian forest buffers, row-crop fields, and continuously-grazed pastures along Bear Creek in central Iowa. Journal of Soil and Water Conservation. 59:19-27.

CHAPTER 2: LIDAR QUANTIFICATION OF BANK EROSION IN BLUE EARTH COUNTY, MINNESOTA

SUMMARY

Sediment and phosphorus transport from the Minnesota River Basin to Lake Pepin on the upper Mississippi River has garnered much attention in recent years. However, there is lack of data on the extent of sediment and P contributions from river banks vis-e-vis uplands and ravines. Using two light detection and ranging (Lidar) datasets taken in 2005 and 2009, a study was undertaken to quantify sediment and associated P losses from river banks in Blue Earth County, MN. Volume change in river valleys as a result of bank erosion amounted to 1.71 million m^3 over 4 years. Volume change closely followed the trend: the Blue Earth River>the Minnesota River at the county's northern edge> the Le Sueur River> the Maple River> the Watonwan River>the Big Cobb River>Perch Creek>Little Cobb River. Using fine sediment content (silt+clay) and bulk density of 37 bank samples representing three parent materials we estimate bank erosion contributions of 48% to 79% of the measured total suspended solids at the mouth of the Blue Earth and the Le Sueur Rivers. Corresponding soluble P and total P contributions ranged from 0.13% to 0.20% and 40% to 49%, respectively. Although tall banks (>3 m high) accounted for 33% of the total length and 63% of the total area, they accounted for 75% of the volume change in river valleys. We conclude that multi-temporal Lidar datasets are useful in estimating bank erosion and associated P contributions over large scales, and for river banks that are not readily accessible for conventional surveying equipment.

INTRODUCTION

Sediment and phosphorus are major causes of surface water impairment throughout the world. The presence of suspended sediments in rivers and lakes increases turbidity which limits light penetration and plant growth for aquatic organisms. In addition, suspended sediments have also been shown to negatively impact aquatic organisms at multiple life stages (Newcombe and Jensen, 1996). Similarly, sediment attached phosphorus has often been linked to eutrophication of water bodies, which can lead to fish kills. One such example of fish kills occurred in Lake Pepin, a floodplain lake on the Mississippi River about 80 km southeast of St. Paul (Figure 1), during the drought of 1988. Sediment attached phosphorus is widely believed to be the cause of the fish kills.

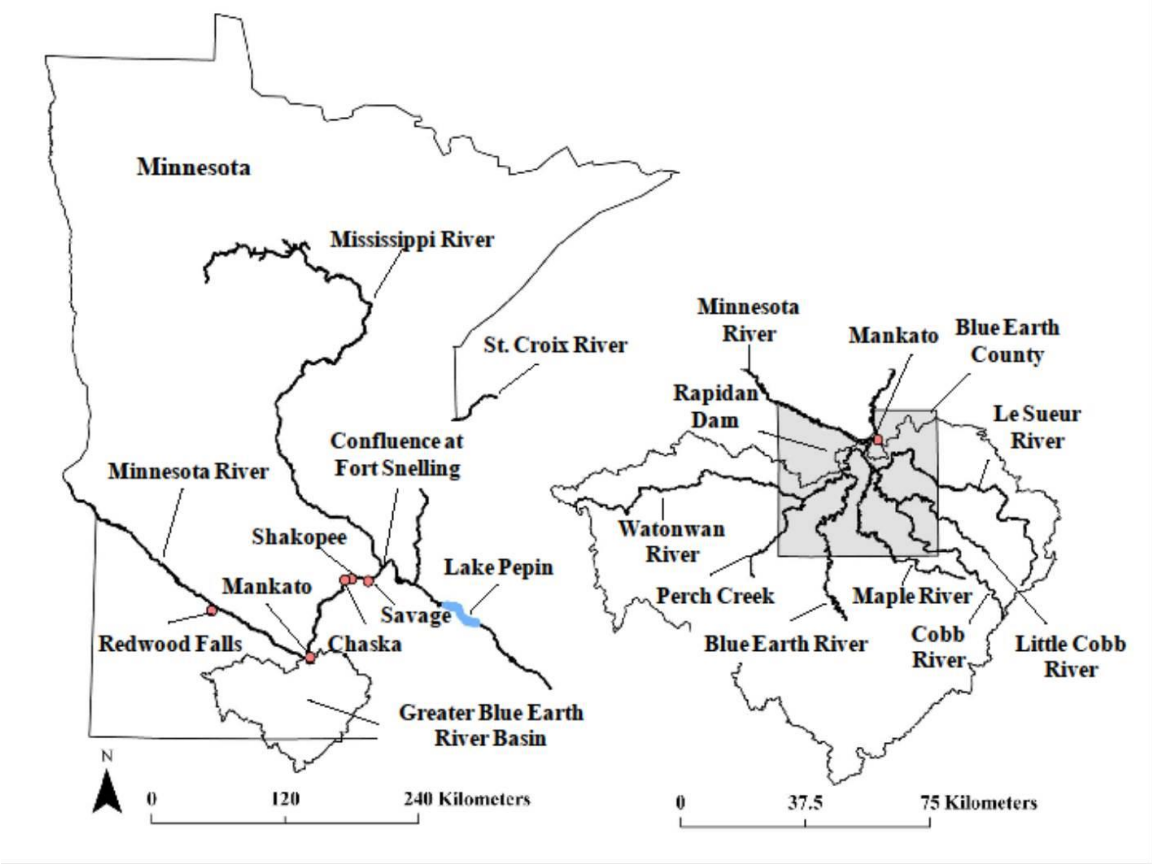

Figure 1. A map of Minnesota showing the location of various rivers in Blue Earth County within the Greater Blue Earth River Basin.

The Minnesota River Basin (MRB, Figure 1) has several major water bodies that are listed as impaired due to the presence of excess sediments. Monitoring studies by the Metropolitan Council Environmental Services (MCES) from 1976-1992 have shown that the water quality of the Minnesota River is worse than that of the Mississippi and St. Croix Rivers near the Twin Cities of St. Paul and Minneapolis, MN (Meyer and Schellhaass, 2002). United States Geological Survey (USGS) monitoring studies have shown that sediment loads in the Minnesota River at Mankato are highly variable ranging from 0.2 to 3.3 million Mg yr^{-1} from 1968 to 1992 (Payne, 1994). About 55% of these

sediments and 46% of the water flow in the Minnesota River at Mankato originates from the Greater Blue Earth River Basin (GBERB, Figure 1), a relatively flat area with 54% of the land having <2% slope and 93% of the land <6% slope.

The GBERB and MRB have been extensively tile drained with numerous surface and side inlets that allow the transport of surface sediments to ditches, and subsequently to streams and rivers (Thoma et al., 2005a; Ginting et al., 2000). There has been controversy on the extent of sediment contributions from agricultural fields compared to stream banks from the MRB. In 1994, Minnesota Pollution Control Agency (MPCA) suggested that bank erosion could not be more than 25% of the sediment load in the Minnesota River (MPCA, 1994). However, Payne (1994) showed that 39% of the sediment load in Redwood River between Seaforth and Redwood Falls, MN originated from river banks over one-week period. Using the rating curve for period without rainfall and the flow data for all periods, Gupta and Singh (1996) estimated that river bank contributions in the Minnesota River at Mankato varied from 48% to 55% of the total sediment load for water years 1990-1992. These authors assumed that if there was no rainfall in the basin for 10 days (recession limb of the hydrograph) then most of the sediments in the river were from bank erosion. The major limitation of Gupta and Singh (1996) analysis is that it does not include catastrophic failures due to floods or seepage during or shortly after rainfall events. Their analysis only considers the sediment contribution due to fluvial erosion for a given flow level and thus significantly underestimates bank erosion.

By conducting ground surveys of seven banks using a total-station surveying instrument, Sekely et al. (2002) estimated that 36% to 48% of the sediments in the Blue

Earth River originated from bank erosion. These authors used bank area as a surrogate variable to extrapolate their measurements on seven stream banks to the entire river. However, this analysis does not account for the variations in bank failure mechanisms through space and time (i.e. not every bank fails every year and the bank failure mechanism on a given bank is not the same every time). In other words, area of the bank has little to do with bank erosion/failure mechanisms and thus should not be used as a surrogate to extrapolate estimates from a few banks to the full length of the reach. This approach was recently adopted by Wilcox (2009) using the tall bank (bank with >3 m relief) erosion rates measured on the Le Sueur and the Maple Rivers with ground-based Lidar and aerial photographs. However, using area as a surrogate variable to extrapolate along the entire length of a river channel has the same limitations as that of Sekely et al. (2002).

Using multi-temporal airborne light detection and ranging (Lidar) scans over 35 miles of the Blue Earth River, Thoma et al. (2005b) calculated that river bank contributions from that portion of the river varied from 23% to 56% of the measured total suspended load between 2001 and 2002. The efforts by Thoma et al. (2005b) differed from others in that it characterized the full length of a reach thus eliminating the need for extrapolation.

Recently, Lidar data has become more widely available (Notebaert et al., 2009; Perroy et al., 2010). An airborne Lidar scan is collected by sending thousands of laser pulses to the ground each second from a Lidar instrument, typically attached to an aircraft, and recording the travel time for their returns. Normally, multiple returns are recorded for each laser pulse with the last being the ground. A global positioning system

(GPS) and inertial measurement unit (IMU) record the aircraft's position and attitude (roll, pitch, and yaw), respectively. The combination of laser return times, GPS derived position, and IMU information allows for the precise estimation of horizontal and vertical positions of objects on the ground. Laser returns from vegetation and other objects, such as buildings, can be removed from the data set to obtain ground positions for constructing a "bare earth" digital elevation model (DEM). Airborne Lidar data of a river valley taken at two different times provide an estimate of the change in the volume of the valley as a result of bank erosion, sloughing and accretion (Thoma et al., 2005b).

Typically surveying companies assure their Lidar data have root mean square errors (RMSE) less than 1 m horizontal and 0.15 m vertical positioning; confirming to the guidelines (Flood, 2004) set by the American Society of Photogrammetry and Remote Sensing (ASPRS). Data accuracy varies depending on aircraft elevation, aircraft speed, laser pulse rate, and laser footprint. Hodgson and Besnahan (2004) presented an error budget model, along with detailed background information, that covers the potential sources of error in Lidar data. In addition, several investigators have examined the accuracy and uncertainty of developing DEMs from elevation surveying data in fluvial systems (Bowen and Waltermire, 2002; Lane et al., 2003; Notebaert et al., 2009; Perroy et al., 2010; Wheaton et al., 2010). Bowen and Waltermire (2002) found that areas with large topographic relief tend to have lower vertical accuracy in steep riparian corridors, primarily due to horizontal positioning limitations (lower horizontal accuracy). This lower vertical accuracy in turn could lead to a higher degree of uncertainty in quantification of valley volume change in steep terrain. As such, a variety of methods have been adopted to account for uncertainty in DEMs (Wheaton et al. 2010). A

minimum level of detection threshold (LD_{min}) is frequently applied to examine uncertainties between actual elevation changes and noise (Fuller et al. 2003). Values falling below the threshold level are generally discarded, while the values above the threshold are considered real. Threshold levels can be set based on the results of accuracy tests, such as those described in the guidelines outlined by the ASPRS (Flood, 2004).

In addition to errors from data collection and varying topography, the manner in which data is processed can also have a significant impact on the accuracy of DEMs derived from Lidar data (Hodgson and Bresnaham, 2004). Several efforts have been made to identify the best spatial interpolation techniques for generating DEMs from Lidar data (Lloyd and Atkinson, 2002; Bater and Coops, 2009; Guo et al., 2010). Liu (2008) has given a review on the limitations of several interpolation techniques such as inverse distance weighted (IDW), natural neighbor (NN), triangulated irregular network (TIN), spline, ordinary kriging (OK), and universal kriging (UK) for generating DEMs from Lidar data. Generally, the results identifying the best spatial interpolation technique have been inconsistent, and often depend upon the specific Lidar data collection method, and how and where the data was applied. For instance, Guo et al. (2010) found IDW, NN, and TIN to be the most efficient methods for generating DEMs from Lidar, but found kriging methods to provide the most accuracy. On the other hand, Bater and Coops (2009) found NN as the best spatial interpolation technique for generating Lidar derived DEMs. Studies have also shown that as Lidar data density increases, the accuracy differences among spatial interpolation techniques for generating DEMs diminishes. (Bater and Coops, 2009; Guo et al., 2010). Currently, no studies have been reported that quantify

the effect of different interpolation techniques on Lidar-based change detection calculation.

The objective of this study was to quantify sediment and associated phosphorus contributions from bank erosion/sloughing along several rivers in Blue Earth County using airborne Lidar. Characterization of phosphorus contributions from bank erosion is included because of its impact on water quality of Lake Pepin on the Mississippi River. Blue Earth County was selected for this study because the Lidar data from an earlier scan was available for this county and also the GBERB contributes over half of the sediment load to the Minnesota River at Mankato (Payne, 1994). In this paper, we also report the accuracy and uncertainties of using airborne Lidar over steep terrains, examine how different spatial interpolation techniques affect Lidar-based DEM change detection calculations of stream bank erosion, and explore the sensitivity of using limited soil characterization to estimate fine sediment and associated phosphorus contributions from bank erosion.

MATERIALS AND METHODS

Study Area Description

The geological setting of Blue Earth County is well described by Bennett and Hurst (1907) and Wright (1972a, b). Gran et al. (2009) has provided more specific details on the geology of the Le Sueur River Watershed. Briefly, the area was glaciated during the Wisconsin glaciations approximately 12,000 years before present. The area predominately consists of fine-textured, carbonate-rich buff colored glacial tills deposited by the Des Moines Lobe. In some places the till is as thick as 80 m. Due to compaction

at the time of deposition, the bulk density of the till often exceeds 1.6 Mg m^{-3}. As the Des Moines Lobe retreated, Glacial Lake Minnesota occupied the region depositing up to 1 m of lacustrine sediment on top of the till. After glaciation and drainage of Glacial Lake Minnesota, river incision began. River bottoms commonly contain thin (< 2 m) deposits of alluvium. The surface soils are black loam to fine clays with high organic matter content derived from prairie grasses native to the region. In most untilled soils, organic matter is generally concentrated in top 15 cm depth.

Blue Earth County, MN lies in the GBERB and contains many rivers that are deeply incised with steep and unstable banks. The county is relatively flat with 71% and 93% of the land <2% and <6% slopes, respectively. Blue Earth County also has the most rivers of any county in Minnesota. The major waterways include the Blue Earth, Le Sueur, Watonwan, Maple, Big Cobb, and Little Cobb Rivers and Perch Creek (Figure 1). The Watonwan River and Perch Creek are tributaries of the Blue Earth River whereas the Maple, Big Cobb, and Little Cobb Rivers are tributaries of the Le Sueur River. The Le Sueur River converges into the Blue Earth River before it joins the Minnesota River at Mankato. For this study, 496 km of rivers including the Minnesota River at the northern edge of the county were investigated. Table 1 lists the length of each river analyzed in this study. These lengths are based on the centerline of the river channel. Some of the sloughing banks are as tall as 50 m (Figure 2) and in some places the valley is as wide as 1.5 km. Lack of vegetation on the banks, exposed tree roots, accumulation of the fallen material at the toe, and presence of dead trees in the rivers are some of the indications of active bank sloughing along these rivers. Most of these rivers are lined with tall trees or shrubs and access to these banks is primarily through the river with a canoe. Generally,

the tall banks are sheer cliffs with slopes as high as 80 degrees (Figure 2). Surveying these banks with conventional surveying equipment such as a total station is dangerous, laborious, time consuming, and for most practical purpose infeasible. Remote sensing techniques, such as Lidar, provide a unique tool to quantify bank sloughing/erosion safely and quickly.

Table 1. River length and the length and area of tall (>3 m height) and short (< 3 m height) banks for each river in Blue Earth County, Minnesota. Sum of tall plus short bank lengths will be greater than the river length as we are considering both sides of the river and river length corresponds to the center line of the river channel.

River	River Length, km	Tall Bank Length, km	Tall Bank Area, km^2	Short Bank Length, km	Short Bank Area, km^2
Blue Earth	103	100	2.14	125	0.82
Watonwan	41	29	0.60	56	0.33
Perch Creek	32	11	0.19	63	0.35
Le Sueur	71	69	1.00	77	0.38
Maple	80	49	0.79	110	0.38
Big Cobb	87	29	0.40	122	0.59
Little Cobb	32	8	0.13	44	0.24

Figure 2. A steep tall bank actively sloughing along the Le Sueur River in Blue Earth County, Minnesota. Accumulated material at the toe is from past bank sloughing from above. Lack of vegetation on part of the bank indicates active sloughing nature of this bank.

Lidar Data

With the exception that the calculations were done with a geographic information system (GIS) software, the procedures used to calculate volume change from two Lidar datasets were similar to those of Thoma et al. (2005b). The data processing utilized three data products (bare earth points, hydrologic breaklines, and 0.6 m contours) derived from the Lidar datasets and delivered by the data vendors. The following text briefly describes the features of the two Lidar datasets used in this study.

2005 Lidar Dataset: The first Lidar dataset was obtained by Optimal Geomatic, Inc., Huntsville, AL with an Optech ALTM 3100 Lidar system flown at 1836 meters above

ground using a laser pulse rate of 70 kHz. The data was collected during 4 flights over two collection periods, 13-14 April 2005 and 23-24 April 2005, with a foot print of 0.45 m and an average of 1 data point per m^2 during leaf off conditions. Raw Lidar data was processed by the vendor using proprietary software to produce bare earth points, hydrologic breaklines, and 0.6 m contours. The accuracy of their data was checked by the Minnesota Department of Transportation (MnDOT) using ground truth data with a total of 351 points collected with real time kinetic (RTK) GPS over a variety of land covers. Points included 204 open terrain, 41 tall weeds and crops, 13 brush lands and low tree, and 93 urban areas. The reported fundamental vertical accuracy was ±0.24 m. Fundamental vertical accuracy is calculated as $RMSE_{(z)}$ x 1.96 and refers to the confidence interval at 95% significance (Flood, 2004).

2009 Lidar Dataset: The second Lidar dataset was obtained by Aero-Metric, Inc., Sheboygan, WI using an Optech ALTM Gemini system flown at 1200 meters above ground with a laser pulse rate of 45 kHz. Data was collected on 28 April 2009 and 2-3 May 2009 during leaf off conditions with a 0.9 m foot print and average of 1.25 data points per m^2. Raw Lidar data was processed by the vendor using proprietary software and included the generation of bare earth points, hydrologic breaklines, and 0.6 m contours. The vendor also collected ground elevation data for 106 points using static and RTK GPS techniques for an accuracy assessment over a variety of land covers. Points included 26 hard surfaces (roads, parking lots, etc.), 20 short grasses, 20 tall grasses/weeds, 20 brushes, and 20 woods. The fundamental vertical accuracy reported for this scan was ±0.17 m.

Lidar Data Processing

Volume Change and Mass Wasting Calculations: The vendor generated bare earth points in both datasets were spatially interpolated to an Environmental Systems Research Institute (ESRI) ArcGIS 9.3 terrain file of a common extent using the breaklines and contours as hard and soft control lines, respectively. Terrain files data structure provides an efficient way to manage large datasets of bare earth points, breaklines and contours to create TINs. Due to the large Lidar data sets, terrain files were selected as a balance between processing efficiency and accuracy. Next, each terrain file was converted to a DEM grid with a 0.76 m spatial resolution (hereafter referred to as user DEMs). The above data processing resulted in county wide bare earth user DEMs with the same spatial alignment for both years of Lidar data. In this study, we define river banks as the area between the breakline of the river and the top of the river bank. The highest water mark indicated by the breaklines in the two scans was used to define the bottom of the bank. Since the Lidar systems used in collecting the data for this study could not penetrate water surfaces, all areas below the high water mark were eliminated from bank erosion calculations. The top of the bank was manually digitized using a combination of aerial imagery (2005 and 2009), hillshade models, and slope grids. Hillshade models and slope grids were calculated for both 2005 and 2009 using the user DEMs. The 2005 aerial imagery was collected in unison with the 2005 Lidar data, while the 2009 aerial imagery was collected from 4 April 2009 to 6 May 2009 by Blue Earth County. This river bank identification procedure was performed for each river examined. The user DEMs were

then subtracted from each other creating a county wide grid showing elevation change from 2005-2009.

The riverbanks in the county wide elevation change grid were identified as the zones for net elevation change calculations. The net elevation change for each river was calculated from the subtracted DEMs (ΔDEM) for all river bank zones using a summary zonal statistic in ArcGIS. This net elevation change for each river was then multiplied by the spatial extent (area) of the river bank zones, resulting in a net volume change. Next, net volume change was multiplied with the mean bulk density of a given parent material (Table 2) to calculate mass wasting. These mass wasting values were in turn multiplied with fine content (silt+clay), soluble P, and total P concentrations (Table 2) to calculate fine sediment, soluble P, and total P losses as a result of bank erosion/sloughing.

Table 2. Mean fine sediment (silt+clay), bulk density, soluble P, and total P in samples representing various parent materials along river banks in Blue Earth County, MN. Number within parenthesis represents the number of samples.

Parent Material	**Silt+Clay %**	**Bulk Density, Mg m^{-3}**	**Soluble P, mg kg^{-1}**	**Total Phosphorus, mg kg^{-1}**
Till	56.3 (27)	1.82 (27)	0.46 (22)	408.8 (24)
Lacustrine	67.3 (5)	1.48 (5)	0.74 (5)	556.2 (5)
Alluvium	52.5 (5)	1.49 (4)	0.73 (3)	558.6 (5)

In addition to the above calculations, further analysis was also undertaken to quantify the extent (volume basis) of soil loss from tall (>3m relief) and short (<3 m relief) stream banks in Blue Earth County, MN. This classification was chosen to be consistent with previous literature (Gran et al. 2009). Gran et al. (2009) defined tall banks as bluffs and short banks as stream banks. Bluffs in our and Gran et al. (2009) studies are not rock outcrop but glacial deposits, mainly tills. Tall banks were identified using a 10 m x 10 m moving window analysis in ArcGIS. Areas identified as tall banks were manually inspected to insure the accuracy of the moving window classification. Remaining areas (< 3 m relief) were considered short stream banks. Extent of volume loss (erosion) from tall and short stream banks was expressed as a percent of the total volume change for each river.

Lidar Data Accuracy

Fundamental vertical accuracies in the Lidar data outlined earlier were the results of accuracy analysis performed on the raw data provided by the vendor. In addition, we also conducted two accuracy analyses on the user DEMs. In the first accuracy analysis, 78 of the 2005 MnDOT hard surface points, collected with an RTK GPS unit, were compared against the corresponding points in the 2005 and 2009 user DEMs. This was done to insure data accuracy in user DEMs across years. Bias in the elevation estimates for the 2005 and 2009 user DEMs were evaluated by comparing the mean vertical errors in the datasets using a paired t-test with a null hypothesis that the vertical errors were equal to zero.

The second accuracy assessment involved testing the vertical accuracy of points on steep terrains. This was done because a large proportion of the volume change in our study area was on steep terrains (>10% slope). The procedure involved subtracting elevations of 124 points representing a variety of land covers on steep terrains between 2005 and 2009 user DEMs. The points were taken on areas with slopes ranging from 4% to 77% and included wooded (26 points), road (77 points), grass (6 points), tall grass (9 points), and a restored bluff (6 points) land covers. These areas were stable and known to have zero elevation change between 2005 and 2009. Differences in elevation between the 2005 and 2009 user DEMs at the selected points were summarized as measurement errors in the Lidar data. A paired t-test was performed between the elevations of the 2005 user DEM and 2009 user DEM found at the 124 steep terrain points with the null hypothesis that the mean difference between their elevations was equal to zero.

Elevation Error Analysis: An additional uncertainty analysis was conducted to determine how various levels of elevation errors in steep terrain could have impacted the net volume change estimates in this study. A series of LD_{min} (0.00, 0.08, 0.15, 0.23, 0.3, 0.46, 0.61, and 0.91 m) were applied to the ΔDEM following methods similar to those developed by Fuller et al. (2003). At each interval, values beneath the minimum threshold (for both erosion and deposition) were removed from the ΔDEM. The net change in volume estimates were then recalculated at each interval for all rivers, and the results were compared to the original volume change to determine whether or not significant change in the volume occurred at various LD_{min}; a potential indicator of possible uncertainty on steep terrains.

Spatial Interpolation Error Analysis: A sensitivity analysis was conducted on one bank (Figure 3) to see how various spatial interpolation techniques for generating DEMs from Lidar data affect volume change estimates for river bank erosion. The techniques tested were IDW (Bartier and Keller, 1996), OK (Cressie, 1990), NN (Sibson, 1981), regularized spline, and regularized spline with tension (Mitasova and Hofierka, 1993). For all techniques, the number of points used for each local approximation was 12. IDW was run with 2, 4, and 6 exponent power options. These power options control the weight of the surrounding points on the interpolated value. Higher exponent values give less weight to points further away from the local interpreted value. OK was applied with spherical, circular, exponential, Gaussian, and linear semivariogram models. Briefly, the procedure for this sensitivity analysis involved first generating DEMs for both 2005 and 2009 Lidar datasets for each spatial interpolation technique using the bare earth point files provided by the vendors and then calculating the net volume change between 2005 and 2009 DEMs. Using summary statistics, the resulting volume change from various interpolation techniques were then compared to the volume change calculations from the terrain to raster technique used for the whole study area.

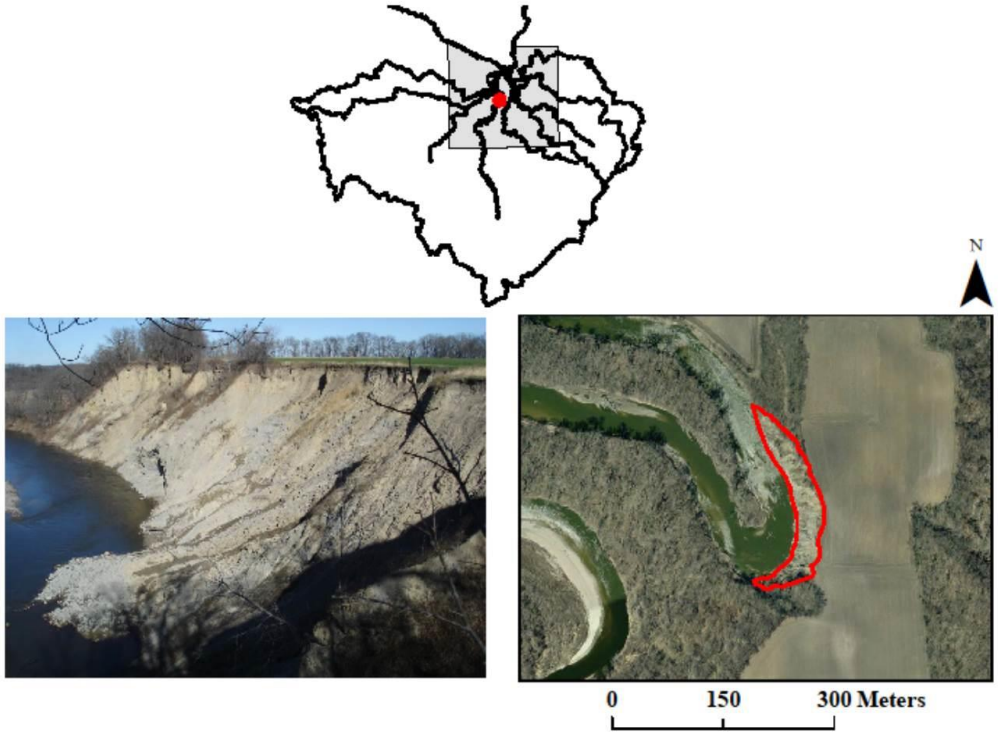

Figure 3. Pictures of a bank in Blue Earth County, Minnesota, used in sensitivity analysis of volume change calculations with various spatial interpolation techniques in construction of digital elevation models.

Fieldwork and Laboratory Analysis

For conversion of volume change estimates from Lidar analysis to mass wasting and then fine sediment losses, 26 soil samples representing materials of various depths and origins were collected from the study area. Because of the difficulty of taking soil samples from tall sheer cliffs, samples were taken from accessible banks, fallen material at the toe of

the river banks, and road cuts. During sampling of road cuts, efforts were made to sample areas representing mid to upper depths of tall banks that are otherwise difficult to sample.

These samples were characterized for bulk density and particle size distribution using the clod method (Grossman and Reinsch, 2002) and the hydrometer method (Gee and Or, 2002), respectively. These samples were also analyzed for soluble P with water using a 1:10 ratio (Kuo, 1986) and total P via microwave acid digestion (USEPA, 1981). Soluble P and total P analysis was done by the Soil Testing Laboratory at the University of Minnesota. Since lacustrine and alluvium materials generally represent less than two meters depth of the bank, their contributions to the total sediment loads from most tall banks will be minor. We combined our data on particle size analysis, bulk density, soluble P and total P with the data base from Thoma et al. (2005b). Table 2 lists the mean values of fine sediment (silt+clay), bulk density, soluble P, and total P in bank samples by parent material.

Sediment loads for the Blue Earth and Le Sueur Rivers were obtained from the Water Resources Center at Minnesota State University, Mankato, MN (Scott Matheson, Personal Communication, 2010). These data represent the measurements at the USGS water gauging stations near the mouth of these rivers. The data for the Blue Earth River represented the contributions from the Blue Earth and Watonwan Rivers plus Perch Creek; whereas the data for the Le Sueur River represented the contributions from the Le Sueur, Maple, Big Cobb, and Little Cobb Rivers. Percent contributions of sediment, soluble P, and total P from river banks to river loads were calculated by dividing the fine sediment (silt+clay), soluble P, and total P loss estimates from the Lidar calculations with the respective measured values of total suspended solids, soluble P, and total P loads at

the gauging stations. We also report the estimated value of fine sediment, soluble P and total P losses due to bank erosion from the Minnesota River touching the northern boundary of Blue Earth County.

RESULTS AND DISCUSSION

Accuracy Assessment of Lidar

The fundamental vertical accuracy ($RMSE_{(z)}$ x 1.96) at 95% confidence interval for the 2005 and 2009 scans when tested against the 2005 MnDOT hard surface points corresponded to ±0.20 m and ±0.14 m, respectively. The corresponding fundamental vertical accuracy between the 2005 and 2009 user DEMs was ±0.25 m. The 2005 user DEM underestimated the actual terrain elevation, based on the 2005 MnDOT hard surface points by 0.029 m ($P = 0.01$) whereas the 2009 user DEM overestimated the actual terrain elevation by 0.032 m ($P < 0.01$). The comparison of mean vertical error between the 2005 and 2009 user DEMs resulted in an average difference of 0.06 m ($P < 0.01$), with the 2009 user DEM producing higher elevation estimates than the 2005 user DEM. This average difference between user DEMs is less than the typical fundamental vertical accuracy (±0.15 m) vendors' guarantee in their processed Lidar data.

The differences in elevation determined from 2005 and 2009 user DEMs for points of varying steepness in parks and roads of Blue Earth County, MN are shown in Figure 4 as a function of percent slope. The average difference in elevation was -0.009 m with a minimum difference of -0.291 m and a maximum difference of 0.303 m. Except for a few outliers, difference in elevation between 2005 and 2009 user DEMs was about same (±0.2m) irrespective of the slope. The differences in elevation between the two

scans showed a fundamental vertical accuracy of ±0.19 m at a 95% confidence level; a value slightly higher than ±0.15m fundamental vertical accuracy specification typically promised by Lidar vendors for a single Lidar data set.

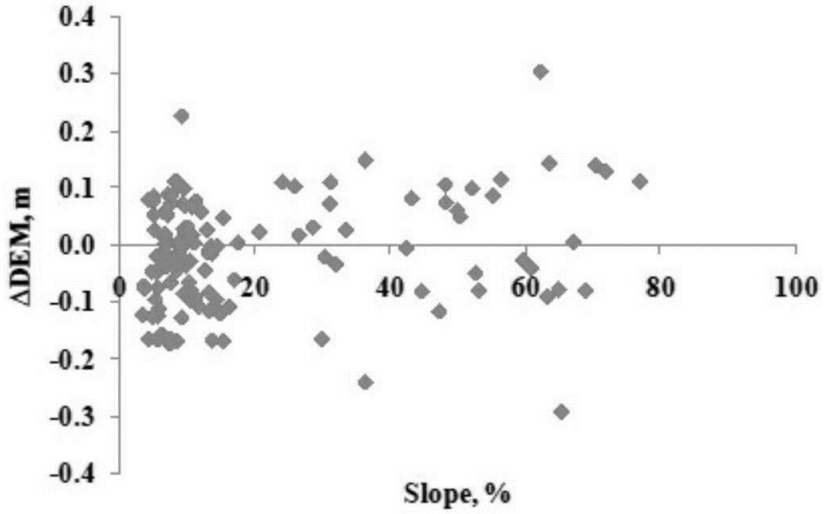

Figure 4. Distribution of elevation difference between 2005 and 2009 user digital elevation models (DEMs) potted as a function of slope for the 124 steep terrain points taken on various land covers in Blue Earth County, Minnesota. All of the points were stable locations known to have zero change in elevation from 2005-2009.

Volume Change in River Valleys

Changes in the volume of river valleys as a result of bank erosion from 2005 to 2009 for several rivers in Blue Earth County, MN are shown in Figure 5. The greatest volume change in the river valley occurred for the Blue Earth River followed by the Le Sueur River, the Maple River, the Watonwan River, the Big Cobb River, the Perch Creek, and the Little Cobb River. This trend in volume loss follows the trends in tall bank area over the scanned rivers kilometers (Table 1): The Blue Earth River >Le Sueur

River>Maple River>Watonwan River>Big Cobb River>Perch Creek>Little Cobb River. Volume change estimates for the Maple, Big Cobb and Little Cobb rivers are somewhat conservative because in some sections there were insufficient Lidar data due to high water levels in the 2005 scan and thus these submerged banks were removed from the bank erosion calculations. Removal of submerged banks also implies that the Lidar analysis in this study does not account for erosion losses from the river bed. Volume change as a result of bank erosion/sloughing in tributaries of the Blue Earth and the Le Sueur Rivers amounted to 1.39 million m^3 from 2005 to 2009. Corresponding volume change in the Minnesota River at the northern edge of Blue Earth County equaled 321,571 m^3 over 4 years.

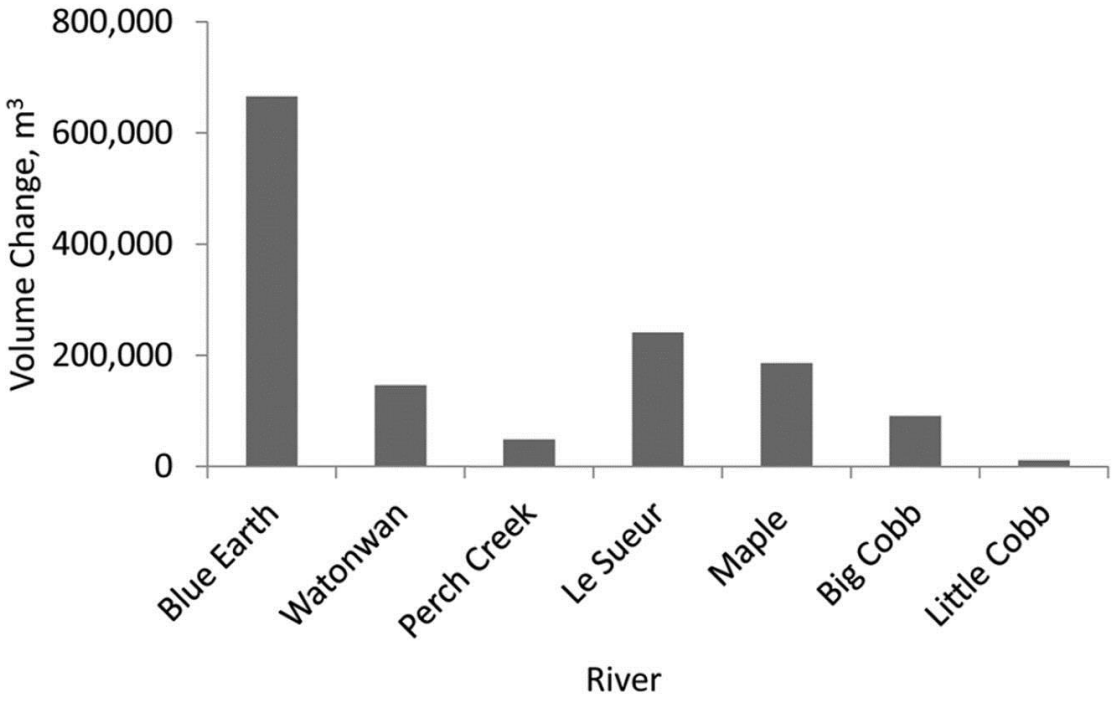

Figure 5. Change in volume of river valleys as a result of bank erosion/sloughing from 2005 to 2009 for various rivers in Blue Earth County, Minnesota.

Contributions from Tall vs. Short Banks

Percent contributions to volume change estimates from tall (> 3 m relief) and short (< 3 m relief) banks for each river in Blue Earth County are shown in Figure 6. When summed over all rivers, tall and short banks, respectively, contributed 75% and 25% of the calculated volume change from the Lidar scans. However, the tall banks account for only 33% of the total length and 63% of the total area along all rivers investigated (Table 1). This further indicates that tall banks, while occupying a small portion of the river lengths in Blue Earth County, are the key producers of sediment in rivers of GBERB. Contributions from short (<3 m relief) banks may be conservative because during the analysis it was quite evident that point bars were forming from the deposition of suspended sediments on the inside of meanders. Although depositional point bars are likely composed of sediments from all sources (fields, ravines, and short and tall banks), this analysis discounted 100% of the point bar deposition from the areas defined as short banks.

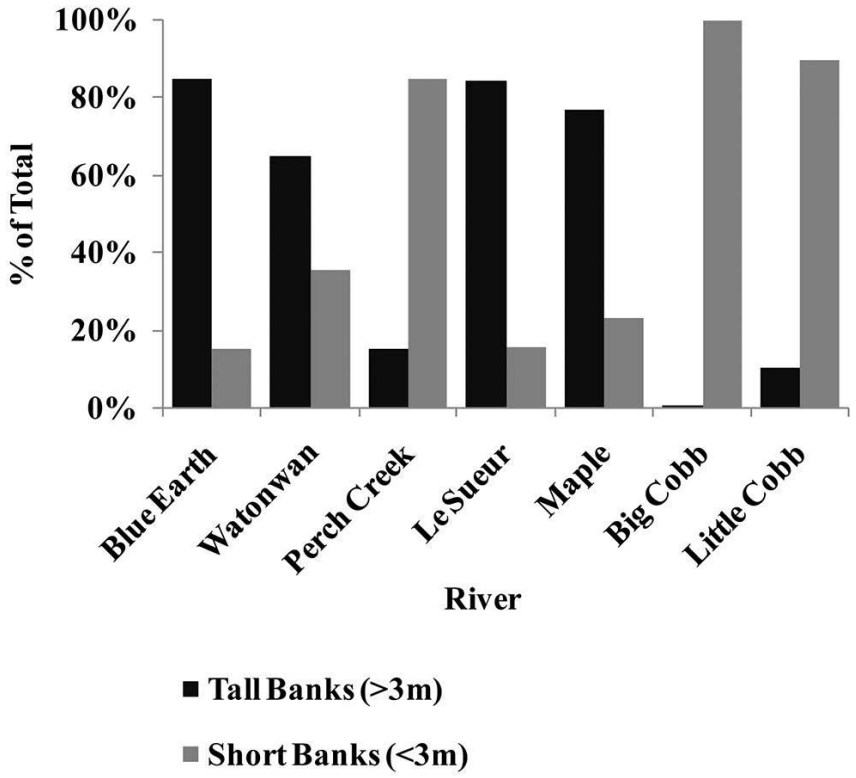

Figure 6. Proportion of soil volume lost due to bank erosion from tall (>3 m high) and short (<3 m high) banks between 2005 and 2009 along various rivers in Blue Earth County, Minnesota.

LD_{min} Uncertainty Analysis

The results of the LD_{min} uncertainty analysis on net volume change from all river banks except along the Minnesota River at the northern edge of the county are shown in Figure 7. These results show that at LD_{min} values <0.46 m, the volume change slightly increases with an increase in LD_{min}. Comparatively, at LD_{min} values >0.46 m there is a decrease in volume change with an increase in LD_{min}. These results are expected considering that a larger portion of small elevation changes are attributed to deposition and thus deletion of areas with small changes in elevation results in an increase in volume

change. Conversely, a majority of large elevation changes are the result of erosion and thus deletion of areas with large elevation changes results in a decrease in volume change. Percent error in volume change corresponded to 0.25, 1.5, 3.3, 4.9, 5.4, 2.6, and -10% for LD_{min} values of 0.08, 0.15, 0.23, 0.30, 0.46, 0.61, and 0.91m, respectively.

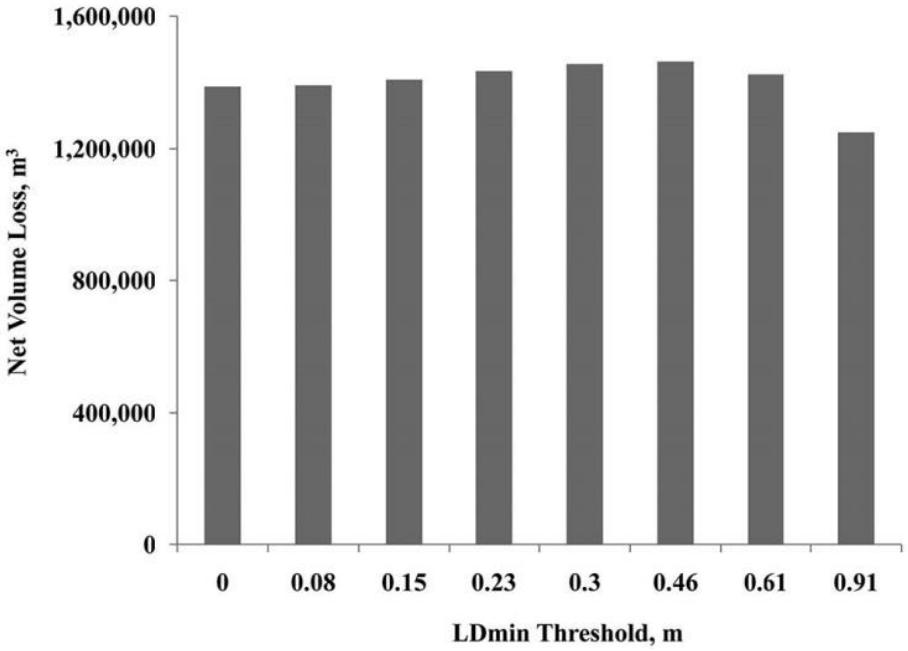

Figure 7. Variation in net volume loss due to bank erosion from all rivers except along the Minnesota River at the northern edge of Blue Earth County, Minnesota, at various threshold levels of LD_{min} in the uncertainty analysis.

Overall, the results in Figure 7 indicate that the removal of data within ± 0.91m has little impact on net volume change estimates for the rivers analyzed in this study. This suggests that the majority of sediments are derived from areas with large elevation changes (>0.91m in ΔDEM). Comparing these results with the range of error values (-0.291 to 0.303m) in the steep terrain accuracy assessment indicates that the range of error in steep terrain is below the threshold level that would have a significant impact on the

net volume change calculations. This further increases the confidence in Lidar quantification of sediment production as a result of mass failure of river banks.

Spatial Interpolation

The results of the spatial interpolation sensitivity analysis on one bank are given in Table 3. The volume loss calculations for all interpolation techniques varied between 10,933 m^3 and 13,143 m^3 with an average value of 11,719 m^3 and a standard error of 202 m^3. This is less than 2% standard error in volume calculations due to spatial interpolation. The calculation from the terrain to raster technique resulted in volume loss of 11,543 m^3, a value close to the average value for all the techniques. These results suggest that the terrain to raster technique used for this study performs similarly to other spatial interpolation techniques used in the literature. It's likely that the high data density provided by the Lidar datasets in our study reduced the error between different spatial interpolation techniques, a result similar to the findings of other studies (Bater and Coops, 2009; Guo et al., 2010). For the purposes of this study, we concluded that terrain to raster was a suitable spatial interpolation technique for quantifying volume loss from river banks of Blue Earth County using Lidar derived DEMs.

Table 3. Sensitivity analysis of volume loss calculations for one bank using various techniques for interpolating Lidar data to construct digital elevation models.

Spatial Interpolation Method	**Volume Loss, m^3**	**Difference from Terrain to Raster, %**
ArcGIS 9.3 Terrain to Raster	11,543	------
Inverse Distance Weighted, Exp. of 2	11,060	-4
Inverse Distance Weighted, Exp. of 4	11,240	-3
Inverse Distance Weighted, Exp. of 6	11,346	-2
Ordinary Kriging Circular	11,332	-2
Ordinary Kriging Exponential	11,941	3
Ordinary Kriging Gaussian	10,933	-5
Ordinary Kriging Linear	11,448	-1
Ordinary Kriging Spherical	11,448	-1
Natural Neighbor	12,539	9
Spline Regularized	13,143	14
Spline with Tension	12,656	10

During the review of the manuscript, a question was raised whether a 0.76 m spatial resolution might be too fine for Lidar data that was collected with an average 1 point m^2? In other words, some of the grid cell values may be derived wholly from interpolated values rather than data points. We hypothesize that if a 0.76 m cell size induced a significant error in our net volume calculations, we would have seen notable differences among the spatial interpolation techniques. Since the above analysis shows

minimal differences between interpolation techniques, we concluded that 0.76 m is appropriate for this investigation.

Characteristics of Stream Bank Sediments

Using Lidar data to estimate bank erosion and the contributions of sediment, soluble P, and total P from banks to river loads requires the conversion of volume change to mass wasting associated losses. For these conversions, representative values of bulk density, soluble P and total P for bank materials are important. As previously mentioned, accurately characterizing river bank materials in the entire study area, both spatially as well as with depth, was not practical. Since the river banks in Blue Earth County consist of varying materials, mass wasting and fine sediment losses were calculated by parent material. Table 2 lists the average bulk density and fine sediment of glacial till, glacial lacustrine, and alluvium samples collected along river banks in the county. This is based on the combined data base both from this study and from Thoma et al. (2005b). As expected, the bulk density of the tills is much higher (1.82 Mg m^{-3}) than that of lacustrine (1.48 Mg m^{-3}) or alluvium (1.49 Mg m^{-3}) materials. This is primarily because tills generally occur at deeper depths buried under a large amount of overburden material including thick ice during the ice age. Fine sediment contents were generally higher in lacustrine soils (67.3%) followed by nearly equal amounts in tills (56.3%) and alluvium (52.5%) materials.

Mean fine sediment content for tills calculated in this study (56.3%) is slightly lower than the 65% value used by Gran et al. (2009) in their calculations for bank sediment contributions in the Le Sueur River Basin. Gran et al. (2009) had over 300

samples in their data base for particle size distribution and they applied the average value to much deeper depths when calculating geologic erosion over thousands of years. No literature values are available for bulk density, soluble P, and total P for bank materials in Blue Earth County to compare with our data base. Gran et al. (2009) used bulk density value of 1.82 Mg m^{-3} from Thoma et al. (2005b). This bulk density value represents an average of 11 samples. The bulk density for tills in the combined data base (Table 2) also equaled 1.82 Mg m^{-3}. We use this value in our calculations.

To address the issue of variation with soil depth, we also obtained particle size analysis at various depths for 5 coring sites in Blue Earth County from the Minnesota Geological Survey (Alan Knaeble and Gary Meyer, Personal Communication, 2011). Table 4 lists maximum depth of sampling, number of samples for silt+clay measurement, mean values of silt+clay to that depth, number of samples for bulk density measurement, and depth weighted mean bulk density at each of the five coring sites. The maximum sampling depth of measurements varied from 12.5 m to 51.6 m. Since silt+ clay contents were measured on random samples, these values represent ordinary means. Comparatively, bulk density was measured on two representative samples for each depth section thus mean values were depth weighted. Averaged over all soil depths at five coring sites (N=133), silt + clay content corresponded to 55.6%; a value close to the mean value of 56.3% in our data base. We used these additional sources of data in our sensitivity analysis to provide a likely range of sediment, soluble, P, and total P contributions from river bank sloughing to river loads.

Table 4. Mean and standard deviation of silt+clay content and bulk density of soil samples from various depths at five Minnesota Geological Survey coring sites in Blue Earth County, MN. Mean silt+clay content represent ordinary means whereas mean bulk density refers to depth weighted mean. N_1 is the number of samples for silt+clay content whereas N_2 is number of samples times two replications for bulk density at each coring site.

Core	Maximum Depth m	N_1	Silt+Clay %	N_2	Bulk Density Mg m^{-3}
SC5	12.5	7	63.9±24.5	20	1.94±0.16
SC5A	27.2	18	46.3±19.8	32	1.92±0.20
SC6	82.2	32	52.3±19.4	142	1.85±0.14
SC7	67.2	44	66.3±22.3	122	1.95±0.14
SC8	51.6	32	47.5±19.2	84	1.97±0.15

Fine Sediment, Soluble P and Total P Losses

Table 5 lists the estimated fine sediment, soluble P, and total P contributions from bank erosion from various rivers as a proportion of the measured values (Table 6) at the mouth of the Blue Earth River below Rapidan Dam, or at the mouth of the Le Sueur River before it joins the Blue Earth River. These values are calculated for various parent materials from volume change in Figure 5 and the corresponding silt+clay, soluble P, and total P contents in Table 2. As stated earlier, contributions for the Blue Earth River, the Watonwan River, and the Perch Creek are relative to USGS water gauge measurements for the Blue Earth River, whereas contributions for the Le Sueur, Maple, Big Cobb, and Little Cobb rivers are relative to the measurements for the Le Sueur River. As expected, fine sediment, soluble P, and total P contributions from bank erosion follow the trends of volume change for various river valleys (Figure 5). The combination of higher density

and lower fine content in tills, or lower density and higher fine content in lacustrine soils resulted in only small differences (<12%) in the total fine sediment losses for various parent materials in a given river system (Table 5). Fine sediment losses followed the trend: till> lacustrine>alluvium.

Table 5. Fine sediment, soluble P, and total P losses as a percentage of the measured values at the mouth of the Blue Earth (Blue Earth River, Watonwan River, and Perch Creek) or the Le Sueur River (Le Sueur River, Maple River, Big Cobb River, and Little Cobb River). The losses were estimated for each of the three parent materials using specific fine sediment content, bulk density, and soluble P and total P contents.

	Sediment Losses, %			**Soluble P losses, %**			**Total P losses, %**		
River	**Till**	**Lacustrine**	**Alluvium**	**Till**	**Lacustrine**	**Alluvium**	**Till**	**Lacustrine**	**Alluvium**
Blue Earth	48.8	47.7	37.2	0.12	0.16	0.16	31.3	34.4	34.7
Watonwan	10.7	10.4	8.2	0.03	0.03	0.03	6.8	7.5	7.6
Perch Creek	3.6	3.5	2.7	0.01	0.01	0.01	2.3	2.5	2.5
Le Sueur	36.1	35.1	27.6	0.06	0.08	0.08	20.0	22.2	22.4
Maple	27.9	27.1	21.3	0.05	0.06	0.06	15.5	17.1	17.3
Big Cobb	13.6	13.2	10.4	0.02	0.03	0.03	7.5	8.3	8.4
Little Cobb	1.7	1.5	1.2	0.003	0.004	0.004	0.9	1.0	1.0

Table 6. Annual suspended solids, soluble phosphorus and total phosphorus measured at the mouth of the Blue Earth and the Le Sueur Rivers for the study period (2005-2009).

Rivers	Sediment, Mg yr^{-1}	Soluble P, kg yr^{-1}	Total P, Mg yr^{-1}
Blue Earth River	216,145	191.1	166.2
Le Sueur River	132,824	117.5	102.1

Depending upon the parent material, combined fine sediment losses from the Blue Earth River, Watonwan River, and Perch Creek within Blue Earth County varied from 48% to 63% of the TSS measurements at the mouth of the Blue Earth below Rapidan Dam. Similarly, combined fine sediment losses from the Le Sueur, Maple, Big Cobb and Little Cobb rivers within Blue Earth County varied from 61% to 79% of the TSS measurements at the mouth of the Le Sueur River before it joins the Blue Earth River. Higher proportion of sediment losses from bank erosion in the Le Sueur River Basin relative to the Blue Earth River Basin are likely (1) due to greater length of the rivers analyzed in the Le Sueur River Basin (270 km) compared to the Blue Earth River Basin (176 km), and (2) because the measured sediment loads at the mouth of the Le Sueur River were lower than at the mouth of the Blue Earth River over the study period (Table 6). Fine sediment contributions from the Minnesota River touching the northern edge of

Blue Earth County corresponded to 82,380 Mg yr^{-1}, 80,079 Mg yr^{-1}, and 62,891 Mg yr^{-1} for the till, lacustrine and alluvium parent materials, respectively.

Both, soluble P and total P losses followed the trend: alluvium>lacustrine> till. Combined soluble P losses from the Blue Earth River, Watonwan River, and Perch Creek varied from 0.16% to 0.20% of the measured value at the mouth of the Blue Earth River whereas the corresponding total P losses ranged from 40% to 45% of the measured value. Depending upon the parent material, combined soluble P losses from the Le Sueur River, Maple River, Big Cobb River, and Little Cobb River varied from 0.13% to 0.17% of the measured value at the mouth of the Le Sueur River. Corresponding total P losses ranged from 44% to 49% of the measured values. Soluble P and total P losses for the Minnesota River at the northern edge of the county varied from 67.3 to 88.1 kg yr^{-1} and 59.8 to 66.9 Mg yr^{-1}, respectively.

Since these rivers extend past Blue Earth County into the neighboring counties, it is likely that bank sloughing also occurred along these rivers in the neighboring counties. This would suggest that our estimates of volume change and in turn bank erosion are somewhat conservative. It is also likely that some of the sediments are settling in floodplains and not necessarily making it to the mouth of these rivers as well as to the confluence with the Minnesota River. The other sources of sediment in Blue Earth County are agricultural fields and near channel ravines. Although relatively flat, agricultural fields do contribute some sediment to rivers through surface and side inlets. The level of erosion in near channel ravines and subsequent sediment transport to rivers has not been documented yet, and should be the focus of future studies.

Sensitivity Analysis of Fine Sediment, Soluble P and Total P Losses

We also ran sensitivity analyses for sediment, soluble P, and total P contributions from bank sloughing using the estimate of fine sediment content (65%) and bulk density (1.82 Mg m^{-3}) from Gran et al. (2009) and mean fine sediment content and depth weighted bulk density measurements on samples from five Minnesota Geological Survey soil coring sites (Table 4). We used our measurements of soluble P and total P (Table 2) for till in both these sensitivity runs.

Table 7 shows the comparison of sediment, soluble P and total P contributions as a proportion of the measured values for three data bases. Using Gran et al. (2009) values, estimates of fine sediment contributions to total suspended solid loads corresponded to 73% and 92% of measured values at the mouth of the Blue Earth River and the Le Sueur River, respectively. Corresponding soluble P contributions from bank erosion for the two rivers equaled 0.18% and 0.16% of the measured values, and total P contributions at 44% and 49% of the measured values.

Table 7. Estimated bank sloughing contributions of sediment, soluble P, and total P to corresponding total loads at the mouth of the Blue Earth and the Le Sueur Rivers for various values of silt +clay content and the bulk density in river banks. Silt+clay content for Minnesota Geological Survey (MGS) cores refer to ordinary mean, whereas the bulk densities are depth weighted values over the length indicated in Table 4. Sediment, soluble P, and total P estimates reported for this study correspond to the till parent material.

Source	**Silt + Clay**	**Bulk Density**	**River**	**Sediment**	**Soluble P**	**Total P**
	%	**Mg m^{-3}**		**----------%----------**		
This study	58.8	1.82	Blue Earth	63.1	0.16	40.4
			Le Sueur	79.3	0.13	43.9
Gran et al.	65.0	1.82	Blue Earth	72.8	0.18	44.4
			Le Sueur	91.5	0.16	48.6
MGS-SC5	63.9	1.94	Blue Earth	76.2	0.17	42.7
			Le Sueur	95.8	0.15	46.8
MGS-SC5A	46.3	1.92	Blue Earth	54.6	0.16	42.3
			Le Sueur	68.7	0.15	46.3
MGS-SC6	52.3	1.85	Blue Earth	59.4	0.16	40.7
			Le Sueur	74.7	0.14	44.6
MGS-SC7	66.3	1.95	Blue Earth	79.3	0.17	42.9
			Le Sueur	99.7	0.15	46.9

MGS-SC8	47.5	1.97	Blue Earth	57.5	0.17	43.4
			Le Sueur	72.3	0.15	47.5

Using the mean silt+clay content and depth weighted bulk densities for five Minnesota Geological Survey coring sites, contributions of fine sediment from bank erosion varied from 55% to 79% for the Blue Earth River and from 69% to 100% for the Le Sueur River. Corresponding contributions for soluble P and total P from river bank sloughing varied from 0.16% to 0.17% and 41% to 43%, respectively, of the measured values for the Blue Earth River and 0.14% to 0.15% and 45% to 48%, respectively, of the measured values for the Le Sueur River. Using the till measurements, our estimates for sediment (63% and 79%), soluble P (0.16% and 0.13%) and total P (40% and 44%) contributions from river bank erosion/sloughing at the mouth of the Blue Earth River and the Le Sueur River (Table 6) are within the range of values obtained with data bases of Gran et al. (2009) or five coring sites of the Minnesota Geological Survey. This further suggests that the soil samples collected and analyzed in this study provide estimates of bank erosion contributions within the range of estimates calculated using soil characterization data from other investigations.

CONCLUSIONS

The results from this study show that bank erosion/sloughing is the primary source of sediments in rivers of Blue Earth County. As much as 1.71 million m^3 of soil sloughed from banks of rivers in the county from 2005 to 2009. Tall banks (>3 m high) accounted for 75% of the volume change in river valleys even though they represented

only 33% of the total length and 63% of the total area. Conversion of Lidar measured volume change into mass wasting and then fine sediment loss suggests that as high as 63% and 79% of the measured total suspended loads at the mouth of the Blue Earth River and the Le Sueur River, respectively, may be from river bank erosion/sloughing. Sensitivity analysis with additional data bases showed that the range of losses calculated in this study could be further refined with characterization of fine sediment content, bulk density, soluble P, and total P from additional bank sites in the basin. We conclude that multi-temporal Lidar scans are useful for estimating bank erosion over large scales and for river banks that are not readily accessible for conventional surveying equipment. This method has an advantage over empirical methods that use areas as a surrogate to extrapolate limited measurements to the full length of a river. An added advantage of this technique is in helping to identify banks that are a major source of sediments in a given river system.

REFERNCES

Bartier, P. M. and C. P. Keller. 1996. Multivariate interpolation to incorporate thematic surface data using inverse distance weighting (IDW). Computers & Geosciences. 22:795-799.

Bater, C.W. and N.C. Coops. 2009. Evaluating error associated with Lidar-derived DEM interpolation. Computers & Geosciences. 35:289-300.

Bennett, H.H. and L. A. Hurst.1907. Soil survey of Blue Earth County, Minnesota. U.S. Department of Agriculture, Bureau of Soils, Government Printing Office, Washington, DC. pp 55.

Bowen, Z.H. and R.G. Waltermire. 2002. Evaluation of light detection and ranging (Lidar) for measuring river corridor topography. Journal of the American Water Resources Association. 38:33-41.

Cressie, N. 1990. The origins of kriging. Mathematical Geology. 22:239-252.

Flood, M. 2004. American Society for Photogrammetry and Remote Sensing Guidelines – Vertical Accuracy Reporting for Lidar Data, ASPRS, Bethesda, Maryland, 15 p. http://www.asprs.org/society/committees/Lidar/downloads/vertical_accuracy_reporting_for_Lidar_data.pdf (retrieved February 18, 2011)

Fuller, I.C., A.R.G. Large, M.E. Charlton, G.L. Heritage, and D.J. Milan. 2003. Reach-scale sediment transfers: An evaluation of two morphological budgeting approaches. Earth Surface Processes and Landforms. 28:889-903.

Gee, G.W., and D. Or. (2002) Particle size analysis. p 255-293. In Dane and Topp (Eds.), *Methods of soil analysis: Part 4, Physical methods*, Soil Science Society of America, Madison, WI.

Ginting, D., J.F. Moncrief, and S.C. Gupta. 2000. Runoff, solids, and contaminant losses into surface tile inlets draining lacustrine depressions. J. Environ Qual. 29:551-560.

Guo, Q., W. Li, H. Yu, and O. Alvarez. 2010. Effects of topographic variability and Lidar sampling density on several dem interpolation methods. Photogrammetric Engineering and Remote Sensing. 76:1-12.

Gupta, S.C., and U.B. Singh, 1996. A review of non-point source pollution models: Implications for the Minnesota River Basin. A report submitted to the Minnesota Department of Agriculture. p77.

Gran, K., P. Belmont, S. Day, C. Jennings, A. Johnson, L. Perg, and P. Wilcox. 2009. Geomorphic evolution of the Le Sueur River, Minnesota, USA, and implications for current sediment loading. The Geological Society of America, Special Paper 451.

Grossman, R.B. and T.G. Reinsch. 2002. Bulk density and linear extensibility. p 201-228. In Dane and Topp (Eds.), *Methods of soil analysis: Part 4, Physical methods*, Soil Science Society of America, Madison, WI.

Hodgson, M.E. and P. Bresnahan. 2004. Accuracy of airborne Lidar-derived elevation: empirical assessment and error budget. Photogrammetric Engineering and Remote Sensing. 70:331-339.

Kuo, S. 1986. Phosphorus, extraction with water or dilute salt solution. In A. Klute (Ed.), *Methods of soil analysis: Part 1. Physical and mineralogical methods,* Soil Science Society of America, Madison, WI.

Lane, S.N., R.M. Westaway, and D.B. Hicks. 2003. Estimation of erosion and deposition volumes in a large, gravel-bed, braided river using synoptic remote sensing. Earth Surface Processes and Landforms. 28:249-271.

Liu, X. 2008. Airborne Lidar for DEM generation: some critical issues. Progress in Physical Geography. 32:31-49.

Lloyd, C.D. and P.M. Atkinson. 2002. Deriving DSMs from Lidar data with kriging. In. J. Remote Sensing. 23:2519-2524.

Meyer, M. L. and S. M. Schellhaass. 2002. Sources of phosphorus, chlorophyll, and sediment to the Mississippi River upstream of Lake Pepin: 1976-1996. A report for environmental studies of phosphorus. Metropolitan Council Environmental

Services. http://www.metrocouncil.org/environment/Riverslakes/documents/LakePepinPhosphorusSources.pdf (retrieved February 18, 2011)

Minnesota Pollution Control Agency (MPCA). 1994. Minnesota River Assessment Project report. Vol. II Physical and Chemical assessment, and Vol. III. Biological and Toxicological Assessment. Report to the legislative Commission on Minnesota Resources. January 1994.

Mitasova, H. and J. Hofierka. 1993 Interpolation by regularized spline with tension: II. Application to terrain modeling and surface geometry analysis. Mathematical Geology 25:657-669.

Newcombe, C.P. and J.O.T. Jensen. 1996. Channel suspended sediment and fisheries: a synthesis for quantitative assessment of risk and impact. North American Journal of Fisheries Management. 16:693-727.

Notebaert, B., G. Verstraeten, G. Govers, and J. Poesen. 2009. Qualitative and quantitative applications of Lidar imagery in fluvial geomorphology. Earth Surface Processes and Landforms. 34:217-231.

Payne, G.A. 1994. Sources and transport of sediment, nutrients and oxygen demanding substances in the Minnesota River Basin, 1989-92. USGS Water Resources Investigations Report 93-4232.

Perroy, R.L., B. Bookhagen, G.P. Asner, and O.A. Chadwick. 2010. Comparison of gully erosion estimates using airborne and ground-based Lidar on Santa Cruz Island, Californian. Geomorphology. 118:288-300.

Sekely, A.C., D.J. Mulla and D.W. Bauer. 2002. Streambank slumping and its contribution to the phosphorus and suspended sediment load of the Blue Earth River, Minnesota. Journal of Soil and Water Conservation. 57:243-250.

Sibson, R. 1981. A brief description of natural neighbor interpolation. Interpolating Multivariate Data. New York, John Wiley & Sons. pp. 21-36.

Thoma, D.P., S.C. Gupta, J.S. Strock, and J.F. Moncrief. 2005a. Tillage and nutrient source effects on water quality and corn yield from a flat landscape. Journal of Environmental Quality 34:1102-1111.

Thoma, D. P., S. C. Gupta, M. E. Bauer, and C. E. Kirchoff. 2005b. Airborne laser scanning for riverbank erosion assessment. Remote Sensing Environ. 95:943-501.

Wheaton, J.M., J. Brasington, S.E. Darby, and D.A. Sear. 2010. Accounting for uncertainty in DEMs from repeat topographic surveys: improved sediment budgets. Earth Surface Processes and Landforms. 35:136-156.

Wilcox, P. 2009. Identifying sediment sources in the Minnesota River Basin: Minnesota River Sediment Colloquium. Minnesota Pollution Control Agency. http://www.lakepepinlegacyalliance.org/SedSynth_FinalDraft-formatted.pdf (retrieved February 18, 2011)

Wright Jr., H.E. 1972a. Quaternary history of Minnesota. p 515-547. *In* Sims and Morey (eds.) *Geology of Minnesota: A Centennial Volume*. Minnesota Geological Survey, Univ. of Minnesota, St. Paul, MN.

Wright Jr., H.E. 1972b. Physiography of Minnesota. p 561-578. *In* Sims and Morey (eds.) *Geology of Minnesota: A Centennial Volume*. Minnesota Geological Survey, Univ. of Minnesota, St. Paul, MN.

CHAPTER 3: ASSESSMENT OF RIVER BANK EROSION IN SOUTHERN MINNESTOA RIVERS POST EUROPEAN SETTLEMENT

SUMMARY

River bank erosion is one of the major sources of sediment for many rivers around the World. With the current emphasis on developing Total Maximum Daily Loads (TMDL) for impaired waters in the United States, there is heightened interest in quantifying the background sediment levels in rivers. Changes in river bank erosion were assessed using a combination of 1855 Public Land Survey System PLATs, aerial photographs from 1938-2009, and light detection and ranging (Lidar) data from 2005 and 2009 for sediment impaired rivers in Southern Minnesota. Results showed that bank erosion was episodic, making comparisons of erosion rates from dissimilar time intervals unreliable. For comparable time intervals from 1855-1938 and 1938-2009 or 1938-1971 and 1971-2009, average river bank retreat rates were statistically similar suggesting that bank retreat rates have remained stable since European settlement. However, a greater number of banks slumped from 1971-2009 relative to 1938-1971. Contrary to the assumptions made in the literature, bank erosion measurements from Lidar data showed a poor relationship (r^2=0.01 to 0.36) with river bank physical features (face area, inclined surface area, length, slope, height, and aspect) indicating that extrapolating a limited number of bank erosion observations to the whole length of a river should be avoided. This lack of relationship was expected considering most of these bank physical features do not fully represent bank erosion processes such as seepage, freeze-thaw, river migration, under cutting and sapping. In assessing conservation measures or developing TMDLs to manage sediments in rivers, we conclude that (1) background levels of

suspended sediments from river bank erosion should be established using comparable time intervals, and (2) up scaling of discrete volume loss measurements to an entire reach should be avoided.

INTRODUCTION

Suspended sediments frequently contribute to surface water impairments in many parts of the world. High concentrations of suspended sediment in rivers and lakes have deleterious impacts on recreational and navigational activities, as well as on fisheries, which in some cases can be lethal to aquatic species (Newcombe and Jensen, 1996). In many areas, river bank erosion is a major source of suspended sediment loads (Thoma et al., 2005; Evans et al., 2006; Wilson et al., 2007; Belmont et al., 2011; Kessler et al., 2012; Day et al., 2013b). In the U.S., once a river is identified as impaired by excess sediment the Clean Water Act requires that the maximum amount of sediment it can receive and still meet local water quality standards be calculated. This maximum amount of sediment is referred to as the Total Maximum Daily Load (TMDL). As TMDLs are being developed for rivers impaired by excess sediment, there is often a need to establish natural background contributions of suspended sediments from river bank erosion. This means determining the degree to which natural processes vis-à-vis anthropogenic activities affect river bank contributions to suspended sediment loads.

In Minnesota, river banks have been identified as a major source of sediments in the Minnesota River and its tributaries (Thoma et al., 2005; Gran et al., 2009; Belmont et al., 2011; Kessler et al., 2012); all of which are classified as sediment impaired. Meyer and Schellhass (2002) estimated that as much as 623,000 Mg yr^{-1} of total suspended solids (TSS) were transported by the Minnesota River at Fort Snelling in the

Minneapolis/St. Paul area. Kelley and Nater (2000) estimated that Minnesota River sediments comprised at least 75% of the sediment in Lake Pepin, a floodplain lake on the Mississippi River about 80 km southeast of St. Paul, MN. Payne (1994) reported that as much as 55% of the sediment in the Minnesota River at Mankato originated from the Greater Blue Earth River Basin (GBERB; Figure 8), a relatively flat basin (54% of the land with < 2% slope and 93% of the land with < 6% slope) with deeply incised streams that are lined with steep and unstable banks that reach heights over 50 m (Figure 9). Using Lidar, Kessler *et al*. (2012) showed that river banks sloughing in Blue Earth County account for 48% to 79% of the TSS measured at the mouth of the Blue Earth and the Le Sueur Rivers. However, a limitation of Kessler et al. (2012) and other bank erosion studies (Sekely et al., 2002; Thoma et al., 2005; Wilcock, 2009; Kronvang et al., 2011) is that the bank erosion rates are only for one period and do not provide information on how erosion may have varied over time. With increased rates of sediment accumulation in flood plains and lakes, such as in Lake Pepin (Engstrom et al., 2009), there is a need to identify how river bank erosion has varied over time.

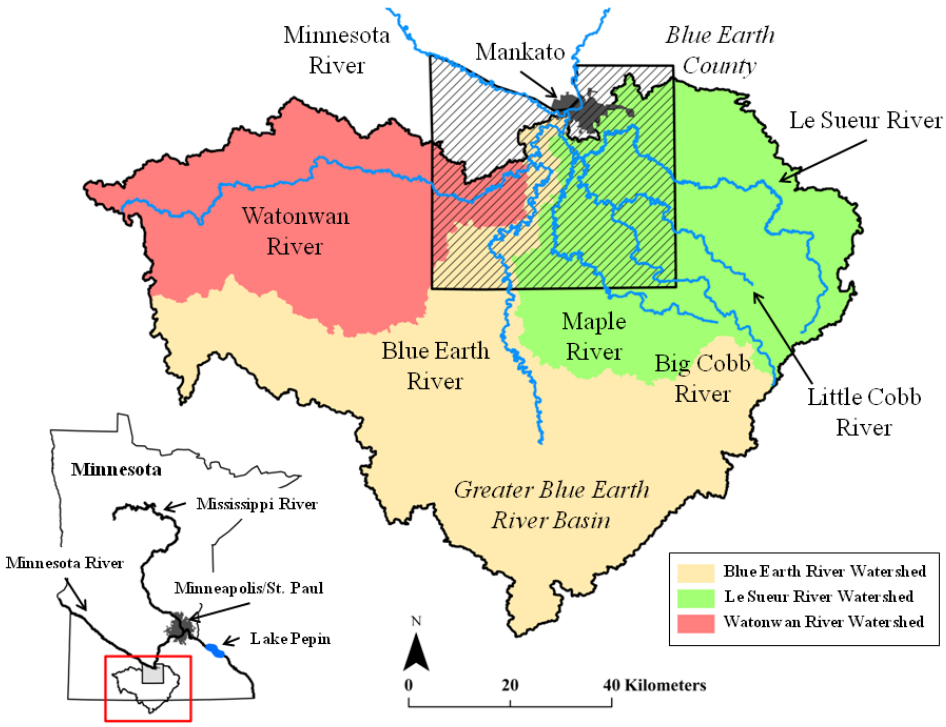

Figure 8. Map of the Greater Blue Earth River Basin and surrounding areas.

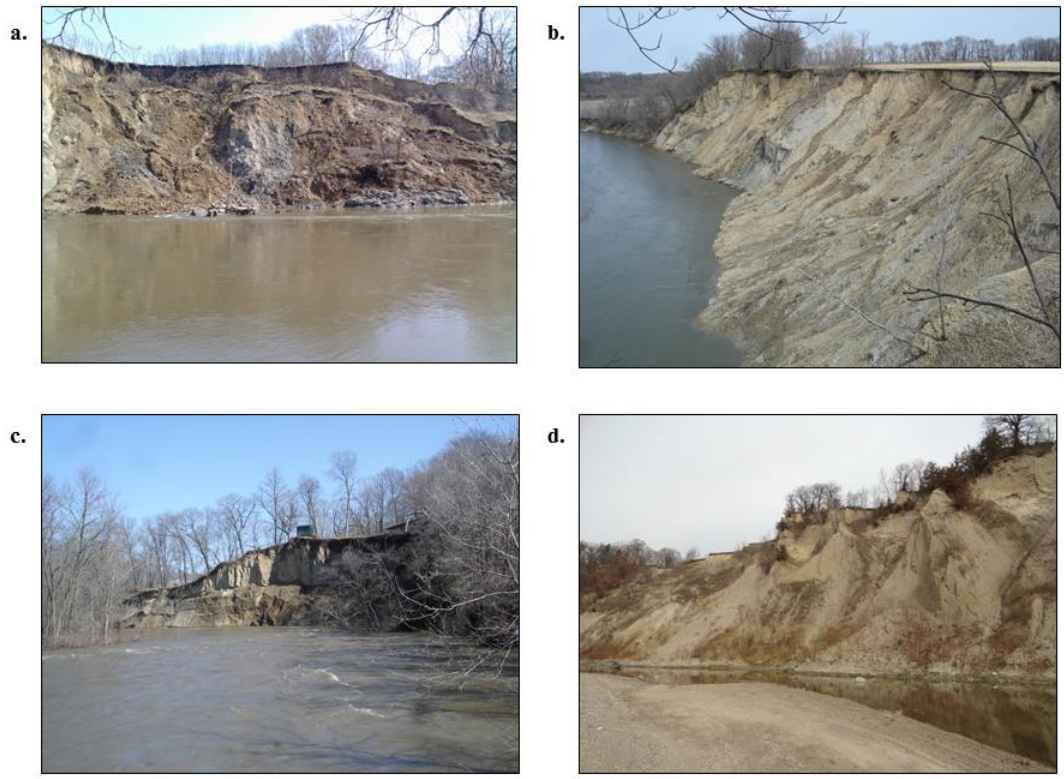

Figure 9. Photographs of tall, unstable, and actively sloughing banks along the Blue Earth and Le Sueur Rivers in Blue Earth County, Minnesota. (a) 23-m-tall bank on the Blue Earth River which has detached from the upper bank. (b) 30-m-tall bank on the Blue Earth River showing wet spots as well as soil deposits at the toe of the bank. (c) 18-m-tall bank on the Le Sueur River where a portion of a residential property is about to fall into the river. (d) 60-m-tall bank on the Le Sueur River which is eroding both near the river as well as at the top 30 m away from the river.

Depending upon the time scale, sediment inputs from river bank erosion can be episodic. For example, Black et al. (2010) described average migration rates ranging from 0.7 to 4.7 m yr^{-1} over a 100 year period across three rivers in the North Eastern

United States. The radionuclide dating technique in that study revealed both nearly constant and episodic migration rates at decadal time scales. Using erosion pins, Zaimes et al. (2004) identified that 60 to 80% of bank erosion along a creek in central Iowa occurred over a period of a few days during a two year study. In spite of the observations that bank erosion processes can be largely episodic, recent research has drawn comparisons between river bank erosion measurements made at dissimilar time intervals (Gran et al., 2009; Belmont et al., 2011; De Rose and Basher, 2011). If bank erosion exhibits episodic characteristics then comparisons made between measurements taken at short (i.e. decadal) and long (> 100 years) time intervals will lead to erroneous interpretations and conclusions.

Worldwide, several different techniques have been used to quantify river bank erosion. In addition to airborne Lidar, erosion pins, terrestrial Lidar scans (TLS), traditional survey, fallout radionuclides, and numerical models have all been used to measure river bank erosion. Erosion pins are commonly used and provide accurate measurements at the locations they are installed (Couper et al., 2002). However, the bank must be accessible in order to insert the pins, inserting the pin can cause localized erosion, and erosion in between pin measurements must be interpolated. Recently, terrestrial Lidar has been shown to provide high resolution measurements of bank erosion (Day et al., 2013a). However, there is a limitation on the number of banks that can be surveyed requiring extrapolation of measurements from a few river banks to the entire length of a river channel. Currently, most extrapolation techniques are statistical and are not based on any bank erosion mechanisms. Another technique for assessing bank erosion includes numerical models. Numerical models are generally based on physical

principles and require substantial inputs for simulating bank erosion from even one bank (Rinaldi and Casagli, 1999; Simon et al., 2000; Pollen and Simon, 2005; Cancienne et al., 2008, Lindow et al., 2009), not to mention a whole reach; which may extend several hundred kilometers. For example, the Bank Stability and Toe Erosion Model (BSTEM) requires several measurements on physical and geometric properties of the bank including effective cohesion, length of failure planes, bank angle, bank failure plane angle, matric suction or soil pore-water pressure, and pore-air pressure (Cancienne et al., 2008).

Aerial photographs also provide a means to assess past river bank erosion rates (Leys and Werritty, 1999; Shields et al., 2000; Hughes et al., 2006; Hooke, 2007; Nicoll and Hickin, 2010; De Rose and Basher, 2011). The advantage of aerial photography is a long record as well as coverage of a wide area. Using a combination of Lidar and historical aerial photographs, De Rose and Basher (2011) showed that meander migration rates of two reaches of the Waipaoa River in New Zealand were comparable to rates over the past 18 ka BP. Using historical aerial photographs from 23 sites on 21 rivers in Alberta and British Columbia, Canada, Nicoll and Hicken (2010) found that meander migration rates varied from 0.01 to 5.8 m yr^{-1}. Although aerial photographs have been used in river bank erosion analysis, there are limited studies that have validated the accuracy of these techniques over larger areas. Recently, Day et al. (2013b) reported a high degree of uncertainty in estimated bank erosion rates based on aerial photograph analysis. These uncertainties included potential errors in delineations of bank crests as well as georectification of aerial photographs. However, Day et al. (2013b) performed no direct accuracy assessment against more precise bank erosion measurements, such as

terrestrial or airborne Lidar. The increasing availability of airborne Lidar data over the whole length of rivers provides a new opportunity to assess the accuracy of bank erosion measurements made with aerial photographs.

Because of the difficulty and the expense of characterizing river bank erosion, some researchers have recently used simpler empirical approaches to estimate bank erosion over the whole length of a river. One such approach is to extrapolate or upscale discrete bank sloughing/erosion measurements based on surrogate variables such as bank inclined surface area, length, or aspect (Sekely et al., 2002; Wilcock, 2009; Belmont et al., 2011; Kronvang et al., 2011; Willet et al., 2012; Day et al., 2013b). However, identifying surrogate variables that uniquely represent most if not all bank sloughing mechanisms is difficult. While this technique has been used, research has yet to validate if extrapolating discrete volume loss measurements on a few banks based on surrogate variables provides accurate erosion estimates for the entire length of a river channel.

The objectives of this study were to assess (1) the accuracy of using aerial photographs to estimate bank erosion, (2) how river bank erosion (bank retreat or volume loss rates) has varied over time for rivers in Blue Earth County, Minnesota, and (3) if extrapolation of discrete river bank volume loss measurements using bank physical features such as face area, inclined surface area, length, height, slope, or aspect is suitable for quantifying net bank erosion for an entire river channel.

STUDY AREA

The waterways investigated in this study are the Blue Earth, Le Sueur, Watonwan, Maple, Big Cobb, and Little Cobb Rivers in Blue Earth County, Minnesota

(Figure 8). The Watonwan River is a tributary of the Blue Earth River whereas the Maple, Big Cobb, and Little Cobb rivers are tributaries of the Le Sueur River. The Le Sueur River joins the Blue Earth River before it empties into the Minnesota River at Mankato. In total, the rivers of the GBERB drain about 9,200 km^2, with the Blue Earth River Watershed draining 4,050 km^2, the Watonwan River Watershed draining 2,260 km^2, and the Le Sueur River Watershed draining 2,880 km^2. The gradient of the Blue Earth, Watonwan, and Le Sueur Rivers range from 0.3 to 1.3 m km^{-1}, 0.4 to 1.6 m km^{-1}, and 0.3 to 2.7 m km^{-1}, respectively (Bohling, 2012). The Blue Earth River is approximately 170 km long and has an average annual discharge of 30 m^3 s^{-1}. Comparatively, the Le Sueur River is approximately 180 km long and has an average annual discharge of 15 m^3 s^{-1}, and the Watonwan River is approximately 180 km long and has an average annual discharge of 11 m^3 s^{-1}. These rivers generally flow north and thus occasionally get blocked by ice jams in early spring. This results in flooding of river valleys and also large scale movement of the river path.

All of the rivers in Blue Earth County are deeply incised with steep and actively eroding banks due to the continuous down cutting that resulted after the River Warren drained the melt waters of Lake Agassiz some 13,400 BP and stranded these tributaries from its master stream, the Minnesota River (Clayton and Moran, 1982; Matsch, 1983; Gran et al., 2009). The area has been well described by Gran et al. (2009), and consists predominantly of fine-textured tills deposited by the Des Moines Lobe, with some areas having tills as thick as 80 m. As the glacier retreated, melt waters deposited lacustrine, deltaic, and outwash materials over much of the county (USDA, 1978).

A majority of the soils in the county are nearly level, poorly drained and derived from lacustrine deposits. The dominant sub orders are Haplaquolls, Agriaquolls, Hapludolls, Argiudolls and Hapludalfs. The dominant soil series are Marna silty clay loam, Minnetonka silty clay loam, Madelia silty clay loam, Cordova clay loam, and Darfur loam (USDA, 1978). Close to the river, soils are somewhat steep and the dominant soil series is Storden loam. The upland surface soils are generally high in organic matter content (4-6%) derived from prairie grasses native to the region, while the river bottoms commonly have thin deposits of alluvium (< 2 m). The majority of the GBERB is under row crop agriculture and the bulk of the land is tile drained.

MATERIAL AND METHODS

Databases

The databases included 1855 Public Land Survey System (PLSS) PLATs, eight different sets of aerial photographs taken in 1938, 1950, 1958, 1964, 1971, 2003, 2005, and 2009, and Lidar data sets from 2005 and 2009. All data were projected to a common coordinate system using North American Datum 1983, and High Accuracy Reference Network (HARN) adjusted for Blue Earth County, Minnesota. Each data set is described below.

PLATs and Aerial Photographs: The 1855 PLSS PLATs were obtained from the Minnesota Geospatial Information Office in digital format and co-registered to section lines using a minimum of seven user selected ground control points while maintaining a RMSE of less than 1 m, with an emphasis on identifying points near the rivers. Here the

RMSE is specific to the georecification processes and does not represent actual ground position error between the PLAT and historic landscape. The PLSS PLATs establish the original land boundaries for much of the United States and are the only formal records of land use before European immigrant settlement in Blue Earth County, Minnesota. These records are still used to establish original property boundaries, and have been used to construct pre-settlement landscapes (Galtowitsch, 1990). Galtowitsch (1990) and others (Rod Squire, University of Minnesota, September 21, 2012; Personal Communication) have also noted that the width and course of rivers at surveyed section lines are well recorded. Thus, PLSS PLATs provide a rare opportunity to gain insights into river geomorphology during initial European settlement for much of the central and western United States.

Georeferenced aerial photographs for 1938 were provided by Blue Earth County, Minnesota. The county had scanned aerial photographs at 600 dpi and georeferenced them with a minimum of nine ground control points (GCP), with an emphasis on road intersections. A maximum 4.7 m RMSE was maintained, and third (> 9 GCP) order polynomial transformations were used with the cubic convolution interpolation technique. Aerial photographs for the years 1950, 1958, 1964, and 1971 were acquired at a scale of 1:20,000 from the University of Minnesota, John R. Borchert Map Library. For each year, multiple photographs were required to cover the entire length of the river channels within Blue Earth County. The 1950, 1958, 1964, and 1971 aerial photographs were scanned with an Epson Perfection V500 photo scanner at 12,800 dpi. The aerial photographs were then co-registered to the 2009 aerial image using a minimum of seven user selected ground control points while maintaining a root mean square error of less

than 1 m, with an emphasis on identifying points near the river at road intersections. A second order polynomial transformation was used to rectify both PLSS PLATs data and historical aerial photographs with bilinear interpolation re-sampling to 0.3 m.

An additional assessment of georectification error was conducted following techniques similar to those developed by Hughes et al. (2006). A minimum of seven additional ground control points (GCP) were selected for every historic aerial photograph that was georeferenced. These GCPs were unique from the original points and were focused on buildings, whereas the initial georeferncing focused on road intersections. The total root mean square error (RMSE) for each year of historic imagery was then calculated as

$$RMSE_t = \sqrt{\frac{\sum_{i=1}^{n} a^2 + b^2}{n}} \quad (1)$$

where a and b are the resultant vectors from residuals between the x and y coordinates of the newly selected GCPs, and n is the number of GCPs.

The other photographs included 2003 NAIP (National Agriculture Imagery Program) image, 2005 aerial photographs collected by Optimal Geomatics, and 2009 aerial photographs collected by Pictometry International Corp. The summer time collection (leaf-on stage) of the 2003 NAIP image, acquired at a 1 m ground distance, significantly reduced the number of bank erosion observations in this imagery. As such, the 2003 NAIP image was only used in the analysis of average volume loss and retreat as a function of period length. The 2005 Optimal Geomatic aerial photographs were collected on April 13-14, 2005 (leaf-off stage), using a Leica RC-30 precision aerial camera at a 15 cm ground scale distance. The 2009 Pictometry aerial photographs were

collected from April 12 to May 2, 2009 (leaf-off stage), using a proprietary georectification technique and camera system. The camera, called Pictometry Penta View, was flown with a 65 mm focal length sensor at a 30 cm ground scale distance.

Lidar Data: The details on the Lidar data and its processing are described in the previous chapter and Kessler et al. (2012). Briefly, the 2009 Lidar data set was collected by Aero-Metric, Inc., Sheboygan, WI using an Optech ALTM Gemini system flown at 1200 m above ground with a laser pulse rate of 45 kHz during leaf-off conditions with a reported horizontal accuracy of 1 m. The data were collected on April 28, 2009, and May 2-3, 2009, and processed by the vendor using proprietary software. The vendor delivered bare earth points, hydrologic breaklines, and 0.6 m contours, which were used to create a 0.76 m bare earth digital elevation model (DEM). The accuracy of the bare earth DEM tested with 106 points from a variety of land covers (26 hard surfaces; 20 short grasses; 20 tall grasses/weeds; 20 brushes; and 20 woods) using static and real time kinematic (RTK) GPS showed a fundamental vertical accuracy of ±0.17 m (Kessler et al., 2012). Based on the guidelines of Flood (2004), fundamental vertical accuracy was calculated as root mean square error ($RMSE_{(z)}$) x 1.96 and refers to the confidence interval at 95% significance.

The 2005 Lidar data set was collected by Optimal Geomatic, Inc., Huntsville, AL using an Optech ALTM 3100 Lidar system flown at 1836 m above ground using a laser pulse rate of 70 kHz. The data was collected during two leaf-off periods, April 13-14, 2005, and April 23-24, 2005, with a total of four flights. The data had a foot print of 0.45 m with an average of 1 data point per m^2 and a reported horizontal accuracy of 1 m. The

vendor processed the raw Lidar data using proprietary software to produce bare earth points, hydrologic breaklines, and 0.6 m contours, which were used to generate a 0.76 m bare earth DEM. The accuracy of the bare earth DEM was checked using 351 points collected with RTK GPS over a variety of land covers including 204 open terrain, 41 tall weeds and crops, 13 brush lands and low tree, and 93 urban areas. The fundamental vertical accuracy of this data set was ±0.24 m (Kessler et al., 2012).

River Bank Erosion Measurements

River bank erosion from aerial photographs was calculated assuming a parallelepiped loss of bank during sloughing (Figure 10). It was assumed that the failure plane angle of river banks remained the same during the study period. The crest of river banks and their length along the river were manually identified in each year of the aerial photographs. The outward shift in the crest of a river bank between two aerial photograph periods represented the top area of river bank lost (Figure 10). Since this study is focused on average rates of volume loss and retreat, and does not attempt to quantify net volume loss from an entire river channel, point bar accretion adjacent to eroding banks was omitted. In some instances, vegetation at the crest of the river bank precluded locating its exact position. Therefore, this study only included river banks where the crest of the river bank was easily identifiable in the aerial photographs and a shift in the position of the stream bank was clearly evident. Because of these restrictions, the number of river banks analyzed varied between each survey period.

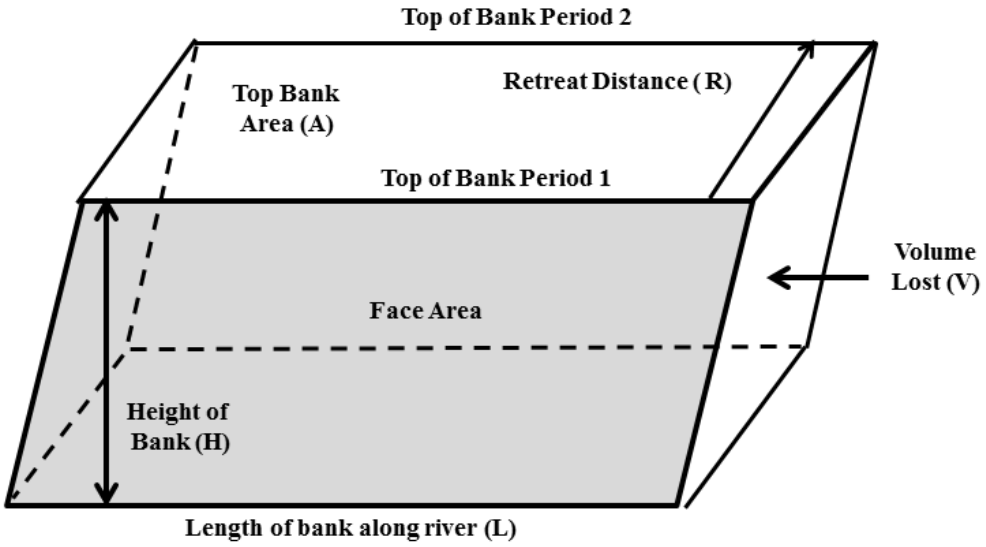

Figure 10. Schematic illustration of volume loss and bank retreat calculations using aerial photographs. The method assumes a parallelepiped loss of soil between the two periods.

For the 1855 PLSS PLATs, data on river positions were only used for locations where rivers crossed section lines. Where these intersections occurred a point was placed on the position of the river bank in the 1855 PLATs. This process was then repeated on the same bank in the 1938 and 2009 aerial photographs. For each identified bank in 1855 PLSS PLATs and in aerial photographs, the height and average slope were calculated from the 2009 Lidar derived DEM. Since long-term historic measurements of height and slope are unavailable, it was assumed that the height and slope of the bank remained the same from 1855-2009.

Bank retreat was calculated using the relationship $R = A / L$, where R equals the retreat distance, A equals the area lost on top of the bank, and L equals the length of the bank along the river (Figure 10). Volume loss (V) was calculated as $V = A * H$, where H equals the average height of the bank, calculated from the Lidar data. Average volume

loss and retreat rate were calculated for each river from the bank positions identified in the aerial photographs. For several consecutive time periods (1938-1950; 1950-1958; 1958-1964; 1964-1971; 1971-1905; 2005-2009), ANOVA was run to determine if significant differences in volume loss and retreat rates existed between periods. In addition, a paired t-test was used to compare retreat rates between 1855-1938 *vs.*1938-2009 and 1938-1971 *vs.* 1971-2009.

River bank heights in the GBERB range from less than 1 m to over 60 m. To differentiate between taller and smaller banks, river banks used in the accuracy assessment and analysis of consecutive periods (described above in section 3.2) were split between banks greater than 5 m (hereafter referred to as tall banks) and those less than or equal to 5 m (hereafter referred to as small banks). Based on 2005 Lidar data, banks greater than 5 m in height occupy 26% of the length of river channels in Blue Earth County.

Accuracy of Aerial Photograph Measurements

The accuracy of bank erosion measurements from aerial photographs was assessed by comparing erosion estimates derived from aerial photographs against airborne Lidar data for the period 2005 to 2009. Studies have shown that multi temporal airborne Lidar data provides accurate estimates of river bank erosion (Thoma et al., 2005; Kessler et al., 2012). The procedure involved identifying river banks in 2005-2009 aerial photographs where volume loss and retreat had occurred and then estimating river bank erosion using the procedures as described above. A total of 124 river banks were analyzed for volume loss and retreat rate from 2005 and 2009 aerial photographs, and the

estimates were then compared against 2005-2009 Lidar measurements using regression analysis. A t-test was used to evaluate if the slope and intercept of the regression relationships between aerial photograph estimates and Lidar measurements of volume loss and retreat differed from one and zero, respectively. In addition, Bland-Altman plots (Altman and Bland, 1983) were developed to identify differences in volume loss and retreat rate between measurements made with aerial photographs relative to Lidar estimates.

Volume Loss as a Function of Bank Physical Features

The 2005 and 2009 Lidar data were also used to test the assumptions of using surrogate variables to predict volume loss over the length of a river channel. This portion of the analyses relied exclusively on the two years of airborne Lidar data to calculate volume loss from 2005 to 2009. The details on volume loss calculations using this data are described in Kessler et al. (2012). Briefly, these calculations involved estimating volume loss based on the difference between the 2009 and 2005 bare earth DEMs. River bank volume loss measurements were then regressed against face area, inclined surface area, length, height, slope, and aspect as has been done in the literature (Sekely et al., 2002; Wilcock, 2009; Belmont et al., 2011; Kronvang et al., 2011; Day et al., 2013b). The face area and inclined surface area used in the above calculations are different than the top area mentioned in section 3.2. Face area refers to the 2 dimensional exposed surface of the bank facing the river (Figure 10), whereas inclined surface area refers to the 3 dimensional exposed surfaces (including small undulations) of the bank facing the river. Comparatively, top area refers to the area lost on the top surface of a river bank

from an outward shift in the bank. The database for this analysis included 339 river banks along the Blue Earth, Le Sueur, Watonwan, Little Cobb, Big Cobb, and Maple Rivers. Since the physical characteristics of river banks may have changed over time, two sets of regression analysis were done using physical features from both 2005 and 2009 Lidar data.

RESULTS AND DISCUSSION

Accuracy of Aerial Photograph Measurements

The RMSE for georectification of all historic images (1938-1971) varied from 4.14 m (1964 images) to 5.12 m (1938 images), with an average RMSE of 4.62 m over all images (Table 8). While these errors limit the ability to detect small changes in the position of river banks, they are similar to those reported by others (Hughes et al., 2006; Day et al., 2013b). The overall accuracy of bank erosion estimates from aerial photographs was also evaluated against measurements from the 2005 and 2009 airborne Lidar (Table 9). With the exception of bank retreat on small river banks, there is a poor agreement between the estimates from aerial photographs and the measurements from airborne Lidar for both volume loss and bank retreat. Blan-Altman plots for volume loss show that this lack of a 1 to 1 relationship was consistently driven by an overestimation by the aerial photograph technique (Figure 11a). The aerial photographs performed better in estimating retreat distance (Figure 11b) especially for small banks, where the slope and intercept of the regression between the aerial photograph retreat estimates and Lidar retreat measurements were not significantly different from 1 ($P = 0.21$) and 0 ($P = 0.68$), respectively. Average difference in bank retreat from the photographs relative to

airborne Lidar was 0.37 m for small banks and 1.62 m for tall banks. The corresponding standard deviation in the retreat distances were 2.24 m and 1.87 m for the small and tall banks, indicating a substantial uncertainty in the absolute measurement of retreat from the aerial photographs for any individual bank.

Table 8. Total root mean square error ($RMSE_t$) for georectified historical images.

Year	$\boldsymbol{RMSE_t}$
1938	5.12
1950	4.82
1958	4.59
1964	4.14
1971	4.47
mean	4.62

Table 9. Regressional analysis ($y = \alpha + \beta x$) between airphoto (x) estimates of bank erosion vs. Lidar (y) measurements. The regression intercepts (α) and slopes (β) for volume loss and retreat distance were tested with t-test to see if they were significantly different from zero and one, respectively.

Measurement		Mean difference	n	r^2	Coefficients		t-stat	p-value
Volume	Tall	5,488	67	0.08	α	82	0.96	0.34
Loss, m^3					β	0.02	-108.6	<0.01
	Short	2,433	57	0.77	α	-287	-2.39	0.02
					β	0.36	-24.52	<0.01
Retreat, m	Tall	1.62	67	0.09	α	0.90	1.66	0.10
					β	0.34	-4.97	<0.01
	Short	0.37	57	0.62	α	0.23	0.41	0.68
					β	0.88	-1.28	0.21

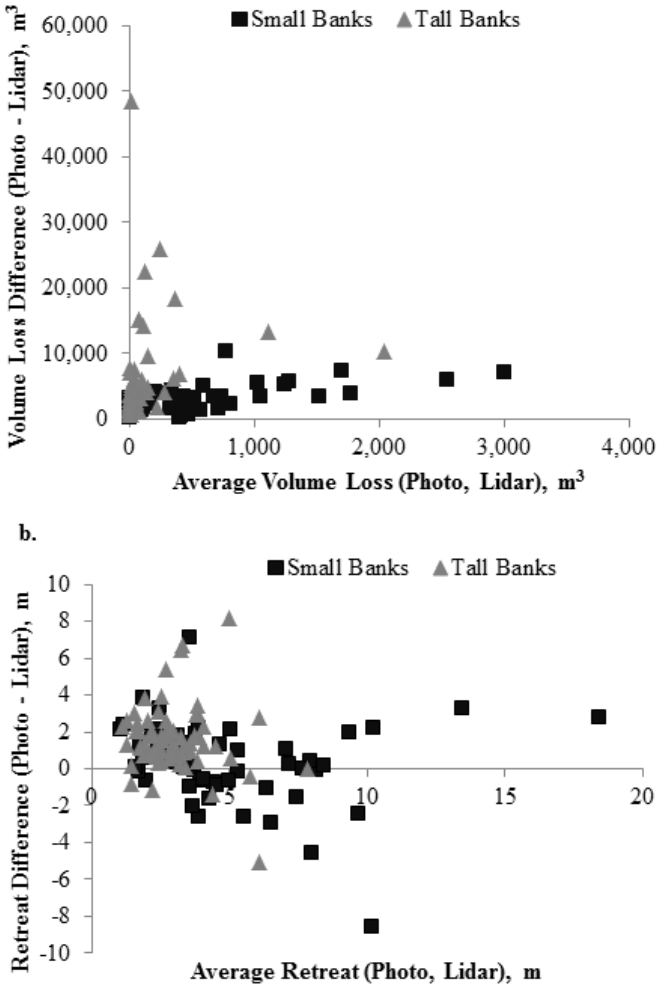

Figure 11. Bland-Altman plots of volume loss (a) and retreat (b). In most instances, aerial photographs overestimated volume loss and retreat distance relative to airborne Lidar estimates from 2005–2009.

The poor estimates of volume loss from the aerial photographs are likely due to greater variability in soil erosion from the large exposed bank surface, especially in tall river banks. It is likely that there were times when only the crest of tall river banks slumped rather than the entire bank, as indicated by the large difference in average volume loss per unit area between the aerial photograph and airborne Lidar estimates.

For example, the aerial photograph analysis over predicted volume loss for tall river banks by 11.3 $m^3 m^{-2}$ relative to the Lidar measurements. Comparatively, the aerial photographs over predicted volume loss from small river banks by only 2.9 $m^3 m^{-2}$. Large variability in tall river bank retreat will likely decrease at longer time intervals because long term erosion over the entire surface will push the river bank further back in alignment with its crest. This suggests that volume loss and retreat rate from aerial photographs may still be valuable if used over longer time scales. Since the over prediction was systematic, the remainder of this paper focuses on the trends in these measurements rather than on their absolute values.

Temporal Variation in Bank Erosion Rates

The average river bank retreat rate for the period 1938 to 2009 was 0.57 m yr^{-1} (n = 107) with a range of 0.06 to 2.94 m yr^{-1}. For a similar period (1938-2005), Day et al. (2013b) reported an average river bank (>3 m) retreat rate of 0.14 m yr^{-1} (n = 183) and a range of 0.00 to 0.96 m yr^{-1}. Much of the difference in average retreat rate between this study and Day et al. (2013b) is due to the differences in bank types characterized, as well as the techniques used to measure retreat rate from aerial photographs. Day et al. (2013b) measured bank retreat rates from banks taller than 3 m, whereas this study included all size banks (taller or shorter than 3 m). In addition, Day et al. (2013b) measured retreat rates for a fixed length along the entire base of a bank whether or not any bank sloughing occurred. They also recorded a number of banks with retreat rates of zero. In this study, the length of the bank only corresponded to the section of the bank that retreated, thus the length of bank was much smaller. The underlying difference between Day et al. (2013b)

and our study is mainly with respect to the objectives. Day et al. (2013) were interested in estimating net volume loss for all river banks > 3 m in the Le Sueur River basin from retreat rates in aerial photographs. The present study focused on the trends over time rather than absolute estimates of net volume loss for the entire channel length of all rivers.

For consecutive periods, an ANOVA test on natural log transformed measurements for consecutive time periods indicated that retreat rate from small banks, and volume loss and retreat rate for tall banks for the period 1971-2005 were significantly lower than other time spans (Table 10). Average volume loss rate was the highest for the period 1958-1964 for both small and tall banks. Comparatively, the average bank retreat rate for the small bank was highest in the period 1958-1964 and for tall banks in the period 1964-1971. Except for small banks in the period 1971-2005, the number of bank retreat observations consistently increased over time. This suggests that even though most rates were similar, sediment production may have increased due to a greater number of banks failing. The lower volume loss and retreat rates for the 1971-2005 (Table 10) appear to be due to differences in time intervals (34 years for 1971-2005 period compared to 4 to 12 years for other periods) over which the averages were calculated. There was also a large coefficient of variation (as high as 142% for small banks and 128% for tall banks) in volume loss and bank retreat rates for various periods in Table 10. The variable bank erosion rates over different periods suggest that large bank failures in the GBERB may be episodic depending upon the dominating mechanism at any given time. Many processes influence bank failure including floods, seepage and pore water pressure build up, undercutting, piping, and sapping (Hooke, 1979; Hagerty, 1991a, b; Lawler, 1995;

Wilson et al., 2007; Fox and Wilson, 2010; Zinger et al., 2011). The predominance of any of these processes in a given period will have a large influence on the rates of river bank failure. The lower apparent volume loss or retreat rate in the larger time interval (1971-2005) demonstrates the potential limitations of comparing annual erosion rates between observations taken from dissimilar time intervals.

Table 10. Temporal variation in short (≤ 5 m) and tall (> 5 m) bank volume loss and retreat rates estimated from consecutive aerial photographs taken along rivers in Blue Earth County, Minnesota.

	Small bank			Tall Bank		
Years	*n*	Mean volume loss, m^3 yr^{-1}	Mean retreat rate, m yr^{-1}	*n*	Mean volume loss, m^3 yr^{-1}	Mean retreat rate, m yr^{-1}
1938–1950	18	553 a†	1.01 a†	13	1,013 a†	0.76 c§
1950–1958	26	652 a	1.29 a	16	1,198 a	0.90 c
1958–1964	31	852 a	1.46 a	19	1,554 a	1.23 c
1964–1971	42	606 a	1.30 a	24	1,731 a	1.33 c
1971–2005	21	394 a	0.69 b	28	496 b	0.37 d
2005–2009	57	512 a	1.10 a	67	862 a	0.89 c

† Different letters within columns indicate a significant difference between natural log transformed erosion estimates at $\alpha = 0.05$ according to a Scheffe test using SPSS version 19.0.

§ Different letters within column indicate a significant difference between natural log transformed erosion estimates at $\alpha = 0.05$ according to a Tamhane test due to unequal variance using SPSS version 9.0

The effects of variable periods on volume loss and volume loss rate were further tested using 823 independent bank erosion measurements that covered a range of time intervals (2 to 71 years) between aerial photographs (Figure 12). These time intervals refer to combinations of time periods between aerial photographs acquired during 8 different years (1938, 1950, 1958, 1964, 1971, 2003, 2005, and 2009). The technique for calculating volume loss and retreat distance was the same as described above for consecutive periods. The number of volume loss and retreat observations for any given period ranged from 1 to 127. Because of the limited number of observations for some time intervals, Figure 12 only includes time intervals where there were 10 or more observations of banks erosion. As expected, volume loss (Figure 12a) and retreat distance (Figure 12c) increases with an increase in time interval between photograph acquisitions. The larger standard error in volume loss at large intervals (Figure 12a) likely indicates the episodic nature of bank erosion in GBERB. When expressed as annual volume loss (Figure 12b) and annual retreat (Figure 12d), there is a decrease in the rate with an increase in time interval. Also, there is a smaller standard error in these estimates (Figure 12b and Figure 12d) at large intervals because of the division by a longer time interval. A power function fit describes the decrease in volume loss rate as a function of time interval between aerial photograph acquisitions. This fit accounts for 66% of the variability ($P < 0.05$) in annual volume loss rate (Figure 12b), and 83% of the variability ($P<0.05$) in annual retreat rate. This exponential decrease in volume loss (Figure 12b) and retreat (Figure 12d) rate with an increase in observation time again suggests that comparing volume loss or retreat rates for variable time periods between aerial photograph acquisitions is not appropriate in areas where bank erosion is episodic.

Instead comparable time intervals should be selected when comparing present day rates with historic rates with an emphasis on longer time periods where variation will be reduced and likely give a more stable estimate.

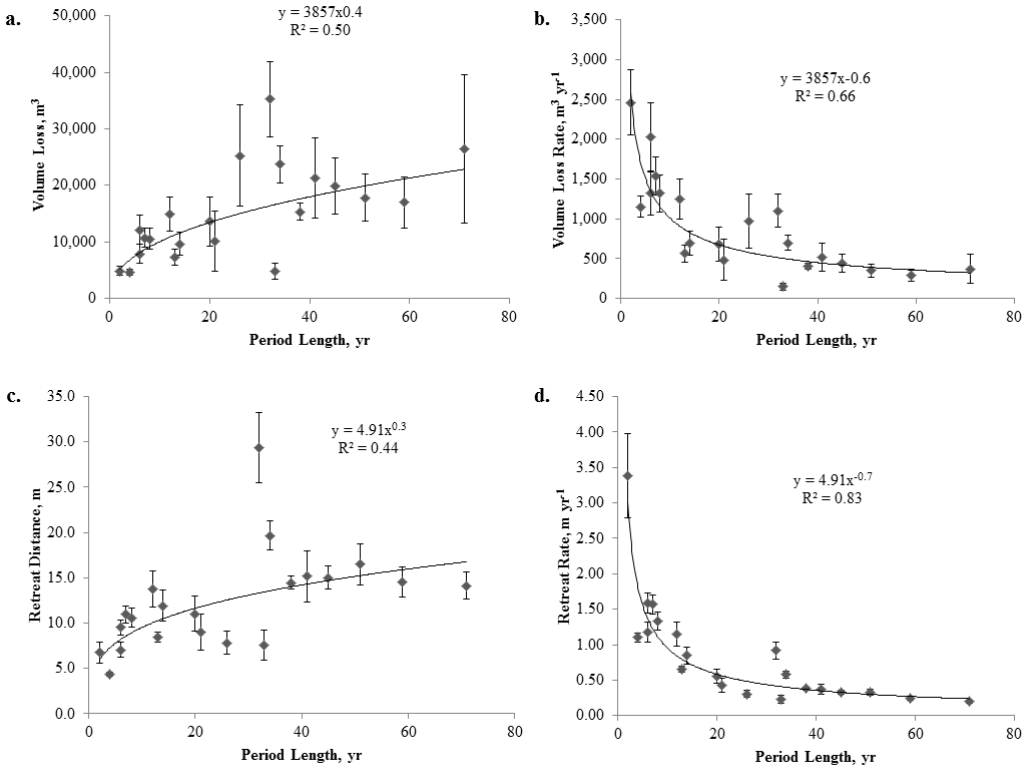

Figure 12. Relationship between volume loss (a), volume loss rate (b), retreat distance (c), and retreat rate (d), *vs*. period length between aerial photographs. The error bars are the standard error of the measurements.

The problems associated with comparisons of annual rates over dissimilar time intervals are well known in studies on rates of sediment accumulation (Sadler, 1981) and have been referred to as a "Sadler effect". Using nearly 25,000 different measurements of sediment accumulation in a variety of environments and time scales, Sadler (1981) found a trend of apparent decrease in the annual rate of sediment accumulation as a function of

increasing period length, similar to the result presented in this study. This would suggest that the "Sadler effect" also applies to rates of bank erosion in the GBERB over dissimilar time periods. The implication of this finding is that natural background rates of suspended sediments in TMDL studies should be established using similar time intervals when bank erosion exhibits episodic characteristics. Furthermore, the emphasis should be on selecting rates over longer time intervals because the variation in measurements decreases with increases in time interval (Figure 12).

Gran et al. (2009) reported a 1.3 to 3.4 times increase in the annual rate of sediment production for the Le Sueur River Basin by comparing measurements from 2000-2006 (6 years of data) to averages for the past 11,500 years. Recently, Belmont *et al.* (2011) compared the efflux of sediment from the Le Sueur River watershed averaged over the Holocene period of 13,400 years (55,000 Mg yr^{-1}) *vs.* averaged over 10 years from 2000-2010 (225,000 Mg yr^{-1}), concluding that the modern day sediment efflux had increased by a factor of four relative to the historic average. De Rose and Basher (2011) also drew similar comparisons between largely dissimilar time steps for the Waipaoa River, New Zealand when they concluded that valley widening rates from 1952 to 2005 and 1956 to 2005 were similar to historic rates from the past 18 ka BP. Based on the evidence presented above, it would be difficult to say whether the differences reported by Gran et al. (2009) and Belmont et al. (2011) are true increases in volume loss in recent years or just an artifact of using two different time intervals (i.e., "Sadler effect"). Similarly, the 18 ka BP rate of river widening presented by De Rose and Basher (2011) may have varied greatly and at times been much higher or lower than the modern day average. The results suggest that comparing average annual rates of river bank erosion,

retreat distance, and sediment efflux for periods with large time differences should be avoided in establishing natural background for TMDL allocations, particularly where bank erosion is episodic. As shown above, averaging over larger time intervals conceals temporal variability in both volume loss and retreat rates.

Bank Erosion Rates for Similar Timer Intervals

To evaluate how bank erosion rates have varied for similar time intervals in Blue Earth County, two sets of bank erosion rates were compared, each set representing similar time intervals but covering different time periods. The first set of 16 river banks selected at section line crossings in 1855 PLSS PLATs were compared over two intervals 1855-1938 (84 yrs) and 1938-2009 (72 yrs). The position of these 16 banks in 1938 and 2009, were taken from the corresponding aerial photographs. The second set, representing 48 river banks, were selected from aerial photographs and comparisons made between the periods 1938-1971 (34 yrs) and 1971-2009 (38 yrs).

For the 16 banks in the first comparison the heights ranged from 3 to 25 m. The bank retreat rates were 0.51 m yr^{-1} and 0.37 m yr^{-1} for the 1855-1938 and 1938-2009 periods, respectively. Both the minimum (0.12 m yr^{-1}) and maximum (2.27 m yr^{-1}) retreat rates were found in the 1938-2009 period. For the 1855-1938 period, the corresponding minimum and maximum retreat rates were 0.12 m yr^{-1} and 1.77 m yr^{-1}, respectively. A paired t-test on natural log transformed retreat rates showed that the average river bank retreat rates between the period 1938-2009 and 1855-1938 were not significantly different (two-tail $t = 2.13$, $p = 0.14$). This suggests that bank retreat rates for the 16 river banks in Blue Earth County remained relatively unchanged since European settlement

starting around 1850. In the second set of retreat rate and volume loss comparisons for 48 banks, a t-test on the natural log transformed data also indicated that total retreat ($P = 0.96$), total volume loss ($P = 0.64$), annual retreat ($P = 0.44$), and annual volume loss ($P = 0.99$) are statistically similar between the two periods 1938-1971 and 1971-2009 (Figure 13). These findings further support earlier conclusions that over longer time periods the retreat rate of individual river banks has remained relatively stable since European settlement.

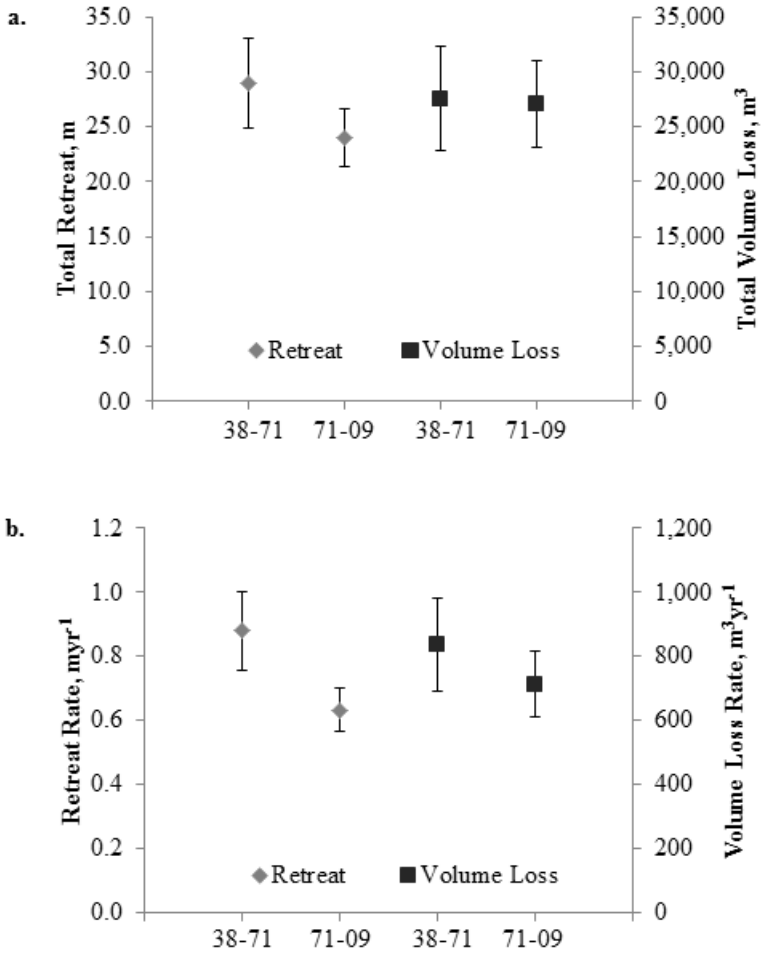

Figure 13. Comparison of bank retreat and volume loss rate. Comparison used 48 river banks in Blue Earth County between two periods (1938–1971 and 1971–2009). (a) Total retreat and total volume loss. Each of them was statistically similar between the two periods (t = -0.05, p = 0.96 and t = -0.48, p = 0.64, respectively). (b) Annual retreat and annual volume loss. Each of them was statistically similar between the two periods (t = 0.76, p = 0.45 and t = 0.01, p = 0.99, respectively).

Although the second comparison was for the same 48 banks in both periods, analysis of the 2009 photographs showed an additional 145 river banks where erosion

had occurred between 1971and 2009. The increased number of banks showing erosion in 2009 photographs could be partially due to better resolution of the modern (2005 and 2009) air photos, as well as their collection in leaf off stage. However, the large difference in the number of observations in 1971 to 2009 relative to 1938 to 1971 (a 120% increase), along with an increasing number of observations between consecutive periods (Table 10), suggests that recent increased sediment production in GBERB is likely from an increased number of banks that are slumping rather than an increased rate of slumping of any given bank. The average annual precipitation for the Blue Earth River Watershed has increased by 37±32 mm from 1972-2009 relative to 1940-1971, with a corresponding increase in annual water yield of 65±47 mm. These changes in precipitation and flow likely caused the increase in the number of eroding banks in recent years.

Volume Loss as a Function of Bank Physical Features

No relationship was observed between the volume loss rate from 2005-2009 derived from airborne Lidar data and the bank physical features (face area, inclined surface area, length, height, and slope) either estimated from 2005 (Figure 14) or 2009 (Figure not included) Lidar data. This is expected considering that none of these physical features represent bank erosion mechanisms such as seepage, piping/sapping, freezing and thawing, undercutting, or fluvial erosion due to migration of rivers from flooding. While sub aerial processes such as seepage and pipping have traditionally been viewed as preparatory, recent research indicates that they can play a large role in bank erosion (Couper, 2003; Fox and Wilson, 2010). Best fit regression lines between the volume loss

rate and the physical features measured from the 2005 Lidar data show that bank face area (Figure 14a), inclined surface area (Figure 14b), slope (Figure 14c), height (Figure 14d), and length (Figure 14e), only explained small fractions (28%, 28%, 1%, 18%, and 24%, respectively) of the variability in the data. The corresponding variability explained by the 2009 Lidar data (Figures not included) were 28%, 28%, 10%, 18% and 24% . This variability is very similar to the variability observed by Day et al. (2013b) when they related erosion rate (Mg/yr) to surface area (m^2) using TLS measurements from 15 tall banks. In these calculations, Day et al. (2013b) had converted volume loss from TLS to erosion using a constant bulk density value (1.8 Mg/m^3). Considering there is a large variability in bulk densities with depth in tall banks (Kessler et al., 2012), it is likely that the variability in their erosion vs. surface area plot would be even greater if the bulk density variability with depth was incorporated in volume loss calculations. Lack of strong statistical relationship between volume loss and the above bank physical features suggests that these physical features are not appropriate surrogate variables for extrapolating discrete volume loss measurements to the entire length of a river channel, as was done by Sekely et al. (2002), Wilcock (2009), Kronvang et al. (2011), Willet et al. (2012), and Day et al. (2013b).

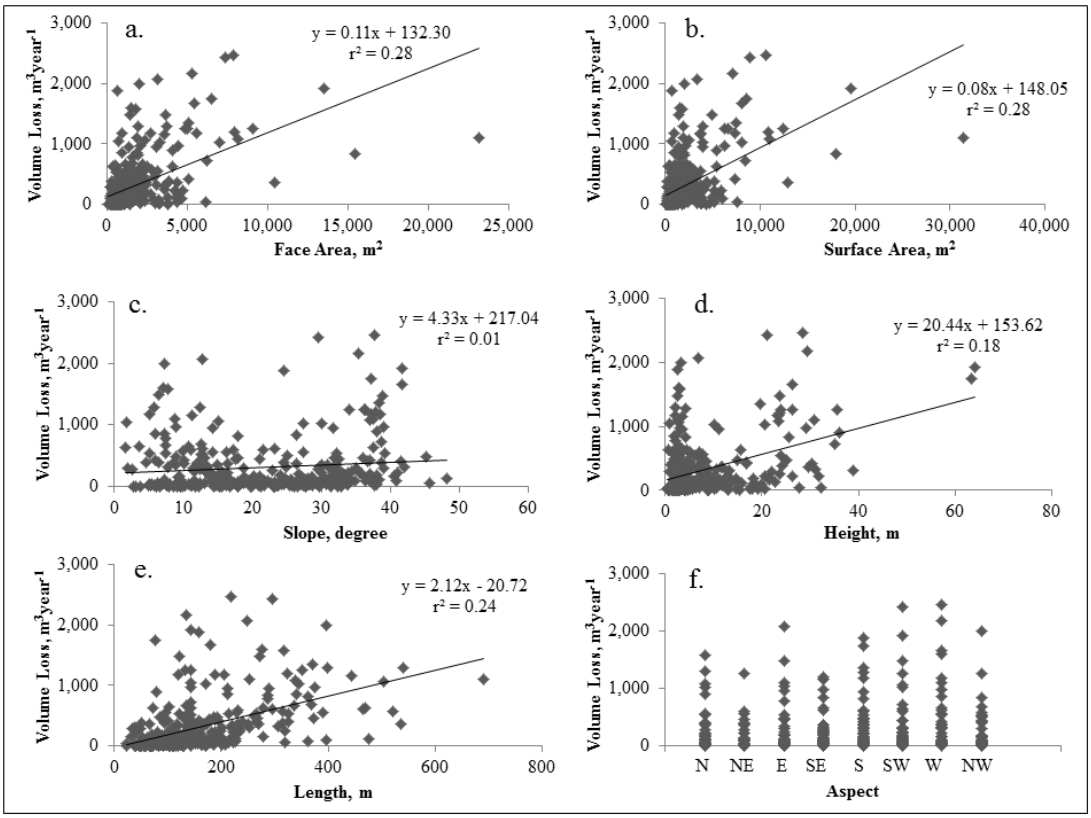

Figure 14. Erosion as a function of bank physical features. Relationships between volume loss per year from various banks along rivers of Blue Earth County, Minnesota and their corresponding (a) face area, (b) inclined surface area, (c) length, (d) height, (e) slope, and (f) aspect measured from the 2005 Lidar data.

Since soils freeze and thaw in northern latitudes, Belmont et al. (2011) and Day et al. (2013b) also used river bank aspect to extrapolate discrete volume loss measurements to the entire length of the Le Sueur River and its tributaries in Minnesota. A plot of volume loss rate from 2005-2009 as a function of bank aspect in 2005 along rivers in the GBERB is shown in Figure 14f. The relationship of volume loss rate as a function of bank aspect measured from 2009 Lidar data set was similar (figure not included). Like other bank physical features, this plot (Figure 14f) also shows a lack of relationship

between volume loss rate and bank aspect. Although there were large variations in volume loss rate across all river bank aspects, some aspects did show slightly higher volume loss rate. As expected, west, southwest, south, and southeast exposures showed greater ranges in volume loss rate, because of the greater potential for soil thawing from direct sun warming during winter and early spring on banks facing these aspects. Contrarily, banks facing north, northeast, and northwest had the lowest variations in volume loss rate. These results differ from those of Day et al. (2013b) and Belmont et al. (2011) who showed the highest retreat rates in north, northwest (315 to 360º), and northeast (0 to 45º) facing banks on the Le Sueur River and north, northwest, northeast and east facing banks on the Cobb River. Only on the Maple River were their results consistent with our data, with the highest retreat rate on the south, southwest (180 to 225°), west, and northwest facing banks.

The lack of relationship between volume loss rate and aspect, or any of other bank physical features measured in this study (Figure 14) suggests that extrapolating discrete volume loss measurements based on aspect or some other bank physical feature will likely provide unreliable net volume loss estimates for the whole length of a river channel. Similar to the discussion on bank physical features, bank aspect only relates to freeze and thaw bank failure mechanism, but ignores other bank failure mechanisms such as seepage, pore water pressure, piping/sapping, undercutting, and fluvial erosion from river migration. This suggests that either airborne Lidar (Thoma et al., 2005; Kessler et al., 2012), or methods based on radionuclide tracers (Walling 2005) and rare earth elements (Kelley and Nater, 2000) may be more suitable alternatives for estimating volume loss over large segments of rivers. In developing empirical methods for

extrapolations, efforts should be made in selecting surrogate parameters that represent the most bank failure mechanisms for a given river reach. Furthermore, those relationships should be validated before wide spread application.

CONCLUSIONS

Annual volume loss rates measured from aerial photographs decreased with an increase in time interval suggesting the episodic nature of bank erosion/sloughing in Blue Earth County, MN. These results confirm the presence of a "Sadler effect" in river bank erosion, thus suggesting that comparison of modern and historic river bank erosion rates should be done not only over similar time intervals, but also over longer time intervals, such as three decades or more. Adaption of such a procedure will give more realistic assessments on the effectiveness of conservation measures to reduce suspended sediments loads from river bank erosion. For various rivers in Blue Earth County, river bank erosion assessment for similar time intervals (1855 to 1938 and 1938 to 2009, and 1938 to 1971 and 1971 to 2009) showed that river bank retreat rates were statistically similar. However, the number of bank erosion observations increased with time, particularly for large river banks, suggesting that increased sediment production in recent years may be a reflection of increases in the number of banks failing, rather than increases in the rate at which individual banks are eroding. The lack of relationship between discrete volume loss rates and individual bank physical features showed that bank physical features do not represent the suite of mechanisms that cause bank erosion. This in turn means, extrapolation or up scaling of volume loss measurements from a few banks to the entire extent of a river channel based on these simple relationships may

result in erroneous predictions. Considering the apparent episodic nature of bank sloughing, we concluded that future efforts should be directed towards quantifying the predominance of different bank failure mechanisms (i.e., seepage, piping/sapping, freeze/thaw, undercutting, and river migration) and the parameters that are representative of these processes in order to predict when and where bank failures may occur in the GBERB.

REFERENCES

Altman, D.G., and J.M. Bland. 1983. Measurement in medicine: the analysis of method comparison studies. The Statistician. 32:307-317.

Belmont, P., K.B. Gran, S.P. Schottler, P.R. Wilcock, S.S. Day, C. Jennings, J.W. Lauer, E. Viparelli, J.K. Willenbring, D.R. Engstrom, and G. Parker. 2011. Large shift in source of fine sediment in the Upper Mississippi River. Environmental Science and Technology. 45:8804-8810.

Black, E., C.E. Renshaw, F.J. Magilligan, J.M. Kaste, W.B. Dade, and J.D. Landis. 2010. Determining lateral migration rates of meandering rivers using fallout radionuclides. Geomorphology. 123:364-369.

Bohling, S., 2012. Turbidity total maximum daily load study: Greater Blue Earth River Basin. Draft report submitted to the Minnesota Pollution Control Agency. Available online: http://www.pca.state.mn.us/index.php/view-document.html?gid=17673, *(accessed on March 18, 2013).*

Cancienne, R., G.A. Fox, and A. Simon. 2008. Influence of seepage undercutting on the root reinforcement of river banks. Earth Surface Processes and Landforms. 33:1769-1786.

Clayton, L., and S.R. Moran. 1982. Chronology of late-Wisconsin glaciations in middle North America. Quaternary Science Reviews. 1:55-82.

Couper, P., T. Scott, and I. Maddock. 2002. Insights into river bank erosion processes derived from analysis of negative erosion pin recordings: observations from three recent UK studies. Earth Surface Processes and Landforms 27, 59-79.

Couper, P. 2003. Effects of silt-clay content on the susceptibility of river banks to subaerial erosion. Geomorphology. 56:95-108.

Day, S.S., K.B. Gran, P. Belmont, and T. Wawrzyniec. 2013a. Measuring bluff erosion Part 2: Pairing aerial photographs and terrestrial laser scanning to create a watershed scale sediment budget. Earth Surface Processes and Landforms. DOI:10.1002/esp.3359.

Day, S.S., K.B. Gran, P. Belmont, and T. Wawrzyniec. 2013b. Measuring bluff erosion Part 1: Terrestrial laser scanning methods for change detection. Earth Surface Processes and Landforms. DOI:10.1002/esp.3353.

De Rose, R.C., and L.R. Basher. 2011. Measurement of river bank and cliff erosion from sequential Lidar and historical aerial photography. Geomorphology. 126:132-147.

Engstrom, D.R., J.E. Almendinger, and J.A. Wolin. 2009. Historical changes in sediment and phosphorus loading to the upper Mississippi River: mass-balance reconstructions from the sediments of Lake Pepin. Journal of Paleolimnology. 41:563-588.

Evans, D.J., C.E. Bison, and R.S. Rossell. 2006. Sediment loads and sources in heavily modified Irish catchments: a move towards informed management strategies. Geomorphology. 79:93-113.

Flood, M. 2004. American Society for Photogrammetry and Remote Sensing guidelines: Vertical accuracy reporting for Lidar data. Available online: http://www.asprs.org/a/society/committees/Lidar/Downloads/Vertical_Accuracy_Reporting_for_Lidar_Data.pdf (*accessed on March 18, 2013*). ASPRS, Bethesda, MD.

Fox, G.A., and G.V. Wilson. 2010. The role of subsurface flow in hillslope and stream bank erosion: a review. Soil Science Society of America Journal. 74:717-733.

Galatowitsch, S.M. 1990. Using the original land survey notes to reconstruct presettlement landscapes in the American West. Great Basin Naturalist. 50:181-191.

Gran, K.B., P. Belmont, S.S. Day, C. Jenning, A. Johnson, L. Perg, and P.R. Wilcock. 2009. Geomorphic evolution of the Le Sueur River, Minnesota, USA, and implications for current sediment loading. The Geological Society of America Special Paper. 451:119-130.

Hagerty, D.J. 1991a. Piping/sapping erosion. I: Basic considerations. Journal of Hydraulic Engineering. 117:991-1008.

Hagerty, D.J. 1991b. Piping/sapping erosion. II: Identification-diagnosis. Journal of Hydraulic Engineering. 117:1009-1025.

Hooke, J.M. 1979. An analysis of the processes of river bank erosion. Journal of Hydrology. 42:39–62.

Hooke, J.M. 2007. Spatial variability, mechanism and propagation of change in an active meandering river. Geomorphology. 84:277-296.

Hughes, M.L., P.F. McDowell, and W.A. Marcus. 2006. Accuracy assessment of georectified aerial photographs: implications for measuring lateral channel movement in GIS. Geomorphology. 74:1-16.

IBM Corp. 2010. IBM SPSS Statistics for Windows, Version 19.0. Armonk, NY.

Kelley, D.W., and E.A. Nater. 2000. Historical sediment flux from three watersheds into Lake Pepin, Minnesota, USA. Journal of Environmental Quality. 29:561-568.

Kessler, A.C., S.C. Gupta, H.A.S. Dolliver, and D.P. Thoma. 2012. Lidar quantification of bank erosion in Blue Earth County, Minnesota. Journal of Environmental Quality. 41:197-207.

Kronvang, B, J. Aude, A. Baattrup-Pedersen, H.S. Jensen, and S.E. Larsen. 2011. Phosphorus load to surface water from bank erosion in a Danish lowland river basin. Journal of Environmental Quality. 41: 304-313.

Lawler, D.M. 1995. The impact of scale on the processes of channel-side sediment supply: a conceptual model. In: Osterkamp W.R. (Ed.), Effects of Scale on Interpretation and Management of Sediment and Water Quality. IAHS Publ. no. 226, pp. 175-184.

Leys, K.F., and A. Werritty. 1999. River channel planform change: software for historical analysis. Geomorphology. 29:107-120.

Lindow, N, G.A. Fox, and R.O. Evans. 2009. Seepage erosion in layered stream bank material. Earth Surface Processes and Landforms. 24:1693-1701.

Matsch, C.L. 1983. River Warren, the southern outlet of Lake Agassiz. In: Teller, J.T., and Clayton, L., (Eds.)., Glacial Lake Agassiz. Geological Association of Canada Special Paper 26, pp. 232-244.

Meyer, M.L., and S.M. Schellhaass. 2002. Sources of phosphorus, chlorophyll, and sediment to the Mississippi River upstream of Lake Pepin: 1976-1996. A report for environmental studies of phosphorus. Metropolitan Council Environmental Services, St. Paul, MN.

Newcombe, C.P., and J.O.T. Jensen. 1996. Channel suspended sediment and fisheries: a synthesis for quantitative assessment of risk and impact. North American Journal of Fisheries Management. 16:693-727.

Nicoll, T.J., and E.J. Hickin. 2010. Planform geometry and channel migration of confined meandering river on the Canadian prairies. Geomorphology. 116:37-47.

Payne, G.A. 1994, Sources and transport of sediment, nutrients and oxygen demanding substances in the Minnesota River Basin, 1989-92. USGS Water Resources Investigations Report 93-4232.

Pollen, N., and A. Simon. 2005. Estimating the mechanical effects of riparian vegetation on stream bank stability using a fiber bundle model. Water Resources Research. 41:W07025. doi:10.1029/2004WR003801.

Rinaldi, M., and N. Casagli. 1999. Stability of river banks formed in partially saturated soils and effects of negative pore water pressures: the Sieve River (Italy). Geomorphology. 26:253-277.

Sadler, P.M. 1981. Sediment accumulation rates and the completeness of stratigraphic sections. The Journal of Geology. 89:569-584.

Sekely, A.C., D.J. Mulla, and D.W. Bauer. 2002. River bank slumping and its contribution to the phosphorus and suspended sediment load of the Blue Earth River, Minnesota. Journal of Soil and Water Conservation. 57:243-250.

Simon, A., A. Curini, S.E. Darby, and E.J. Langendoen, E.J. 2000. Bank and near-bank processes in an incised channel. Geomorphology. 35:193-217.

Shields, F.D. Jr., A. Simon, and L.J. Steffen. 2000. Reservoir effects on downstream river channel migration. Environmental Conservation. 27:54-66.

Thoma, D.P., S.C. Gupta, M.E. Bauer, and C.E. Kirchoff. 2005. Airborne laser scanning for riverbank erosion assessment. Remote Sensing Environment. 95:943-501.

USDA SCS (U.S. Department of Agriculture Soil Conservation Service), 1978. Soil Survey of Blue Earth County, Minnesota. USDA, SCS, Washington, DC.

Walling, D. E. 2005. Tracing suspended sediment sources in catchments and river systems. Science of the Total Environment. 344.159-184.

Willet, C.D., R.N. Lerch, R.C. Schultz, S.A. Berges, R.D. Peacher, and T.M. Isenhart. 2012. River bank erosion in two watersheds of the Central Claypan Region of Missouri, United States. Journal of Soil and Water Conservation. doi:10.2489/jswc.67.4.249.

Wilson, G.V., R. Periketi, G.A. Fox, S. Dabney, D. Shields, and R.F. Cullum. 2007. Soil properties controlling seepage erosion contributions to river bank failure. Earth Surface Processes and Landforms. 32:447–459.

Wilcock, P. 2009. Synthesis Report for Minnesota River Sediment Colloquium. Report for Minnesota Pollution Control Agency, St. Paul, MN. Available online: http://www.pca.state.mn.us/index.php/view-document.html?gid=8099 (*accessed on March 18, 2013*).

Zaimes, G.N., R.C. Schultz, and T.M. Isenhart. 2004. Stream bank erosion adjacent to riparian forest buffers, row-crop fields, and continuously-grazed pastures along Bear Creek in central Iowa. Journal of Soil and Water Conservation. 59:19-27.

Zinger, J.A., B.L. Rhoads, and J.L. Best. 2011. Extreme sediment pulses generated by bend cutoffs along a large meandering river. Nature Geoscience. 4:675-678.

CHAPTER 4: QUANTIFYING SEEPAGE INDUCED RIVER BANK EROSION USING LIDAR

SUMMARY

Seepage has gained significant recognition as an important mechanism of river bank failure. Yet, methods to quantify seepage induced river bank erosion across large scales are lacking. The objective of this study was to assess if laser return intensities from terrestrial and airborne light detection and ranging (Lidar) could be used to detect seepage locations on river banks and if these seepage locations relate to the extent of bank erosion calculated from multi-temporal Lidar change detection. We tested the above concept (1) on a river bank in South-Central Minnesota with terrestrial Lidar acquired in 2012 and 2013, (2) on a developing ravine with terrestrial Lidar acquired in 2014 and 2015, and (3) on a second bank in South Central Minnesota with airborne Lidar collected in 2009 and 2012. The results indicate that both terrestrial and airborne Lidar return intensities provide a means to identify seep locations on river banks and this in combination with Lidar measured elevation change may provide a means to evaluate seepage induced bank erosion.

INTRODUCTION

Seepage is gaining recognition as an important mechanism of river bank erosion (Fox et al., 2007; Wilson et al., 2007; Chu-Agor et al., 2008; Chu-Agor et al., 2009; Lindow et al., 2009; Midgley et al., 2013). In field investigations, Midgley et al. (2013) showed that shallow interflow exiting the face of river banks (i.e. seepage) reduces soil strength thus destabilizing banks and in turn contributing substantial amount of sediments to rivers already impacted by high sediment loads. In spite of the recognition that seepage

is an important process controlling bank erosion, there is a lack of research on techniques that can remotely identify seepage areas on river banks at a broader scale (Deitchman and Loheide, 2009). To date, ground based thermal imaging is the only technique that has been used to locate seeps along the face of river banks (Deitchman and Loheide, 2009; Pfister et al., 2010). However, ambient air temperature at different times of the day and year can mask the thermal detection of seepage on the face of river banks (Deitchman and Loheide, 2009; Pfister et al., 2010).

Numerous remote sensing technologies have been utilized to examine the relationship between reflectance and soil moisture (e.g. Moran et al., 2004; Moran et al., 2000; Muller and Decamps, 2001; Lobel and Asner, 2002; Weidong et al., 2002). However, many of these technologies are based on the use of radar from satellites such as synthetic aperture radar (see Moran et al., 2004). In field studies, Bryant et al. (2003) found that ground based hyperspectral, thermal and satellite radar instruments were sensitive to soil moisture. However, the thermal and radar were the only instruments that were insensitive to soil type. These authors concluded that for optical wavelengths (400 to 700 nm), soil moisture was uniquely related to percent reflectance but this relationship varied with soil types. In reviewing techniques to estimate soil moisture, Moran et al., (2004) concluded that satellite-based radar in combination with soil vegetation atmosphere transfer models, is capable of providing consistent soil moisture measurements at a watershed scale (10 m – 1000 m). However, watershed scale measurements of soil moisture using radar will be unable to isolate seep locations on the face of river banks.

Recent soil research has shown that measurements taken in the near-infrared portion of the electro-magnetic spectrum are capable of detecting variations in soil moisture (Lobel and Asner, 2002). For short-wave radiation (200-2500 nm), Lobel and Asner (2002) showed an exponential decrease in reflectance with an increase in soil moisture. However, this relationship was dependent upon soil type. The authors also reported a strong potential for relating reflectance in short-wave infrared spectral region to soil moisture.

The spatial resolution of many satellite platforms are too coarse (i.e. ≥ 30 m) for detecting seepage on river banks or hillslopes. Also, satellite platforms will have difficulty penetrating through vegetation found around rivers. Recently, studies have begun testing the relationship between soil moisture and return intensity from light detection and ranging (Lidar) at much finer (i.e. ≤ 1 m) spatial scale (Narayana et al., 1993; Brennan and Webster, 2006). In a laboratory experiment, Narayana et al. (1993) demonstrated that laser reflectance collected at 928 nm, 957 nm, and 1024 nm wavelengths could detect variations in soil mass wetness. Brennan and Webster (2006) showed that intensity data from Lidar was able to detect variation in soil moisture and thus aid in land cover classification. The underlying principle of both these studies was that near infra-red light is adsorbed by water thus decreasing the return intensity, an indication of increasing soil moisture content. The increased availability and use of terrestrial and airborne Lidar thus provides opportunities to detect river bank seepage from return Lidar intensity, and simultaneously quantify bank erosion from Lidar measured elevation change. In this study, we present the results of tests on the suitability of terrestrial and airborne Lidar to quantify seepage effects on bank erosion.

METHODS

Study Areas

The study area was two banks along the Blue Earth River in Blue Earth County, Minnesota and a newly developed ravine along Carver Creek, in Carver County, Minnesota (Figure 15). Blue Earth County in South Central Minnesota (Figure 15a) have been shown to be the primary contributor of sediments to waterways of the Greater Blue Earth River Basin (GBERB) and then to the Minnesota River at Mankato (Payne, 1994; Thoma et al., 2005; Belmont et al., 2011; Kessler et al., 2012). The major rivers of the GBERB include the Le Sueur, Blue Earth, Watonwan, Big Cobb, Little Cobb, and Maple Rivers. The Big Cobb, Little Cobb and Maple Rivers are tributaries of the Le Sueur River, and the Watonwan River and the Le Sueur River are tributaries of the Blue Earth River which joins the Minnesota River at Mankato, MN (Fig. 15a). All of the major rivers in the GBERB have been actively incising since the last glaciation over 13,000 years BP (Gran et al., 2009). This post-glaciation incision has led to the formation of tall river banks, referred to as bluffs (see Gran et al., 2009; Belmont et al., 2011). These large bluffs reach heights over 60 m and lengths of over 300 m (Kessler et al., 2012).

Carver Creek, a tributary of the Minnesota River, has also experienced mass wasting along its' river banks. Over 6 inches of rain from June 11 to June 18, 2012 in Carver Creek watershed resulted in one mass wasting event that led to the development of a large ravine (Figure 15c). This ravine has since been expanding.

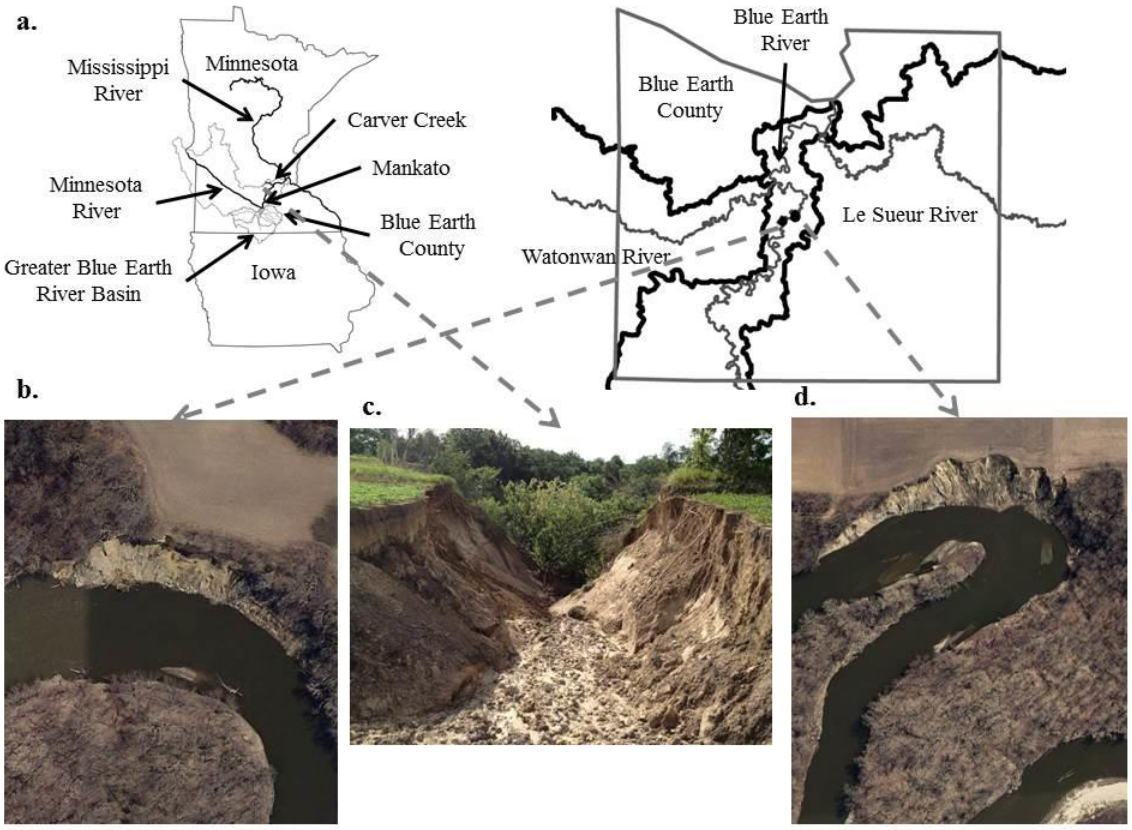

Figure 15. (a) Map of study sites within the Minnesota River Basin and Blue Earth County. (b) The bank on the Blue Earth River where terrestrial Lidar and thermal imagery were collected to characterized seepage caused bank erosion. (c) A developing ravine on Carver Creek where terrestrial Lidar measurements were taken to characterize soil wetness effects on return Lidar intensity. (d) Another river bank along the Blue Earth River where airborne Lidar intensity was used to identify the location of seeps as well as characterize the extent of seepage caused erosion.

The first study site along the Blue Earth River has a river bank that reached a height of 30 m and was 130 m long (Figure 15b). At this site we tested the feasibility of using terrestrial Lidar to identify seepage induced bank slumping. Data collection

included multi-temporal (2012-2013) terrestrial Lidar intensity and elevation data, as well as thermal imagery. The second study site, a ravine along Carver Creek was used to quantify the relationship between terrestrial Lidar return intensities and soil moisture and soil color (Fig. 15c). The third study site, a 27 m tall and 270 m long river bank along the Blue Earth River was used to evaluate if the techniques developed at the first and the second sites could be extended to a larger area using the airborne Lidar data.

First-Site: A Bank on the Blue Earth River

At this site, we evaluated the potential of using thermal imagery and return intensity from terrestrial Lidar to delineate seeps on a river bank. Both the terrestrial Lidar return intensity and thermal imagery were collected in unison during two campaigns on 5 December 2012 and 26 September 2013. All Lidar and thermal imagery data were projected to Universal Transverse Mercator (UTM), zone 15 North, North American Datum of 1983 (NAD83). The collection dates were restricted to a low stream stages (< 0.5 m) to allow access to a point bar across from the river bank. Unfortunately, dense vegetation was present on parts of the river bank during the 2013 terrestrial Lidar survey thus restricting the analysis to the non-vegetated portion of the river bank. Two semi-permanent benchmarks were established in 2012 to align the data from two different collection years. In addition, the bank was also scanned from 2 different angles (locations) on 5 December 2012 to characterize the accuracy of the terrestrial Lidar system. Theoretically, there should be no change in elevation between the two scans taken from two different positions on the same date. The terrestrial Lidar was collected with a Leica ScanStation 2 using a laser beam diameter of 4 mm, a pulse rate of 50 kHz, and a wavelength of 532 nm. The system had a horizontal look angle of 360 degrees and

a vertical look angle of 270 degrees. The distance between the scanner and the river bank during data collection ranged from 42 m to 50 m. The vendor processed the raw data using proprietary software and provided both raw and bare earth points. The processed bare earth points for both the 2012 and 2013 collections had point densities of 460 points m^{-2}. The vendor reported a horizontal and vertical accuracy of 0.007 m from the tie in bench marks between the 5 December 2012 and 26 September 2013 data.

The thermal imagery was collected using a FLIR System (North Billerica, MA) T420 thermal infrared camera. This camera uses a 320 by 240 focal plane array uncooled microbolometer with a spectral range of 7.5 to 13 μm. Table 11 shows the calibration parameters used for two separate collection campaigns. Wet and dry bulb air temperatures were collected to calibrate the thermal imagery for relative humidity and air temperature. Following Deitchman and Loheide (2009), an emissivity of 0.96 was used to produce thermal images of the river bank. The thermal images were then georeferenced to the terrestrial Lidar data.

Table 11. Calibration parameters used for acquiring terrestrial thermal imagery at site #1 along the Blue Earth River.

Parameter	5 December 2012	26 September 2013
Emissivity	0.96	0.96
Distance, m	55	55
Reflected Temperature, °C	-3	23
Atmospheric Temperature, °C	6	20
Relative Humidity, %	65	65

After the second terrestrial scan in 2013, twelve soil samples were also collected around a seep for soil water content measurements. The samples were spaced 25 cm apart on three vertical transects laid at 0 m, 0.5 m and 1 m across the seepage location. The samples were oven dried at 105 °C for 24 hrs and mass wetness determined from the loss in weight during drying (Topp and Ferré, 2002). The number of samples collected was limited due to the difficulty of accessing other seep spots on this steep and unstable river bank. For the same reasons, we were also unable to gather elevation data with real time kinematic (RTK) survey and assess the horizontal accuracy of the georeferenced thermal images. We addressed these concerns at the second site in Carver Creek.

Second Site: Carver Creek Ravine

At this site, we characterized soil moisture and soil color effects on Lidar return intensity. The terrestrial Lidar data at this site were collected during two campaigns on 11 June 2014 and 23 April 2015. All Lidar data were projected to Universal Transverse Mercator (UTM), zone 15 North, North American Datum of 1983 (NAD83). Three semi-permanent benchmarks were established in 2014 to align the data from two different collection campaigns. During the 2014 collection, the terrestrial Lidar was collected with a Leica ScanStation 2 using a laser beam diameter of 4 mm, a pulse rate of 50 kHz and a wavelength of 532 nm. The system had a horizontal look angle of 360 degrees and a vertical look angle of 270 degrees. The distance between the scanner and the river bank during data collection ranged from 1 m to 14 m.

Prior to the 2015 campaign, the vendor acquired an upgraded terrestrial scanner, a Leica ScanStation C10. As such, the Lidar data collected with this instrument used a

laser beam diameter of 4.5 mm, a pulse rate of 50,000 points sec^{-1} and a wavelength of 532 nm. This system also had a horizontal look angle of 360 degrees and a vertical look angle of 270 degrees. The distance between the scanner and the site also ranged from 1 m to 14 m. For both the 2014 and 2015 campaigns, the vendor processed the raw data using proprietary software and provided both raw and bare earth points. The processed bare earth points for both the collection campaigns had point densities greater than 400 points m^{-2}.

The Carver Creek site provided greater accessibility thus allowing a collection of greater number of soil samples and other measurements. During the 2014 terrestrial Lidar collection, 62 soil samples were collected from different soil layers within the failure zone. Mass wetness was measured from loss in weight of these samples after oven drying at 105 °C for 24 hrs (Topp and Ferré, 2002). In addition, volumetric water content measurements were also taken using a Decagon GS3 time domain reflectometry (TDR) probe. The TDR probe was only used during the first Lidar data collection as it proved difficult to fully insert the probe into the naturally compacted subsoil.

Before the Lidar scan, a series of 62 nails with 5 cm diameter plastic heads were inserted into various soil layers on the sides of the ravine (Figure 16). These nail heads serve as the positions for downloading Lidar return intensity as well as for subsequent soil moisture and bulk density measurements. Real time kinematic (RTK) survey was used to locate the nail heads and insure that the spatial locations of the nails could be associated with the terrestrial Lidar data. The data vendor conducted the RTK survey using the same datum, projection, and benchmarks as the terrestrial Lidar survey.

Figure 16. Sampling locations where nails with 5 cm diameter plastic heads where inserted for soil moisture measurements.

During the 2015 terrestrial Lidar data collection, the same nail head procedure was repeated for an additional 60 sites in 6 different soil layers. However before nail insertions, half of area in each layer was wetted with a spray bottle (Figure 17). This technique was followed because during the 2014 survey there was not a wide enough range in soil moisture within each soil layer to assess soil moisture effects on light return intensities. Mass wetness adjacent to each nail head was measured using the procedures described above. The results for the Carver Creek site are shown by soil layer only for the 2015 collection (second scan). Again, the real time kinematic (RTK) survey was used to locate the nail heads and insure the terrestrial Lidar data matched the spatial locations of

the nails. The RTK survey was done using the same datum, projection, and benchmarks as the terrestrial Lidar survey.

Two weeks prior to 2015 field Lidar survey, 10 soil cores each from 5 different layers were also collected using 76 mm diameter aluminum rings. These cores were collected to evaluate soil color and soil wetness effects on Lidar return under controlled conditions. Half of the soil cores from each layer were allowed to air dry whereas the other half were sprayed with water; two extremes of the soil moisture regime. For each soil layer and soil wetness condition, a set of two cores were spray painted with a latex paint of brown, yellow, black, or red color. For each layer, a set of two cores were also left unpainted (natural color) both at air dried and wetted conditions. Moisture in wet cores was maintained by continuous spraying water leading up to the terrestrial Lidar data collection. The painted and natural color cores were then placed in a wooden box and scanned with the Lidar system (Figure 18). Due to smaller size of the wooden box relative to the number of soil cores, we repeated the Lidar data collection process four times; 2 times for wet cores and 2 times for dry cores. After the Lidar collection, the samples were then oven dried at 105 °C for 24 hrs and mass wetness determined from the loss in weight during drying (Topp and Ferré, 2002).

Figure 17. Example of the plastic nails used to identify locations where Lidar data was collected for characterizing the effects of soil wetness on Lidar intensity returns. Wet areas were created by spraying water with a spray bottle.

Figure 18. A set-up of painted and natural soil cores used to characterize color and moisture effects on Lidar return intensity.

On 20 May 2015, the core rings were again used to collect 3 additional soil samples for bulk density measurement from each of the 6 soil layers. Bulk density was calculated as the ratio of oven dried soil mass to ring volume (Topp and Ferré, 2002).

For both terrestrial Lidar surveys at the Carver Creek site, return intensity values were extracted from the bare earth point data close to the locations where the plastic nail heads were inserted (see example in Figure 18). For each soil layer, a linear relationship was developed between Lidar return intensity and soil color or soil moisture using the Excel (Office, 2009) software.

Third Site: Another Bank on the Blue Earth River

At this site, we characterize seepage induced bank erosion using airborne Lidar. The airborne Lidar data at this site were collected during leaf off conditions in the spring of 2009 and 2012. Both data sets were taken from the Lidar surveys of Blue Earth County, MN. The 2009 Lidar survey was commissioned by the authors whereas 2012 survey was commissioned by Minnesota Department of Natural Resources. The 2009

airborne Lidar data was collected in April and May using an Optech ALTM Gemini system with a laser (pulse rate of 45 kHz, wavelength 1064nm) flown at 1200 m above ground. The data had a nominal point spacing of 1.25 m. The 2012 airborne Lidar was collected in April using a Leica ALS70 scanner (with a laser pulse rate of 229 kHz, wavelength of 1064) at 2400 m above ground level. The data had a nominal point spacing of 1.4 m. Reported vertical accuracies of 2009 and 2012 airborne Lidar data were 17 cm and 19 cm, respectively (Kessler et al., 2012).

Estimating Bank Erosion and Identification of Seepage Locations

Bank erosion was estimated by overlaying concurrent digital elevation models (DEM) developed from terrestrial and airborne Lidar data at two different times (Kessler et al., 2012). The DEM models were based on the elevation of bare earth points. Similar to DEMs, concurrent return intensity models (RIM) were also developed using the return intensity values of the bare earth points. The procedures used to develop RIMs were similar to that of DEMs. These models were used to locate seepage locations on river banks. The terrestrial Lidar DEMs and RIMs were interpolated to a grid size of 0.2 m whereas the airborne Lidar DEMs and RIMs were interpolated to a grid size of 1 m.

The DEMs developed from the terrestrial and airborne Lidar surveys at two different times were subtracted using the Geomorphic Change Detection (GCD) 5.0 software (http://gcd.joewheaton.org) to produce a DEM of difference (DOD). The interpolation and differencing technique used to produce DODs has been shown to impact geomorphic change detection (Kessler et al., 2012; Day et al., 2013). As such, several interpolation techniques were tested to generate DEMs and subsequent DODs and

RIMs. These interpolation techniques included the triangulated irregular networks (TIN), inverse distance weighted (IDW), natural neighbors (NN), and ordinary kriging (OK).

Accounting for the uncertainty in DODs derived from high resolution elevation surveys has been a focus of several recent studies (Wheaton et al., 2010; Milan et al., 2011; Schurch et al., 2011; Wheaton et al,. 2013). Wheaton et al. (2010) proposed a spatially variable uncertainty analysis using a fuzzy inference system (FIS) and spatial coherence filter to distinguish between real and uncertain elevation change in GCD studies (see also Wheaton et al., 2013). In this study, we used the technique presented by Wheaton et al. (2010) to develop raw (no threshold) DODs as well as DODs with spatially variable probalistic thresholds for each of the DEM interpolation techniques. Briefly, the bare earth point density and river bank slope were used in the FIS to spatially estimate the uncertainty as an error term in the DEM surfaces. This error term was then propagated into the DEM by comparing the DOD values to the FIS error surface using a t score. An additional uncertainty check was performed by generating a spatial coherence filter on erosion and deposition. The probability surface generated from the FIS t score and the spatial coherence filter were then combined using Bayes' Theorem. Those areas that met or exceeded a 95% confidence interval were deemed real elevation change in the threshold DODs.

The DODs, RIMs, and thermal images were then overlain to evaluate if Lidar return intensities could be used as an alternative to thermal imagery for delineation of seepage locations on river banks and also whether or not elevation loss (bank erosion) in the DODs corresponds with seepage locations.

RESULTS AND DISCUSSION

Seepage Characterization with Lidar Return Intensity and Thermal Imagery

At the first site on the Blue Earth River, both terrestrial Lidar returns and thermal imagery taken in 2012 and 2013 data collection campaigns were able to delineate seepage locations on the river bank (digital photographs Figure 19a and Figure 19b; thermal images, Figure 19c and Figure 19d; Lidar return intensity, Figure 19e and Figure 19f). Seepage locations identified in thermal imagery aligned very well with seepage locations identified by RIMs on both 5 December 2012 (Figure 19g) and 26 September 2013 (Figure 19h). A regression analysis indicated a statistically significant ($F = 32.09$, p value < 0.01, $r^2 = 0.39$) direct relationship between Lidar return intensity and temperature in 2012. Uneven heating from partial shading by vegetation on 26 September 2013 (Figure 19b) created some false positives (i.e. vegetation was the same temperature as seepage water) for seepage locations, thus negatively affecting the ability of thermal imagery to detect correct seepage areas (Figure 19d). However, RIM identified seepage areas match perfectly with visual observation (Figure 18 a, b). These results indicate that under certain conditions RIMs provide a better alternative than thermal imaging for detecting seepage locations on river banks. The soil moisture measurements confirmed the results of thermal imagery and RIM by showing that the highest mass wetness (mean = 30%, Std. dev. = 13) occurred at the water outflow plane in the seepage area. The outflow plane occurred 0.25 m down from the top of the water content sampling grid. The area below the outflow plane (between 0.5 to 1 m from the top of the sampling grid) had a mean mass wetness of 21% (Std. dev. = 3), thus indicating a decrease in soil

moisture away from the seepage outflow plane. The sampling points at the top of the sampling grid had a mean mass wetness of 24% (Std. dev. = 7.6).

The terrestrial Lidar elevation data collected from two different positions on 5 December 2012 exhibited a mean difference of < -0.0001 m (Std dev. = 0.001 m) with a maximum difference of 0.012 m. This elevation difference was much smaller than expected. As such, a conservative approach was taken in applying the FIS thresholds by setting the mean error to 0.03 m. This conservative approach was taken to ensure that the reported changes in elevation and volume loss were representative of actual erosion. Raw and threshold DODs generated from all spatial interpolation techniques indicated over 350 m^3 of net volume loss (Table 12). Relative to the raw DODs, the threshold net volume loss only decreased by an average of 17 m^3 (Std. dev. = 5) with all interpolation techniques.

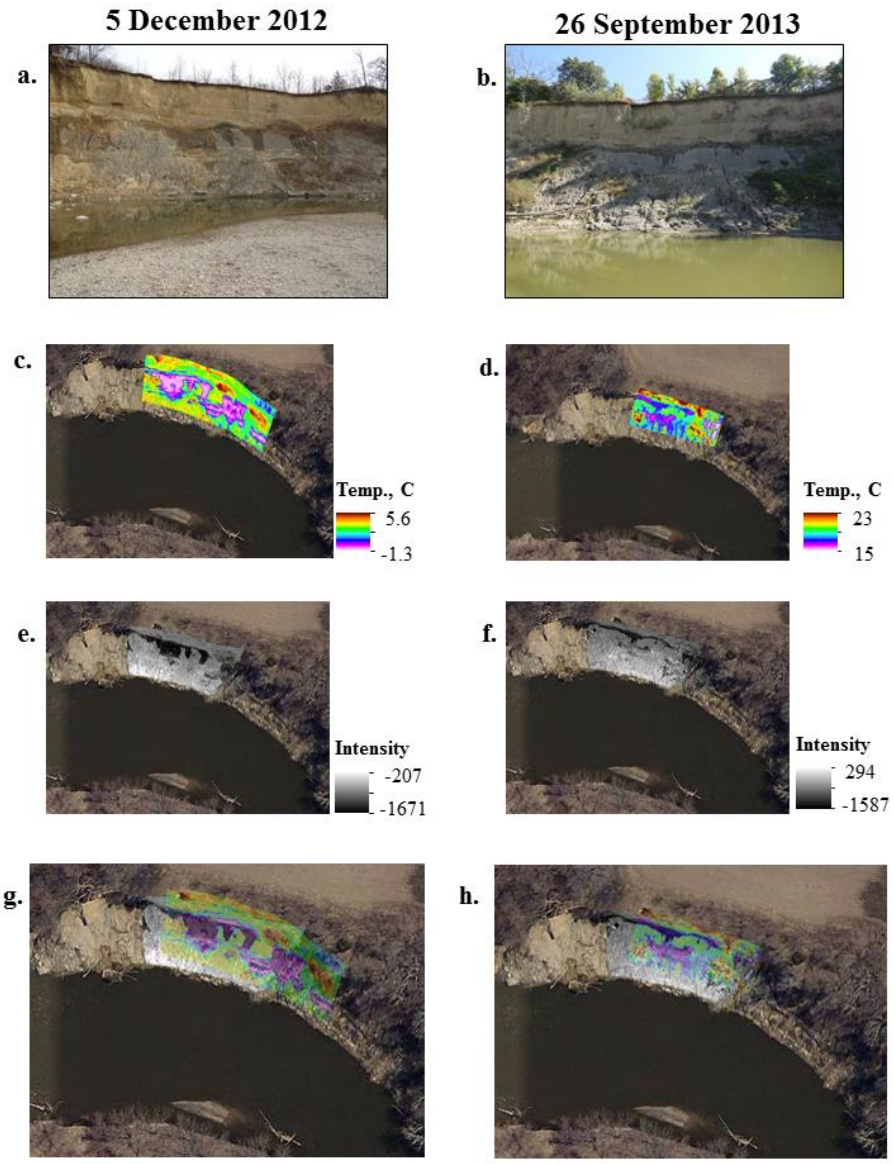

Figure 19. Digital images of a river bank (site #1) along the Blue Earth River in 2012 (a) and 2013 (b), the corresponding thermal imagery in 2012 (c) and in 2013 (d), and terrestrial Lidar return intensities in 2012 (e) and in 2013 (f). A composite image from all three techniques (2012 (g) and 2013 (h)) showed good correspondence between the thermal and the Lidar return intensity data for seep locations.

Table 12. Geomorphic change detection results using triangulated irregular networks (TIN), inverse distance weighted (IDW), natural neighbors (NN), and ordinary kriging (OK) spatial interpolation techniques for raw and threshold data.

Interpolation Technique	Deposition		Erosion		Net Change	
	Raw	Threshold	Raw	Threshold	Raw	Threshold
	---------- Volume, m^3 ----------					
TIN	187	160	-565	-521	-378	-361
IDW	186	160	-564	-525	-378	-365
NN	186	161	-564	-525	-378	-364
OK	187	160	-565	-514	-378	-354

Figure 20 shows an example of TIN generated DEMs for both 5 December 2012 (Figure 20a) and 26 September 2013 (Figure 20b) collection campaigns. As shown in Table 12, the results of the GCDs from other spatial interpolation techniques were similar to the results using TINs. The raw DOD indicated nearly uniform erosion across the top half of the river bank with deposition occurring across most of the bottom half (Figure 20c). Although 703 m^2 of the area (an equivalent to 30% of the total area) was removed from the raw DODs during the threshold process (Figure 20d and Figure 20e), 91% of the change in volume was still maintained (Figure 20f) due primarily to large changes in elevation from bank erosion. Kessler et al. (2012) found similar results in a GCD study along various rivers in Blue Earth County using 2005 and 2009 airborne Lidar data.

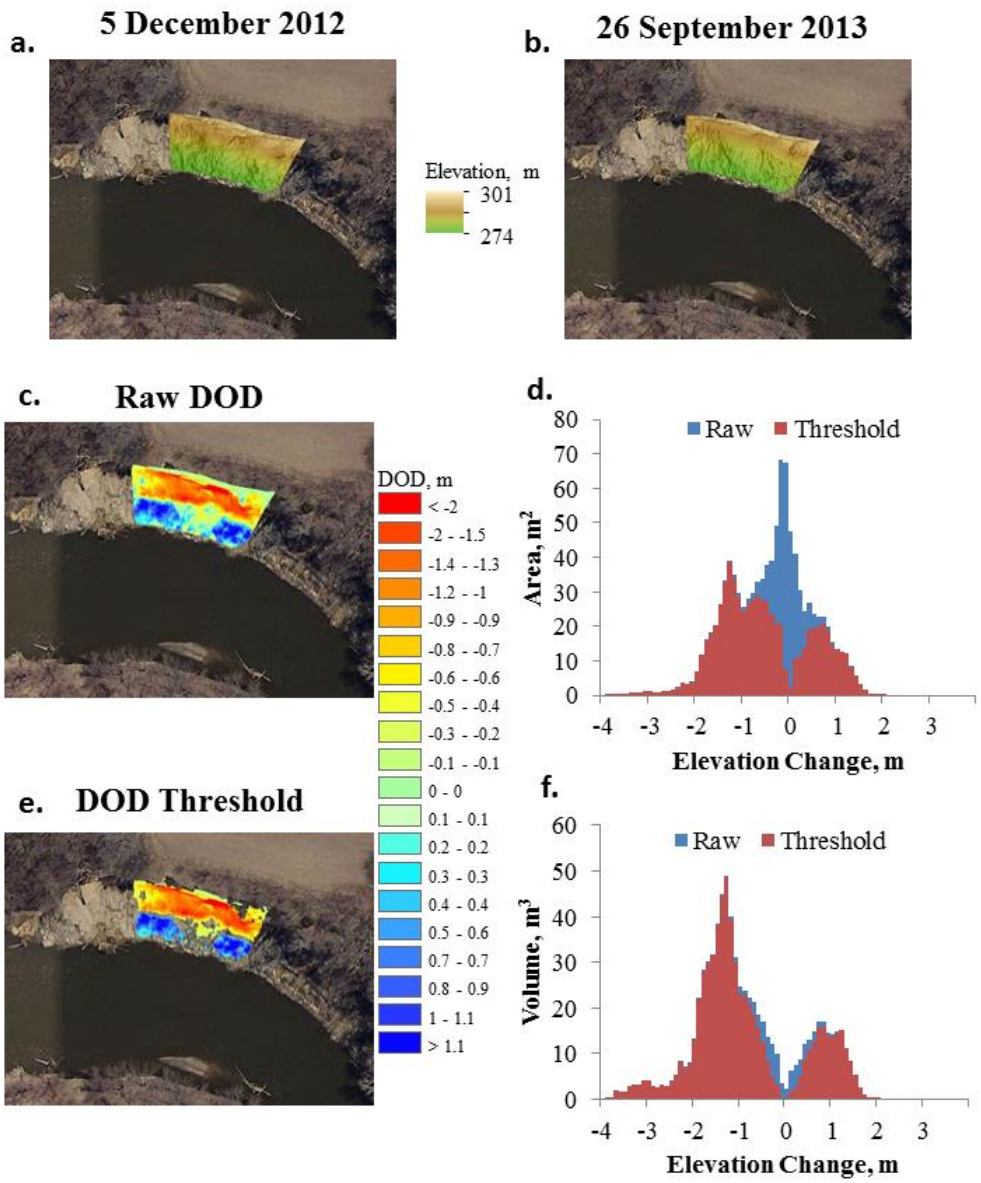

Figure 20. Digital elevation models (DEM) of a river bank (site #1) along the Blue Earth River generated using triangulated irregular networks (TIN) for the 2012 (a) and 2013 (b) collection dates and the corresponding difference in raw DEMs indicating large change in elevation across the site (c). Additional figures show that a considerable portion of the DOD area (d) was removed by the threshold (e), while most all of the change in volume was maintained (f).

The composite image of the threshold DOD (Figure 19e) and the 5 December 2012 RIM image (Figure 21) shows that most of the observed volume loss was directly related to the large seep areas (Figure 19), with 387 m^3 of the volume loss occurring in the zone b (Figure 21) where active seeps were observed during the field data collection campaign and could also be observed in the Lidar return intensity data. This is equivalent to 69% of the total erosion (564 m^3; see Table 12) measured for the site. This indicates that the areas of greatest volume loss correspond to the plane where seepage exited the face of the river bank (Figure 21).

Visual observations during the terrestrial data acquisition showed that a sand lens confined between two glacial till layers was the plane where seepage existed (see Figure 22). Measurements from the terrestrial Lidar DEMs indicate that the sand lens occurs 10 to 13 m below the soil surface. This observation was supported by a well driller's log (provided by the Minnesota Geological Survey) for a private residence 230 m east of the river bank also showing the presence of a sand lens between 12 to 13 m depth below the soil surface. This sand layer served as a preferential flow path for interflow water thus creating conditions for seepage led bank failure either through weakening of the bank material and/or from movement of soil particles by water flow (erosive seepage). Midgley et al. (2013) found a similar erosive seep layer on Dry Creek in Mississippi during a constant head experiment. These authors also showed that the ground water flux and erosion increased with increasing subsurface contributing area. An interesting extension of present research will be to assess if the size of the seepage area identified in the RIM is an indication of the below ground contributing area or volume of the interflow water existing the face of the river bank? The above results demonstrate that RIMs

generated from terrestrial Lidar can be used to identify seep areas and this in association of Lidar elevation change measurements could be used to quantify seepage impact on river bank erosion.

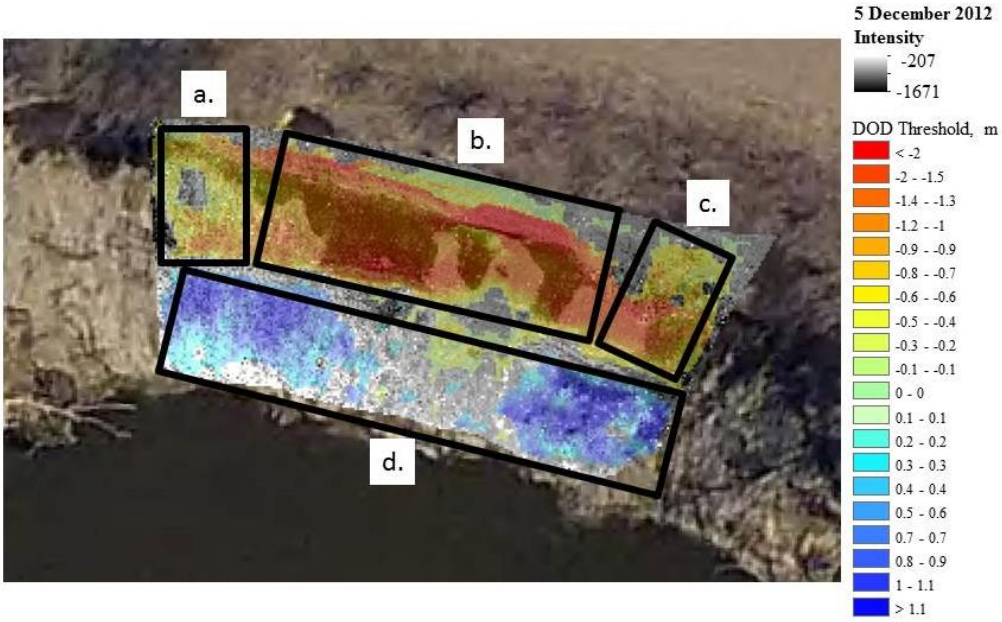

Figure 21. Composite image of the elevation difference grid and return intensity derived from terrestrial Lidar data showing zones with areas impacted by non-seepage erosion mechanisms (zone a), seepage caused mass wasting (zone b), seepage covered by failed bank material (zone c), river bank material deposition (zone d).

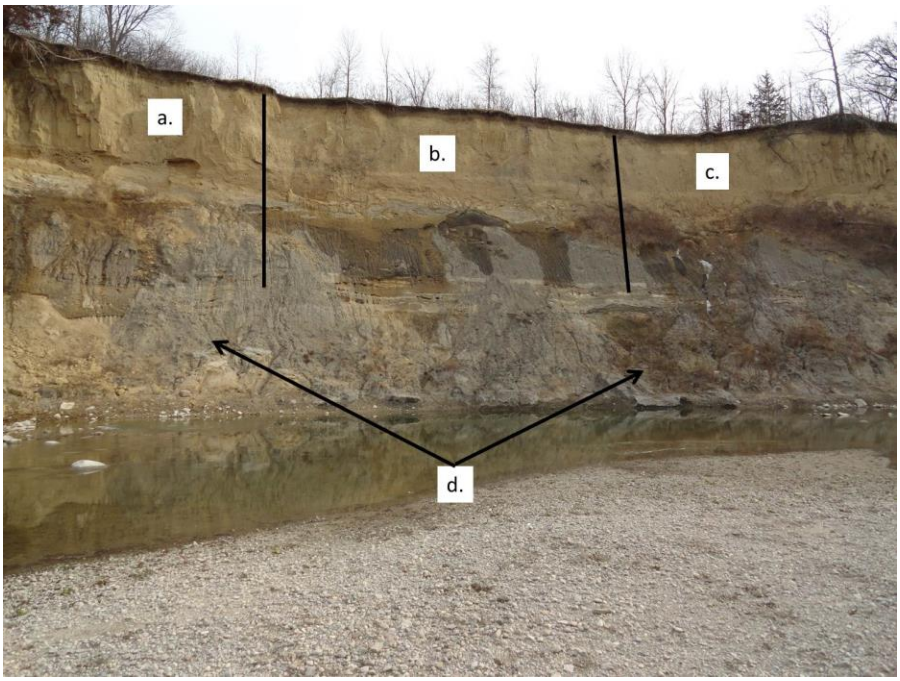

Figure 22. Picture of the Blue Earth River terrestrial Lidar study site # 1 taken on 5 December 2012 showing zone "a" with freeze-thaw caused fissure, zone "b" where seepage caused mass wasting occurred, zone "c" where seepage area is covered by failed bank material and some vegetation and zone "d" where failed bank material from the top has been deposited.

Other processes, such as freeze- thaw cycles, also likely played a role in mass wasting at this site. Zone "a" in Figure 21 shows a location where field observations detected cracks and fissures in the top half of the river bank indicating freeze thaw processes likely played a role in erosion at the site. Based upon field observations at this and other sites, oxidized tills near the top of river banks (2 to 5 m) often allow water to infiltrate where it freezes over winter and thaws in the spring causing cracks and fissures to form. The oxidized tills are typically underlain by a tight unoxidized dark gray till that retards the vertical movement of water leading to the presence of a perched water table

and thus interflow. Hayashi et al. (1998) reported water flux of 1-3 mm/year through unoxidized tills in wetlands located in Southern Saskatchewan.

This site also had seeps that were covered with collapsed bank materials (zone "c" Figure 21) making them undetectable with the terrestrial Lidar or thermal imagery data. One of the limitations of both techniques is that the seep must be exposed in order for it to be detected. Erosion at this site occurred predominantly from the top of the river bank (zone "a", "b", and "c" in Figure 21), with the bottom half of the river bank serving as a deposition zone (zone "d" in Figure 21) between 2012 and 2013 collection periods. The material at the toe of the river bank during the field investigations was primarily failed bank material from the top of the bank. During the next spring discharge events, the deposited materials will be partially or fully excavated allowing the erosion processes to continue.

Effect of Soil Moisture and Soil Color on Lidar Return Intensity

The Lidar return intensities in both 2014 and 2015 data collection campaigns at Carver Creek varied inversely with soil water content (Figure 23). However, the relationships differed between the two dates. An analysis of variance using the multiple regression approach as used by Gupta et al. (2015) showed that the intercepts between the two relationships were significantly different ($t = -18.85$, p value < 0.01) but the slopes of the relationships were statistically similar ($t = -0.17$, p value $= 0.86$). This indicates that the relative change in Lidar return intensity between the two collection periods was similar and this shift in the intercept is likely due to the use of a different Lidar system.

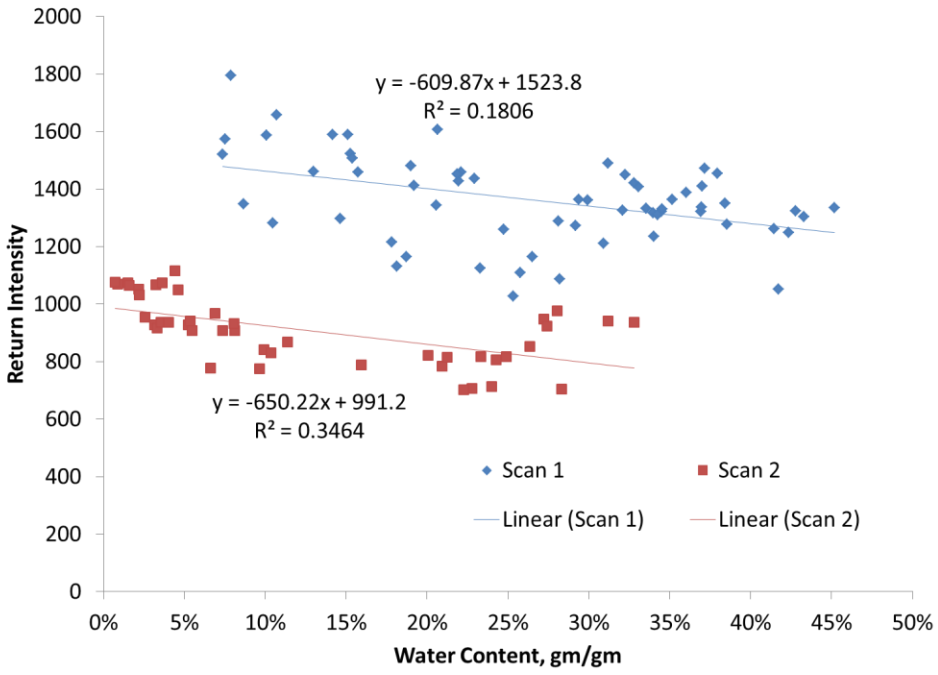

Figure 23. Relationships between Lidar return intensity from terrestrial Lidar and soil water content during the 2014 and 2015 data collection campaigns at the Carver Creek site.

In 2014 scan, there was also more variability in return intensities at a given water content (Figure 22). We envisioned this variability as result of varying colors of different layers at the site. Preliminary analysis using soil colors from Munsell color charts showed some merits to this hypothesis. Since we had not collected our data by soil layer in 2014 campaign, we were unable to fully parse color effects in 2014 return intensities. To address the effect of soil color on return intensity, in 2015 campaign we collected data by soil layer as well as devised a controlled experiment to simultaneously test soil color and wetness effects on terrestrial Lidar return intensities.

Consistent with 2014 scan as well as published literature (Lobell and Asner, 2002), the 2015 data showed a general decreasing trend in return intensity as a function of soil water content (Figure 24). However, there were some differences in the relationship among various soil layers (Figure 24). For example, layers 1, 2, and 5 all showed similar relationship between return intensity and soil water content but layers 3, 4, and 6 all indicated different relationships. These results supported our hypothesis that return intensity is also a function of other soil properties such as soil color. As such, the controlled experiment with natural and painted cores at two water contents (Figure 17) evaluated to what extent soil color may be affecting return intensity values (see Figure 18).

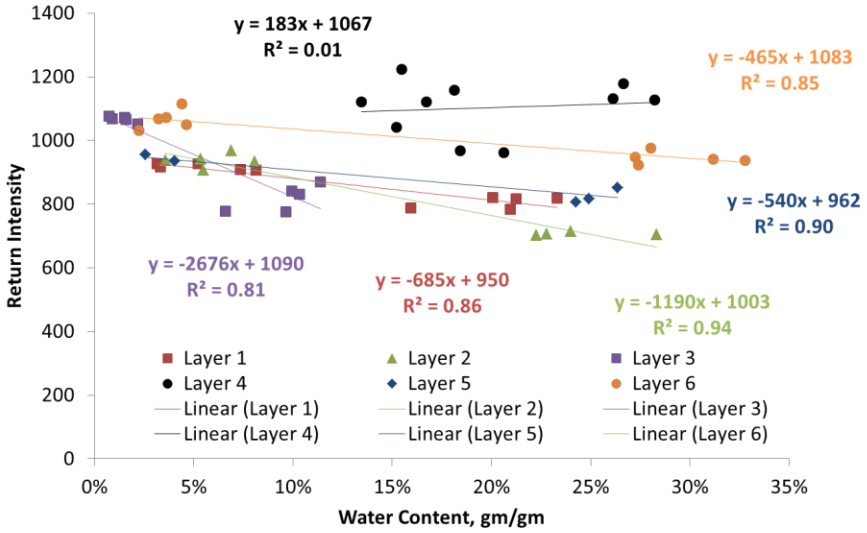

Figure 24. Regression relationships between Lidar return intensity and soil water content for various soil layers in the Carver Creek ravine.

Figure 25 shows the relationships between Lidar return intensity and water content of soil cores that had been painted with various color latex paint. The results show that Lidar return intensities are influenced more by soil color than by soil water content. For example, return intensities from black, red, and brown painted soils showed little variation as a function of water content. Comparatively, yellow colored soil cores followed by natural colored soil cores (i.e. no paint applied) showed a decrease in return intensity with an increase in soil water content; observations similar to in-situ field measurements plotted in Figure 23 and Figure 24. These results suggest that while there is a relationship between Lidar return intensity and soil moisture in relatively light colored soils, other factors such as soil type and/or color may be dominating or at least need to be considered. Although the core experiment covered a range of colors from highly adsorbent (black) to moderately reflective (yellow), in many soil profiles or river banks, it is unlikely that there will be such a wide variation in color at any given location.

In addition to characterization of soil moisture effects on Lidar return intensity, a GCD analysis was also conducted for the Carver Creek ravine using the 2014 and 2015 Lidar data. Only the inverse distance weighted spatial interpolation technique was used in the GCD calculations since previous analysis at site #1 (The Blue Earth River) indicated little impact of different spatial interpolation techniques on net volume loss estimates (see Table 12). The GCD results showed that over 1,178 m^3 of net soil erosion occurred at this site between 11 June 2014 and 23 April 2015 (Figure 26). Considering that the bulk density values at the site ranged from 1.3 Mg m^{-3} to 1.6 Mg m^{-3}, the mass

wasting estimates ranged from 1,531 Mg to 1,885 Mg of soil loss from the site in less than one year.

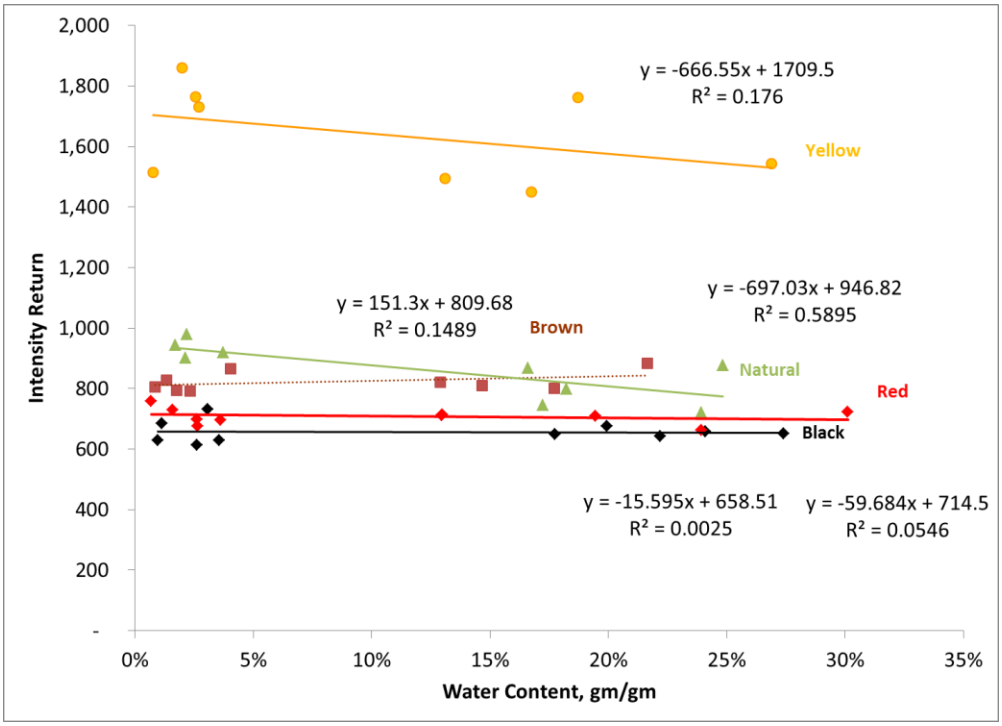

Figure 25. Relationship between Lidar intensity and water content of soil cores that had been painted with various colors.

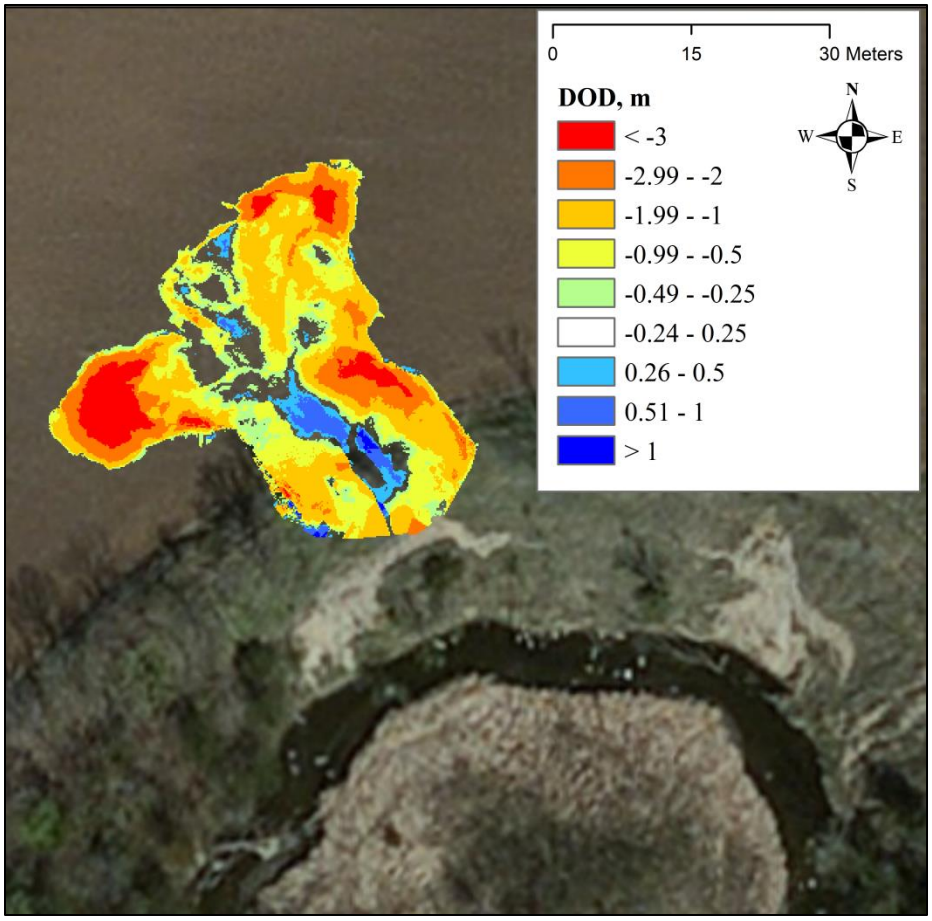

Figure 26. Geomorphic change detection (GCD) analysis of the Carver Creek ravine showing erosion (red) and deposition (blue) between 11 June 2014 and 23 April 2015. Areas with no color corresponds to areas with 0.25 m of erosion or deposition.

Characterization of Seepage Induced Bank Erosion Using Airborne Lidar

The 2009 RIM derived from airborne Lidar data readily identified the seep locations on a river bank in Blue Earth County, MN (Figure 27a). The threshold DOD indicated a net volume loss of 17,234 m^3 (18,316 m^3 of erosion and 1,082 m^3 of deposition) between 2009 and 2012 (Figure 27b). These results are similar to the DOD generated estimates using terrestrial Lidar at site#1 as well as consistent with the findings of Kessler et al. (2012) that the majority of volume change in river banks was driven by large (> 2 m)

changes in elevation. These results further show that the seepage location causing bank erosion could also be delineated in RIM derived from airborne Lidar (Figure 27c).

In both the 2009 (Figure 27a) and 2012 (Figure 27c) RIMs, the seepage locations corresponded directly with the location of mass failures of the river bank (Figure 27b). This suggests that RIMs derived from airborne Lidar have the potential to delineate the seep locations on river banks. Furthermore when used in conjunction with Airborne Lidar, DODs can provide a technique to evaluate the effect of seepage on river bank erosion. However in this bank, substantial erosion also occurred on the left side of the river bank (Figure 27b) without an indication of seepage in the 2009 (Figure 27a) or 2012 (Figure 27c) RIMs. Since we have observed several seepage spots along that portion of the bank at other times during our field visits, it is likely that the seepage area was masked by deposited bank material. However, it is also possible that other physical processes drove the failure on the left side of the river bank. Several mechanisms including floods, freeze/thaw, undercutting, and sapping have been identified to cause river bank failures (Hooke, 1979; Hagerty, 1991a, b; Wilson et al., 2007; Zinger et al., 2011). It is likely that all or some of these processes played a role in river bank erosion even in this stretch of the river. The techniques presented in this study provide a tool to evaluate where and how often the seepage drives river bank failures in the GBERB and other watersheds in the Upper Midwestern United States.

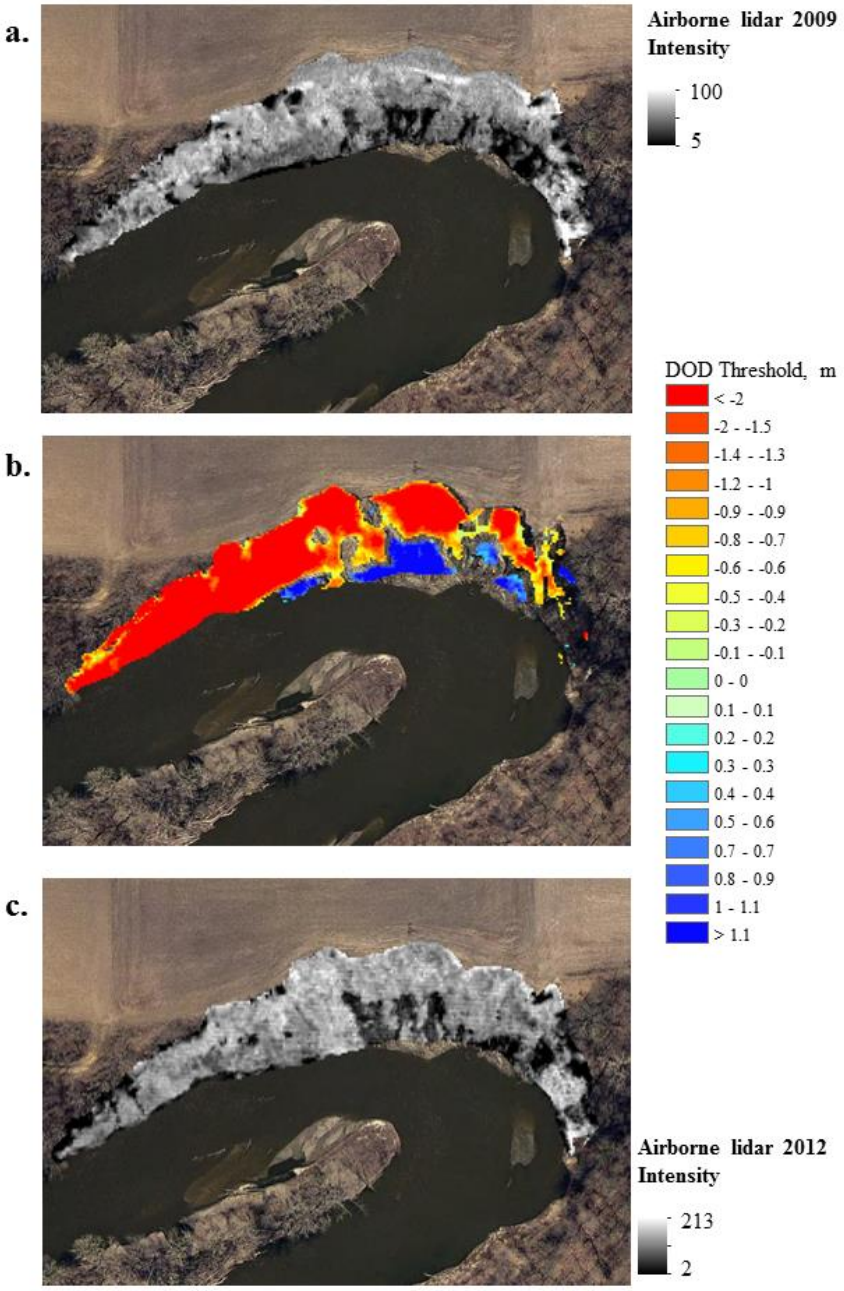

Figure 27. The 2009 Lidar return intensities (a), the difference in digital elevation models with a fuzzy inference system threshold (b), and the 2012 Lidar return intensities (c) for a 27 m tall river bank on the Blue Earth River.

CONCLUSIONS

Both terrestrial and airborne Lidar derived return intensities successfully delineated seepage locations on river banks at two different locations in Blue Earth County, MN. The results also established that Lidar derived RIMs are a suitable alternative to thermal imaging techniques for identifying seepage locations along river banks. Furthermore, all three different Lidar systems (1 airborne, 2 terrestrial) with laser wavelengths in two different portions of the electromagnetic spectrum were able to delineate seepage locations, indicating the technique is robust across different platforms. The field experiments conducted at the Carver Creek ravine show a significant relationship between Lidar return intensity and soil moisture for various soil layers. However, a controlled experiment with painted soil cores at various soil water contents suggests that the Lidar return intensities are also affected by soil color. In general, darker color soil will overwhelm the differences in return intensity from differences in soil water contents. This suggests that Lidar based system may have limitations in delineating seep areas in darker colored soils. This is, particularly important if a Lidar system used to characterize bank erosion operates in the green portion (i.e. 532 nm) of the electromagnetic spectrum.

We also demonstrate that seepage locations from RIMs could be combined with DODs either from terrestrial or airborne Lidar to evaluate the impact of seepage on river bank mass failures. As multi-temporal airborne Lidar becomes more commonly available, it presents an opportunity to use the method developed in this study to quantify the extent of seepage driven river bank erosion across river networks especially in the

Upper Midwestern United States where bank erosion is a major source of sediments to the rivers.

REFERENCES

Belmont, P., K.B. Gran, S P. Schottler, P R. Wilcock, S.S. Day, C. Jennings, J.W. Lauer, E. Viparelli, J.K. Willenbring, D.R. Engstrom, and G. Parker. 2011. Large shift in source of fine sediment in the upper Mississippi River. Environmental Science and Technology. 45:8804-8810, DOI: dx.doi.org/10.1021/es2019109.

Brennan, R., and T. L. Webster. 2006. Object-oriented land cover classification of Lidar-derived surfaces. Canadian Journal of Remote Sensing. 32:162-172.

Bryant, R., D. Thoma, S. Moran, C. Holifield, D. Goodrich, T. Keefer, G. Paige, D. Williams, and S. Skirvin. 2003. Evaluation of hyperspectral, infrared temperature and RADAR measurements for monitoring surface soil moisture. In Proceedings of the First Interagency Conference on Research in the Watersheds Symposium. Benson, AZ, USA, Oct. 27-30: pp. 528-533.

Chu-Agor, M.L., G.A. Fox, and G.V. Wilson. 2009. Empirical sediment transport function predicting seepage erosion undercutting for cohesive bank failure prediction. Journal of Hydrology. 377:155-164, DOI: 10.1016/j.jhydrol.2009.08.020.

Chu-Agor, M.L., G.A. Fox, R.M. Cancienee, and G.V. Wilson. 2008. Seepage caused tension failures and erosion undercutting of hillslopes. Journal of Hydrology. 359:247-259. DOI: 10.1016/j.jhydrol.2008.07.005

Deitchman, R.S., and S.P. Loheide II. 2009. Ground-based thermal imaging of groundwater flow processes at the seepage face. Geophysical Research Letters. 36:L14401, DOI: 10.1029/2009GL038103.

Fox, G.A., G.V. Wilson, A. Simon, E.J. Langendoen, O.Akay, and J.W. Fuchs. 2007. Measuring streambank erosion due to ground water seepage: correlation to bank pore water pressure, precipitation and stream stage. Earth Surface Processes and Landforms. 32:1558-1573, DOI: 10.1002/esp.1490.

Gran, K., P. Belmont, S.S. Day, C. Jennings, A. Johnson, L. Perg, and P. Wilcox. 2009. Geomorphic evolution of the Le Sueur River, Minnesota, USA, and implications for current sediment loading. Special Paper 451. Geological Society of America, Boulder, CO.

Gupta, S.C., A.C. Kessler, M.K. Brown, and F. Zvomuya. 2015. Climate and agricultural land use change impacts on streamflow in the upper Midwestern United States. Water Resources Research. DOI:10.1002/2015WRO17323.

Hagerty, D. J. 1991a. Piping/sapping erosion. I: basic considerations, Journal of Hydraulic Engineering. 117:1009-1025. DOI: 10.1061/(ASCE)0733-9429(1991)117:8(991).

Hagerty, D. J. 1991b. Piping/sapping erosion. II: identification-diagnosis. Journal of Hydraulic Engineering. 117:991-1008. DOI: 10.1061/(ASCE)0733-9429(1991)117:8(1009).

Hayashi, M., G. van der Kamp, and D.L. Rudolph. 1998. Water and solute transfer between a prairie wetland and adjacent uplands, International Water Balance. Journal of Hydrology. 207:42-55.

Hooke, J.M. 1979. An analysis of the processes of river bank erosion, Journal of Hydrology. 42:39-62. DOI: 10.1016/j.bbr.2011.03.031.

Kessler, A.C., S.C. Gupta, H.A.S. Dolliver, and D.P. Thoma. 2012. Lidar quantification of bank erosion in Blue Earth County, Minnesota. Journal of Environmental Quality. 41:197-207, DOI: 10.2134/jeq2011.0181.

Lenhart, C.F., M.L. Titov, J.S. Ulrich, J.L. Nieber, and B.J. Suppes. 2013 The role of hydrologic alteration and riparian vegetation dynamics in channel evolution along the lower Minnesota River. Transactions of the ASABE. 56:549-561.

Lindow, N., G. A. Fox, and R. O. Evans. 2009. Seepage erosion in layered stream bank material. Earth Surface Processes and Landforms. 34:1693-1701, DOI: 10.1002/esp.1974.

Meyer, M.L. and S.M. Schellhaass. 2002. Sources of phosphorus, chlorophyll, and sediment to the Mississippi River upstream of Lake Pepin: 1976-1996. A report for environmental studies of phosphorus. Metropolitan Council Environmental Services. http://www.metrocouncil.org/environment/Riverslakes/documents/LakePepinPhosphorusSources.pdf (retrieved February 18, 2011)

Microsoft Office. 20009. Microsoft Excel (computer software), Microsoft, Redmond, Washington.

Midgley, T.L., G.A. Fox, G.V. Wilson, D.M. Heeren, E.J. Langendoen, and A. Simon. 2013. Seepage-induced streambank erosion and instability: in situ constant-head experiments. Journal of Hydrologic Engineering. 18:1200-1210, DOI: 10.1061/(ASCE) He.1943-5584.0000685.

Milan, D.J., G.L. Heritage, A.R.G. Large, and I. C. Fuller. 2011. Filtering spatial error from DEMs: implications for morphological change estimation. Geomorphology. 125:160-171, DOI: 10.1016/j.geomorph.2010.09.012.

Moran, M.S., C.D. Peters-Lidard, J.M. Watts, and S. McElroy. 2004. Estimating soil moisture at the watershed scale with satellite-based radar and land surface models. Canadian Journal Remote Sensing. 30:805-826.

Moran, M.S., D.C. Hymer, J. Qi, and E.E. Sano. 2000. Soil moisture evaluation using multi-temporal synthetic aperture radar (SAR) in semiarid rangeland. Agricultural and Forest Meteorology. 105:69-80.

Muller E. and H. Decamps. Modeling soil moisture-reflectance. Remote Sensing of the Environment. 76:173-180.

Narayanan, R.M., S.E. Gree, and D.R. Alexander. 1993. Mid-infrared laser reflectance of moist soils. Applied Optics. 32:6043-6052.

Pfister, L., J.J. McDonnell, C. Hissler, and L. Hoffmann. 2010. Ground-based thermal imagery as a simple, practical tool for mapping saturate area connectivity and dynamics. Hydrological Processes. 24:3123-3132, DOI: 10.1002/hyp.7840.

Schurch, P., A.L. Densmore, N. J. Rosser, M. Lim, and B. W. McArdell. 2011. Detection of surface change in complex topography using terrestrial laser scanning: application to the Illgraben debris-flow channel. Earth Surface Processes and Landforms. 36:1847-1859, DOI: 10.1002/esp.2206.

Thoma, D.P., S.C. Gupta, M.E. Bauer, and C.E. Kirchoff. 2005. Airborne laser scanning for river bank erosion assessment. Remote Sensing of Environment. 95:493-501, DOI: 10.1016/j.rse.2005.01.012.

Topp, G.C., and P.A. Ferré. 2002. Water Content. In Dane and Topp (eds.) Methods of Soil Analysis, Part 4, Physical Methods. Soil Science Society of America, Madison, WI.

Wheaton, J.M., J. Brasington, S.E. Darby, A. Kasprak, D. Sear, and D. Vericat. 2013. Morphodynamic signatures of braiding mechanisms as expressed through change in sediment storage in a gravel-bed river, Journal of Geophysical Research: Earth Surface. 118:759-779, DOI: 10.1002/jgrf.20060.

Wheaton, J.M., J. Brasington, S.E. Darby, and D.A. Sear. 2010. Accounting for uncertainty in DEMs from repeat topographic surveys: improved sediment budgets. Earth Surface Processes and Landforms. 35:136-156, DOI: 10.1002/esp.1886.

Weidong, L., F. Baret, G. Xingfa, T. Qingxi, Z. Lanfen, and Z. Bing. 2002. Relating soil surface moisture to reflectance. Remote Sensing of the Environment. 81:238-246.

Wilson, G.V., R.K. Periketi, G.A. Fox, S.M. Dabney, F.D. Shields, and R.F. Cullum. 2007. Soil properties controlling seepage erosion contributions to streambank failure. Earth Surface Processes and Landforms. 32:447-459, DOI: 10.1002/esp.1405.

Zinger, J.A., B.L. Rhoads, and J.L. Best. .2011. Extreme sediment pulses generated by bend cutoffs along a large meandering river. Nature Geoscience. 4:675-678 DOI: 10.1038/ngeo1260.

CHAPTER 5: DRAINAGE IMPACTS ON SURFICIAL WATER RETENTION CAPCITY OF A PRAIRIE POTHOLE WATERSHED

SUMMARY

Wetland restoration has been proposed as a tool to mitigate excess runoff and associated non-point source pollution in the Upper Midwestern United States. This study quantified the surficial water retention capacity of existing and drained wetlands for the Greater Blue Earth River Basin (GBERB), an intensively drained agricultural watershed. Using airborne light detection and ranging, the historic depressional storage was determined to be 152 mm. Individual depression analysis suggested that the restoration of most drained areas would have little impact on the storage capacity of the GBERB because the majority (53%) of retention capacity was in large depressions (> 40 ha) which comprised only a small proportion (<1.0%) of the observed depressions. Accounting for change in storage and the difference in annual evapotranspiration (ET) between wetlands and the croplands that replaced them, restoration of all depressions in the Minnesota portion of GBERB would provide a maximum of 131 mm additional capacity over and above the modern day capacity (193 mm; 56 mm depressional storage; 60 mm wetland ET; and 77 mm cropland ET). Considering that depressional depths in smaller areas are within the range of uncertainty of the Lidar DEMs and larger depressions have the most storage, we conclude that efforts to increase the surficial water holding capacity of the GBERB would be best served in the restoration of large (>40 ha) depressions.

INTRODUCTION

Non-point source pollution (NSP) has been singled out as one of the major causes of existing water quality impairment in the United States. Recently, agricultural drainage has been identified as a significant factor contributing to NSP (Skaggs et al., 1994; Woltemade, 2000; David et al., 2010). For example, agricultural drainage in the Upper Mississippi River Basin (UMRB) has been blamed for excessive flows in waterways (Skaggs et al., 1994), as well as a primary source of nitrogen that is reaching the Gulf of Mexico and causing its hypoxic conditions (Mitsch et al., 2001; Rabalais et al., 2002; David et al., 2010). Some of the recent efforts to mitigate NSP in the UMRB have focused on increasing surface storage through natural, constructed, and restored wetlands (Delgado and Berry, 2008; Strock et al., 2010; Tomer et al., 2012). Since the effectiveness of wetlands in reducing excess flow and NSP is dependent upon their capacity and retention time (Crumpton, 2001), their strategic placement in the landscape is also critical for effective NSP reduction (Tomer et al., 2012; Babbar-Sebens et al., 2013).

Wetlands have been widely acknowledged for the functions they provide including flood attenuation, sediment and nutrient retention, and species habitat (see Richardson, 1985; Mitsch et al., 2005a; Mitsch et al., 2005b; Mitsch and Day, 2006). Some efforts have been made to quantify the storage capacity of wetlands in the Upper Midwestern United States (Haan and Johnson 1967; Haan and Johnson 1968a,b;; Moore and Larson, 1979; Ludden et al., 1983; Miller, 1999; Gleason et al., 2007; Liu and Wang, 2008; Minke et al., 2010; Huang et al., 2011). However, several of these studies have focused on small study area, existing wetland, or were done with low resolution elevation

data thus creating uncertainty on the quantity of additional water that the restored wetlands could store. Haan and Johnson (1968a; 1968b) took measurements on only 120 drained depressional areas in Iowa and developed a model to estimate the impacts of tile drainage on river flows. These authors found that for most storm events, tile drainage had a minimal effect on peak discharge in rivers. Moore and Larson (1979) performed a similar modeling study on two small (8 square miles and 17 square miles) watersheds in Jackson County, Minnesota and concluded that drainage increased annual runoff and the peak discharge significantly. For example, Gleason et al. (2007) showed that wetland volume (V) follows a power function relationship of wetland area (A) in the Prairie Pothole Region (PPR) and that relationship varies depending upon the topography of the PPR. For wetlands varying in size from 0.002 ha to 1.29 ha, Gleason et al. (2007) found that there is a greater increase in wetland volume per unit area in the Prairie Coteau and Missouri Coteau regions, than in the rest of the PPR. Using stereoscopic mapping, Ludden et al. (1983) estimated a maximum storage depth of 83 mm for both existing and historic wetlands in 136 km^2 of the Devils Lake Basin in North Dakota. In this analysis, the authors considered only wetlands that were less than 65 ha.

In the past, efforts to calculate the water retention capacity of wetlands across large areas have been hampered due to lack of high resolution topographic data. For example, using a FORTRAN hydrologic simulation program (HSPF), Miller (1999) estimated that the pre-settlement wetlands in the Little Cobb River watershed in Minnesota would reduce modern annual water yield by 67% to 72% at the outlet of the watershed. However, the input to the simulation program was hydric soils from the STATSGO database (USDA, 1994) for pre-settlement wetlands (Miller, 1999). This

author estimated that 63% of the land area was once wetlands, a value far greater than other reports (see Dahl, 2006). Haan and Johnson (1967) used 2 foot contour maps to develop relationships between depression volume, depth and area for two counties in Iowa. The authors concluded that there was a definable relationships between volume, surface area, and depth for the depression in these counties. Later, Wilson (1997) used the data from Haan and Johnson to estimate the storm return period needed to fill these depressions. The author found that the majority of depressions measured by Haan and Johnson (1967) were small in surface area and depth. The above discussion suggests that alternative methods that take advantage of emerging high resolution topographic data for delineating historic wetlands may be helpful in improving the estimates of water retention in prairie pothole region of the Upper Midwestern United States.

With increased availability of high resolution topographic data from light detection and ranging (Lidar), techniques have been developed to quantify the water retention capacity of wetlands (Liu and Wang, 2008; Huang et al., 2011; Shook and Pomeroy, 2011; Shaw et al., 2012). For example, Huang et al. (2011) used airborne Lidar data to quantify the volume of existing wetlands and equivalent runoff depth (floodwater regulation) in Stutsman County, North Dakota. These authors estimated that the maximum amount of runoff that existing wetlands could retain varied from 15% of a 1500 mm runoff event to 63% of a 50 mm runoff event. Shaw et al. (2012) improved upon Huang et al. (2001) estimates by using a fill-spill approach that continuously increased the contributing areas until the upstream wetlands spilled into downstream wetlands. However, both Huang et al. (2011) and Shaw et al. (2012) applied their techniques on small portions of the landscape and also on existing wetlands, thus failing

to account for spatial variation in water retention capacity at larger scales and landscape conditions prior to wetland drainage.

The loss of wetlands in the UMRB has been widely acknowledged. Dahl (2006) estimated a wetland loss of 50% and 89% in Minnesota and Iowa, respectively. In Minnesota, much of this loss in wetlands occurred in the southern part of the state. Although drainage in the Upper Midwestern United States began in the early 1900's, just over 9 million hectares of agricultural land had benefitted from drainage enterprises by 1940 (U.S. Bureau of the Census, 1940). In addition to loss of storage capacity, the drainage of wetlands and their eventual conversion to row crop (corn, *Zea mays* and soybeans, *Glycine max*) agriculture likely led to some loss of evaporative capacity. Studies conducted in the Upper Midwest indicate that annual wetland evapotranspiration (ET) varies from 134 mm to 796 mm (Shjeflo, 1968; Allred et al., 1971; Winter, 1989) as compared to an ET varying from 500 mm to 650 mm for corn and soybeans (Bauder and Emen, 1981**;** Hattendorf et al., 1988; Suryker and Verma, 2009). This further suggests that both Huang et al. (2011) and Shaw et al. (2012) likely underestimated the impact of wetland drainage because they did not account for ET from wetlands.

The goal of this study was to quantify historic and present day water retention capacities in the Greater Blue Earth River Basin (GBERB) and the impact that wetland drainage likely had on surficial storage and ET. The GBERB, a predominantly agricultural watershed in the UMRB (Figure 28), has been heavily tile drained. There is a pervasive belief that tile drainage of wetlands and the predominance of row crop agriculture have altered the landscape hydrology in the GBERB and more broadly in the UMRB, thus increasing sediment and associated NSP (Schilling and Helmers, 2008).

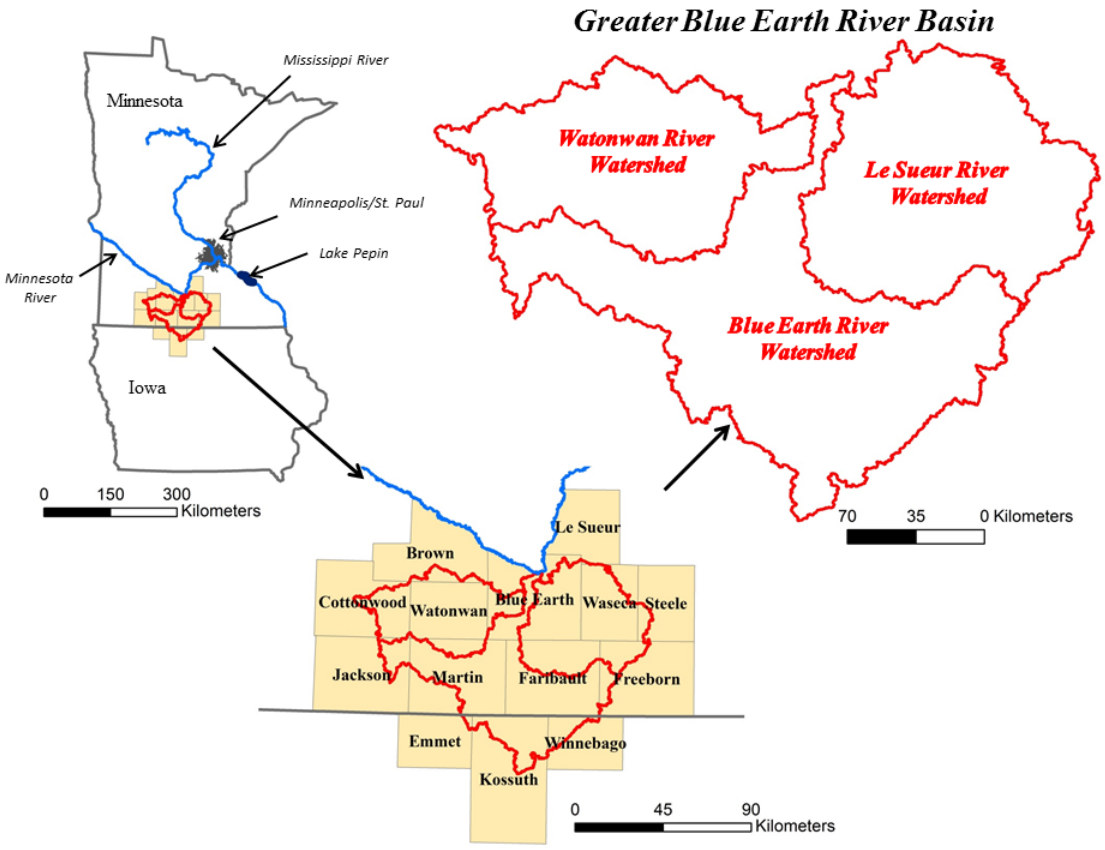

Figure 28. A map of the Greater Blue Earth River Basin (GBERB) showing counties and Hydrologic Unit Code 008 Level watersheds in the GBERB.

The specific objectives of this study were: (1) to quantify the potential water retention capacity of both existing and drained depressions across three eight-digit hydrologic unit code watersheds (hereafter, HUC 8 watersheds) in the GBERB, and (2) to identify the areas at three landscape levels, from individual depressions to HUC 12 and HUC 8 watersheds, where major water retention capacity exists and can potentially be restored. The analysis for the last objective also accounts for changes in ET from the replacement of wetlands by row crop agriculture.

METHODS

Study Area

The GBERB is made up of three major watersheds; the Blue Earth River, Le Sueur River, and Watonwan River watersheds (Figure 28). After the glaciers retreated, a large portion of the area was covered by Glacial Lake Minnesota that subsequently drained and deposited deltaic and outwash materials over much of the watershed (USDA, 1978). The glacial retreat occurred at a fairly even rate creating an undulating, low-relief ground moraine with a number of shallow poorly drained depressions that filled up with surface runoff and groundwater, thus creating many wetlands (Huang et al., 2011). Historically, tall grass prairies were the primary vegetation in the GBERB. Today tile drainage has become common in the area and as much as 74% of the landscape is under row crop agriculture (based upon National Agricultural Statistical Service 2012 Cropland Data Layer). The average annual precipitation (1981 to 2010) for the three HUC 8 watersheds in the GBERB ranges from 751 to 817 mm with rainfall increasing on a gradient from the Northwest to the Southeast.

The rivers in the GBERB generally flow northward draining an area of around 9,200 km^2. The Blue Earth River, Le Sueur River, and Watonwan River watersheds drain approximately 4,050 km^2, 2,280 km^2, 2,260 km^2, respectively, covering portions of 11 counties in Minnesota and three counties in Iowa. The Blue Earth River and the Watonwan River drain the Blue Earth River and the Watonwan River watersheds, respectively, whereas, the Le Sueur, Maple, Big Cobb, and Little Cobb rivers drain the Le Sueur River watershed. Similar to wetlands, the rivers of the GBERB formed at the

end of the last glaciation when the River Warren drained the melt water of Glacial Lake Agassiz (Clayton and Moran, 1982; Matsch, 1983; Gran et al., 2009).

Database

The databases used in this study included Lidar data collected county by county from 2007 to 2010, the location of wetlands based on the national wetlands inventory (NWI) from U.S. Fish and Wildlife Service (USFWS) and drained wetlands based on the restorable wetlands inventory (RWI) from Ducks Unlimited (USFWS, 2011). All data were projected to Universal Transverse Mercator (UTM), zone 15 North, North American Datum of 1983 (NAD83). It was assumed that the differences in collection year and the techniques employed to gather the Lidar data had a minimal impact on topographical measurements since the vertical accuracy amongst all county Lidar scans was similar (17 cm to 28 cm, Table 13). A 3 m bare earth digital elevation model (DEM) generated from the Lidar data was used to estimate the surficial water retention capacity.

Table 13. The reported vertical accuracies of Lidar data sets.

County	State	Vertical accuracy (±), cm
Blue Earth	MN	17
Brown	MN	26
Carver	MN	17
Cottonwood	MN	19
Emmet	IA	≤ 18.5
Faribault	MN	17
Freeborn	MN	28
Jackson	MN	20
Kossuth	IA	≤ 18.5
Le Sueur	MN	18
Martin	MN	22
Steele	MN	23
Waseca	MN	27
Watonwan	MN	27
Winnebago	IA	≤ 18.5

The Lidar data for Minnesota Counties used in this study were collected by Aero-Metric, Inc. Sheboygan, WI. The Blue Earth County, MN Lidar data were collected in April and May 2009 (leaf off conditions) using an Optech ALTM Gemini system flown at 1200 m above ground with a laser pulse rate of 45 kHz and a nominal point spacing of 1 m. The vendor processed the data using proprietary software and delivered bare earth

points, hydrologic breaklines, and 0.6 m contours. Lidar data for all other Minnesota Counties used in this study were collected in May 2010 and November 2010 using Optech ALTM Gemini system flown at 1700 m above ground during leaf off conditions with a laser pulse rate of 34 kHz and a nominal point spacing of 1.3 m. Again, the vendor processed the data using proprietary software and provided a 3 m bare earth digital elevation model. The Iowa Lidar data were collected over multiple periods between May 2007 and May 2010 with a minimum of 18.5 cm RMSE vertical accuracy and 1 m horizontal accuracy. Information on specific sensor, flight altitude, and laser pulse rate for Iowa Lidar scans was unavailable. Independent testing by the U.S. Department of Agriculture, Natural Resources Conservation Service, and the U.S. Department of Transportation confirmed that all Iowa Lidar data used in this study met or exceeded the 18.5 cm RMSE vertical accuracy level. The vertical error in the Lidar data is a potential source of uncertainty that was not accounted for in this study.

The NWI is the official wetland inventory of USFWS and relies on stereo paired photo interpretation to identify wetlands (Cowardin et al., 1979). The RWI was developed to compliment the NWI by using the same mapping protocols, and identified completely drained wetland basins in Minnesota and Iowa that the original NWI did not delineate (USFWS, 2011). The RWI used stereo paired color infrared photographs at 5x magnification to delineate drained wetlands.

Precipitation data were acquired from the Minnesota State Climatology Office. As described by Johnson et al. (2009), the data were created by summing daily observations to create monthly precipitation totals for various monitoring stations. These monthly values were then interpolated to regularly spaced 10-km grid nodes using a

"kriging" technique and a semi-variogram relationship (Davis, 1973). Precipitation for a given watershed was then calculated by overlaying the outline of the watershed boundary on the 10 km grid nodes and taking the average of all grid node values within the polygon. This averaging process was completed via the Surfer program (Keckler, 1994) and additional software created by the State Climatology Office (G. Spoden, personal communication, 2009). Annual precipitation for various watersheds in the GBERB was calculated for the period 1981 to 2010.

Lidar Data Processing

In order to accurately calculate the water retention capacity of drained depressions and wetlands in a landscape, their locations must first be identified. Accurately identifying the location of existing and drained wetlands is problematic and has been the focus of numerous research efforts (see Ozesmi and Bauer, 2002). As a metric for drained depressions and wetlands (hereafter referred to as depressions), a Geographic Information System (GIS) was used to identify surface flow sinks in a landscape. These surface flow sinks were subsequently used to calculate water retention capacity of depressions. This technique has also been used by others (Liu and Wang, 2008; Huang et al., 2011; Shook and Pomeroy, 2011; Shaw et al., 2012) to estimate the volume of wetlands.

In this study, a 3 m DEM derived from the Lidar data was filled to identify flow sinks in the GBERB. Huang et al. (2011) demonstrated that the filled surface can be used to identify the maximum water level in a depression. The difference between the filled surface DEM and the original DEM (showing the bottom of the depression) was used to identify areas where flow sinks are located and the associated storage volume. After all

areas within the GBERB requiring filling were identified, the flow sinks with a filled surface area ≥ 50 m^2 were characterized as depressions and were assumed to have the potential to retain water. Flow sinks with surface area ≤ 50 m^2 were considered erroneous or too small to impact the total retention capacity estimates. The volume of flow sinks was summed together to calculate the water retention capacity of the GBERB, HUC8, and HUC 12 watersheds. Since the DEM fill analysis also indicated several flow sinks in the river channels, those were manually removed from the depressions database. A sensitivity analysis was also run to characterize the impact of removing depressions with area < 50 m^2 on surficial water retention capacity. This analysis was done at 10 m^2 increments until 50 m^2 was reached. At each increment of depression removal, the number, area, and volume of the remaining depressions were re-calculated.

Surficial Water Retention Capacity

Four tiers of depressional water retention capacity were estimated for the GBERB. These tiers were: (1) individual depressions, (2) 111 HUC 12 watersheds, (3) three HUC 8 watersheds, and 4) the entire GBERB. For tiers 2-4, individual depression volumes and areas were aggregated and the retention depth was then calculated as the aggregated volume divided by the watershed area corresponding to that tier. In addition, the individual depressions data were also grouped by surface area to quantify the degree to which a class of depression contributes to net retention capacity of the GBERB. The depth of an individual depression was assessed by dividing the depressional volume with its surface area.

The methods used above have the potential to overestimate retention capacity by including flow sinks that are a result of errors inherent in all DEMs rather than due to real depressions (Lindsay and Creed, 2005). To evaluate the degree to which Lidar derived depressions might overestimate retention capacity, we also calculated the modern retention capacity based on the location of current wetlands from NWI data and restorable wetlands from RWI data. While NWI data were available for the entire GBERB (including Iowa), RWI data were only available for the Minnesota portion of the GBERB at the time of this study. The modern retention depth provides a conservative estimate of modern surficial storage.

Volume of Existing Water Bodies

At a few locations, water was present at the time of the Lidar data acquisition. Since lasers in near-infrared wavelengths were used to collect the Lidar data and since these lasers do not penetrate water, the bottom of water filled bodies could not be identified. As such, the technique described above underestimates the depressional retention capacity of areas where water was present during near-infrared Lidar acquisition. To account for water filled depressions at the time of Lidar acquisition, the volume beneath the water surface was estimated from the relationship between the surface area and volume of empty depressions (Gleason et al., 2007; Huang et al., 2011). The hydrologic breaklines provided by the Lidar vendors for the Minnesota portion of the GBERB, were used to identify areas where water was present at the time Lidar data were acquired. Since hydrologic breaklines were not provided by the vendors for the Iowa portion of the study area, retention volume below the water surfaces for that portion of

GBERB was not estimated. This lack of data likely underestimated the retention capacity for the Iowa portion of the study area.

Relationship between Volume and Area of Wetlands

Gleason et al. (2007) showed that differences in wetland morphology and landscape topography results in different volume to surface area relationships. In this study, a volume to surface area relationship was also developed for depressions < 10 ha in the GBERB and compared to the relationships developed by Gleason et al. (2007). This comparison was made to assess if regional water retention capacity trends exist in the PPR of the UMRB. The threshold of < 10 ha was selected in our analysis to be consistent with the size of wetlands included in Gleason et al. (2007) analysis.

Wetland Drainage Impacts on ET and Surficial Storage

Since drained wetlands in the GBREB are presently occupied by row crops such as corn and soybean, an additional analysis was also performed that accounted for differences in ET of crops versus ET from wetlands on surficial water retention capacity. This analysis was done for two extreme annual precipitations representing a drought (500 mm) and an extremely wet condition (1200 mm). The lowest and highest annual precipitations in the Blue Earth, Le Sueur and Watonwan River watersheds from 1930-2009 were 412 mm in 1976 and 1147 mm in 1993 (G. Spoden, personal communication, 2009). The premise of this analysis was to estimate the increase in surficial storage after accounting for higher ET losses from historic wetlands relative to modern agricultural landscape. For large wetlands, deep and shallow ground water infiltration is a minor part

of wetland hydrology (van der Kamp and Hayashi, 2009) and was not considered in this analysis. As such, the estimates of wetland ET in this analysis were explicit to standing water only.

The change in surficial retention depth, R_c, resulting from depression and wetland drainage was calculated by subtracting the modern retention depth, R_m, from the historic retention depth, R_h. The modern retention depth was set equal to the retention depth estimated using the NWI data, whereas the historic retention depth was set equal to the retention depth estimated from Lidar DEMs. Because of the differences in wetland delineation technique in NWI classification relative to the method used to identify depressions with Lidar data, it is possible that there was some impact on estimates of R_c. It is also likely that some level of depression filling occurred from agricultural erosion that is not accounted for in R_c calculations.

Since drained wetlands in GBREB are presently occupied by row crops such as corn and soybean, we searched the literature for annual ET values for wetlands and row crops. In the Upper Midwestern United States, wetland and lake ET varies from 134 to 796 mm y^{-1} (Shjeflo, 1968; Allred et al., 1971; Winter, 1989) as compared to 500 to 631 mm y^{-1} for row crops (Bauder and Emen, 1981; Hattendorf et al., 1988, Suryker and Verma, 2009). The difference between wetland ET and row crop ET thus ranges from -366 mm yr^{-1} to 165 mm yr^{-1}.

The historic ET (ET_h) of depressions and wetland was estimated as:

$$ET_h = \frac{A_d * ET_{wet}}{A_{GBERB}} \quad (1)$$

where A_d is the historic area of all depressions derived from Lidar, ET_{wet} is the annual ET for wetlands from the literature, and A_{GBERB} equals the area of the GBERB. The modern ET (ET_m) from existing wetlands and the cropland areas where historic depressions had been drained was calculated as:

$$ET_m = \frac{(A_d - A_{nwi}) * ET_{row} + A_{nwi} * ET_{wet}}{A_{GBERB}} \qquad (2)$$

where A_{nwi} equals the modern day wetland area from NWI database, and ET_{row} equals the annual ET from row crops, the change in ET (ET_c) was then calculated as the difference between ET_h and ET_m.

The above calculated ET_c, assumes that all areas of surficial water storage evaporated/transpired at the same simulated rate, thus providing an estimate of the maximum reduction in annual ET that might have occurred when wetlands were drained and converted to row crop agriculture. However, shallow wetlands can dry out earlier in the season thus reducing their annual ET to a maximum of their retention capacity (Shjeflo, 1968). To account for depressional drying, another simulation was conducted where annual ET of depressions was restricted to its average depth when the simulated annual ET was greater than the average depth of a depression. In both simulations, three sets of scenarios were run where maximum annual ET for depressions was set at 600 mm, 700 mm and 800 mm, whereas the row crop annual ET was set at 550 mm for all scenarios.

RESULTS AND DISCUSSION

Threshold Sensitivity Analysis

A total of over 9 million flow sinks covering an area of 208,794 ha (23% of the GBERB area) were identified within the GBERB (Table 14). On average, these flow sinks represented 4 depressions per hectare of basin area. To cut down the number of computations, various threshold values of depressions were tested (Table 14). Setting a threshold of 50 m^2 surface area for depressions removed over 8 million sinks which were equivalent to 5.1% of the total surface area of the depressions, 0.06% of the total water retention capacity, and 0.01 mm of retention depth. This indicates that setting a 50 m^2 threshold did not significantly impact the retention capacity estimates for the GBERB. Expanding the threshold to exclude erroneous flow sinks (<5000) within river channels (0.3% of depressional surface area) further decreased the water retention capacity by 0.48%, and retention depth by 0.79 mm. This analysis indicates that even with removing 93% of the initial flow sinks, the majority of the water retention capacity of the basin was maintained. The remainder of the analysis described below, used depressions > 50 m^2 with the erroneous flow sinks within river channels removed.

Table 14. The results of the threshold sensitivity analysis showing percent volume and surface area unaccounted for when depressions less than 50 m^2 were dropped from the

final calculations. Dropped depressions show the impacts of removing artificial flow sinks found within active river channels.

Threshold	Count	Area, ha	Volume, Mm^3	Depth, mm	Area removed, %	Volume removed, %
All	9,010,802	208,794	-	-	-	-
> 10 m^2	2,731,026	203,142	1,400.8	152.4	2.7%	-
> 20 m^2	1,493,311	200,914	1,400.5	152.3	3.8%	0.02%
> 30 m^2	1,030,254	199,664	1,400.3	152.3	4.4%	0.04%
> 40 m^2	799,915	198,835	1,400.1	152.3	4.8%	0.05%
> 50 m^2	666,043	198,232	1,399.9	152.3	5.1%	0.06%
Drop rivers	661,368	197,147	1,393.3	151.5	5.6%	0.54%

Surficial Water Retention Capacity

The historic water retention depth of the GBERB was estimated at 152 mm from over 600,000 depressions covering 21% of the GBERB area (Table 15). Considering the average annual precipitation (751 mm to 817 mm from 1981 to 2010) for the three HUC 8 level watersheds in the GBERB, historic depressions when empty could potentially store 19% to 20% of the modern annual precipitation. Individually, the historic water retention capacity of the Blue Earth, the Le Sueur and the Watonwan River watersheds equaled 143 mm, 193 mm, and 114 mm, respectively. The higher historic retention capacity (152 mm) of the GBERB was from disproportionately more contributions of surface storage in the Le Sueur River watershed. This is well apparent from the greater

average depth of the depressions in the Le Sueur River watershed (0.88 m) relative to the Blue Earth River watershed (0.65 m), or the Watonwan River watershed (0.58 m) (Table 15). This greater average depth of depressions in the Le Sueur River watershed is likely due to slightly greater topographic variation in the Le Sueur River watershed (average slope =3.4%, std. dev. = 5.9), as compared to the Blue Earth River (average slope = 3.3%, std. dev. = 5.1) and the Watonwan River (average slope = 2.8%, std. dev. = 5.1) watersheds.

Table 15. The water retention capacity and area of depressions in the Greater Blue Earth River Basin.

Watershed	Watershed area, km^2	Count	Volume, Mm^3	Area, ha	Retention depth, mm	Percent of GBERB, %
GBERB	9,194	661,368	1,393	197,147	152	21%
Blue Earth	4,054	253,411	578	89,255	143	22%
Watonwan	2,262	183,527	259	44,657	114	20%
Le Sueur	2,878	224,430	557	63,235	193	22%

Figure 29 shows the distribution of water retention depth (Figure 29a) and volume (Figure 29b) of 111 HUC 12 watersheds in the GBERB. The historic water retention depth of HUC 12 watersheds ranged from 23 mm to 915 mm. Comparatively, the historic volume of HUC 12 watershed ranged from 1.8 Mm^3 to 53.8 Mm^3. Of the 111 HUC 12 watersheds, five had retention depths $\geq$ 400 mm and 20 had retention depths $\geq$ 200 mm, thus leaving 82% of watersheds with retention depths of < 200 mm and 34% of

the watersheds with retention depths < 100 mm. This suggests that while the retention capacities of most areas in the GBERB were relatively small, portions of the historic landscape had a very large capacity to retain water.

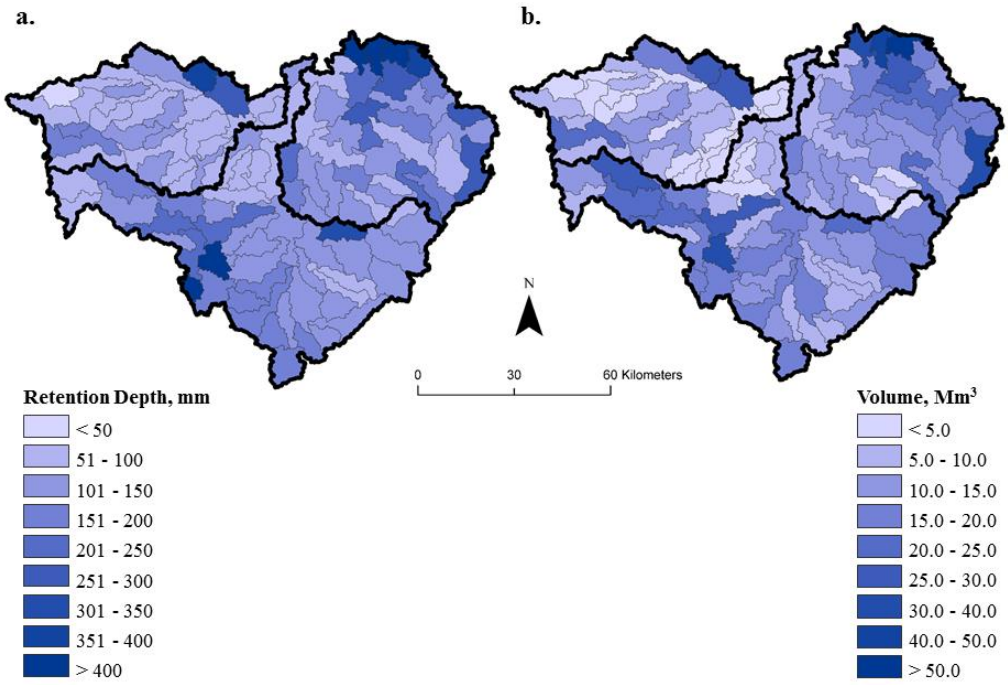

Figure 29. Historic retention depth (a) and volume (b) of depressions within HUC 12 watersheds in the Greater Blue Earth River Basin.

The uneven distribution of the historic water retention capacity in the GBERB landscape is further confirmed by the water retention capacity of individual depressions (Figure 30). This analysis shows that 53% of the total retention capacity (Figure 30a) in the GBERB was in depressions > 40 ha in area. This is equivalent to < 1.0% of the total number of depressions (Figure 30b) and 29% of the total depressional area (Figure 30c) in the GBERB. This analysis also shows that larger depressions have a greater potential

to provide retention due to greater depressional depth (Figure 30d). For example, depressions with area > 40 ha had an average depth of 1.28 m compared to 0.15 m for depressions < 1 ha in size. This again suggests that a vast majority of depressions in GBERB provided a very small retention capacity and most of the historic capacity was concentrated in relatively few large volume water bodies. While depressions with smaller surface areas have average depths within the range of Lidar data uncertainties, they only account for a small portion of the net retention depth. This also shows that, erroneously including false depressions or missing some real depressions would have little impact on the net retention depth estimates.

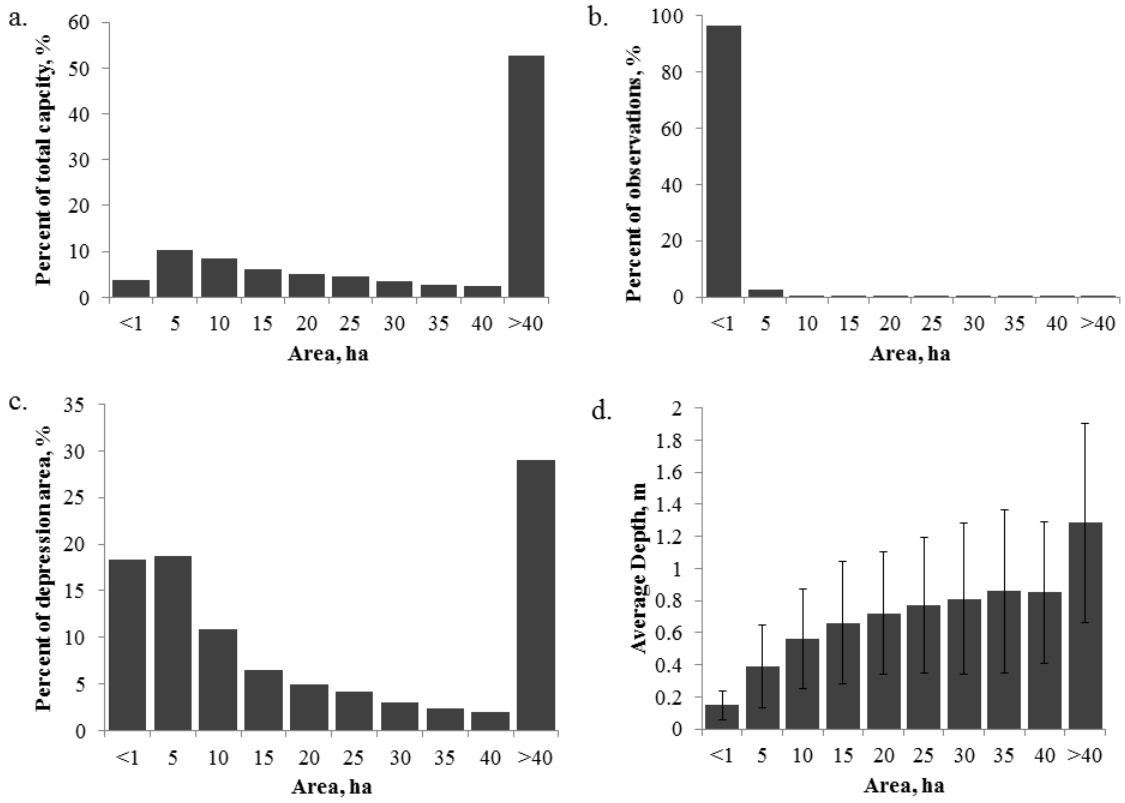

Figure 30. The water retention capacity (a), percent of total observations (b), depressional area as a percent of the watershed area (c), and average depth with standard deviation (d) for various categories of depressional area in the Greater Blue Earth River Basin.

The 57 largest depressions by volume, or 0.009% of total observed depressions, accounted for 25% of the historic retention capacity (Figure 31a); whereas the 460 largest depressions by volume, or 0.07% of total observed depressions, accounted for 50% of the historic retention capacity (Figure 31b). Similarly, 0.4% (2301 depressions) and 1% (8403 depressions) of the depressions accounted for 75% (Figure 31c) and 90% (Figure 31d) of total historic retention capacity. These results indicate that efforts to increase surficial storage capacity to reduce river flows and NSP through restoration of

drained depressions would likely be most effective by focusing on large depressions that have the potential to retain the greatest volume of water or account for the majority of historic water holding capacity. For a similar landscape in Iowa, Tomer et al. (2013) found 11 sites that could store water through restored or constructed wetlands and in turn reduce excess flow. Using the AnnAGNPS watershed simulation model, Tomer et al. (2013) also showed that wetland restoration could reduce nitrogen transported to rivers by 11% to 13%. The results of our analysis indicate that the majority of depressions in the GBERB have a limited capacity to provide surficial water storage that will reduce excess flows and NSP to rivers. However, targeted opportunities similar to those described by Tomer et al. (2013) do exist at a finer scale. The data in Figure 29 indicates that efforts directed at restoring depressions that are > 40 ha in area would likely be most effective in increasing the retention capacity of the GBERB. These depressions account for <1% of the observed depressions but 53% of the retention capacity in the GBERB.

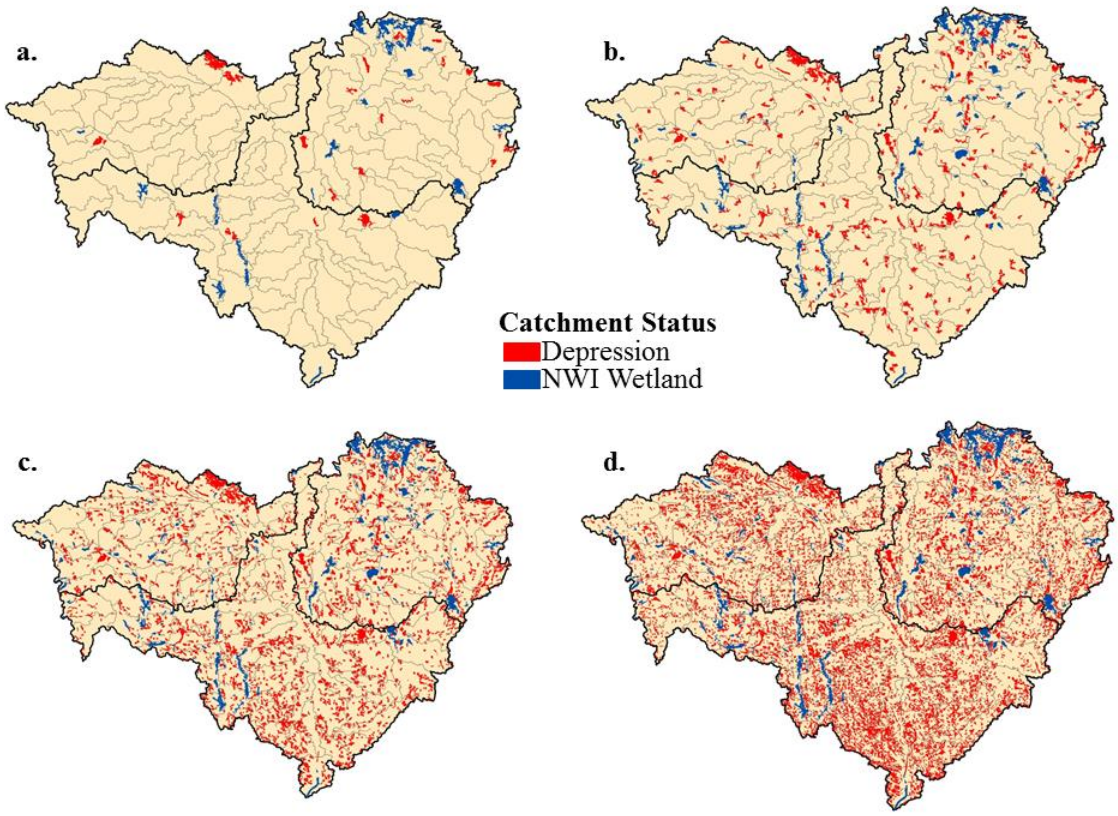

Figure 31. Location of depressions from the Lidar analysis and existing wetlands from the National Wetlands Inventory that account for 25% (a), 50% (b), 75% (c), and 90% (d) of the total historic retention capacity.

A comparison of the modern water retention capacities estimated using the NWI and RWI databases versus the Lidar measurements (historic depressions) showed that the Lidar based water retention capacities were higher (Table 16). For example, the retention capacities estimated using the RWI (56 mm) plus NWI (42 mm) databases were 98 mm; 54 mm less than the Lidar derived depressional retention capacities in the Minnesota portion of the GBERB. Since over 450,000 more depressions were identified in the Lidar analysis relative to the NWI and RWI estimates (Table 16**Error! Reference source not**

ound.), it is likely that some of the Lidar identified depressions were not historically wetlands. For example, there are locations within the GBERB where roads cross large ravines. These areas would likely have been identified as depressions capable of retaining water with the road acting a false dam in the Lidar derived DEM. Although not a historic wetland, a ravine crossed by a roadway certainly could be modified to retain water. In addition, Table 16 does not account for historic wetlands for the Iowa portion of the GBERB as they are not included in the RWI database. This suggests that the retention capacity estimates from the Lidar derived depressions provide an approximation of the maximum retention capacity of the GBERB. However, it is possible that some depressions have been filled overtime due to anthropogenic activities and those depressions are unaccounted for in the present study.

Table 16. Comparison between retention capacity estimates from the Restorable (RWI) and National (NWI) Wetlands Inventory and the Lidar DEM based historic depressions.

Database	Count	Wet area, ha	Volume, m^3	Retention depth, mm
RWI	123,160	109,016	46,931	57
NWI	13,436	32,095	34,662	42
RWI & NWI	136,596	141,112	81,593	98
Historic Depressions	623,993	173,310	125,915	152

Volume-Area Relationship of Drained Depressions

A close relationship (Eq. 3) existed between the volume (V) and surface area (A) of dry depressions (i.e. depressions not under water at the time of Lidar scan) in the GBERB ($r^2 = 0.88$).

$$V = 0.204A^{1.46} \quad (3)$$

Next we used this relationship to calculate the volume of water present in depressions that were filled with water during Lidar acquisition. The surface area of the water filled depressions was calculated from the Lidar derived hydrologic breaklines. This area was then used in Eq. (3) to estimate the retention capacity of water filled depressions. These calculations showed that the retention capacity concealed beneath water surface during Lidar acquisition provides another 29 mm of retention depth to the historic estimates for the entire GBERB. Large water bodies (> 10 ha) accounted for 26 mm of the 29 mm

additional capacity in water filled depression at the time of Lidar acquisition for the Minnesota portion of the GBERB. This additional retention depth suggests that the historic surficial retention capacity of the GBERB may have been as high as 181 mm. The remainder of the analysis in this paper did not include storage beneath water present during Lidar acquisition, because the areas where water was present during Lidar acquisition were not available for the Iowa portion of the GBERB.

To further compare volume-area relationship of depressions in the GBERB with depressions in other areas of the PPR, a similar regression analysis was also done with a subset of dry depressions (< 10 ha in area). The subset (<10 ha in size) was chosen to match the range in depressional sizes used by Gleason et al. (2007). This analysis also showed a strong power function relationship ($R^2 = 0.87$, $P < 0.01$, Figure 32) similar to those reported by Gleason et al. (2007). However for the GBERB, there was a slightly lower increase in storage capacity with an increase in surface area compared to other parts of the PPR (Figure 32). This suggests that depressions in the GBERB are relatively more flat than other parts of the PPR or the Upper Midwestern United States. These differences are likely a reflection of the inherent topography left after the last glaciation some 13,000 years BP. It is also possible that some of the differences between the results of this study and Gleason et al. (2007) relationships may be due to the differences in the methods used to estimate retention capacity.

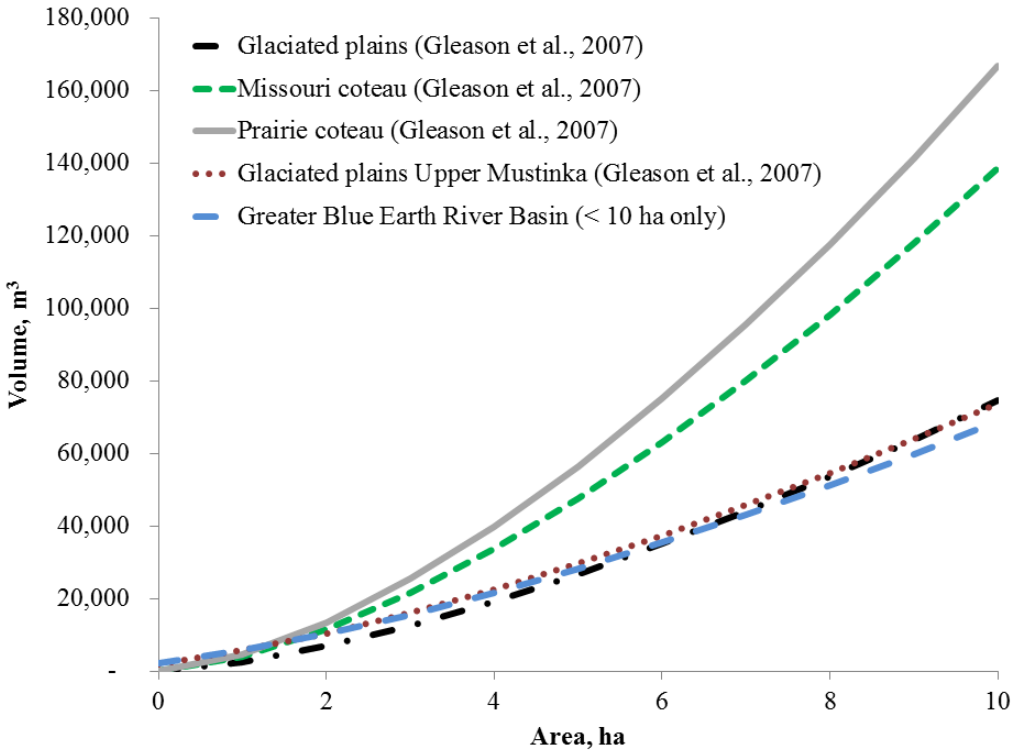

Figure 32. Comparison of regression relationships between volume and surface area of wetlands and depressions in the Greater Blue Earth River Basin relative to other areas in the Upper Midwestern United States.

Drainage Impact on ET and Surficial Storage

Two sets of simulations were conducted for the GBERB to evaluate the change in retention depth as a result of changes in ET (Table 17). The first simulation assumed ET was uniform across all depressional areas. The second simulation restricted ET to a maximum of the average depth of each depression. Under each simulation, three sets of scenarios were simulated. The scenarios corresponded to a maximum ET of 600 mm, 700 mm, and 800 mm from wetlands. For both sets of simulations, the difference between

historic (152 mm) and modern retention (56 mm based on NWI data) was 96 mm (Table 17). This is equivalent to an additional storage of 19% and 8% of the annual precipitations of 500 mm and 1200 mm, respectively. However, 92% of this change in capacity was in drained wetlands > 10 ha, which represent only 0.5% of the depressions. This again demonstrates that the majority of wetland drainage (i.e. drainage of wetlands < 10 ha in area) had very little impact on the retention capacity of the GBERB.

Table 17. Comparison of annual depressional evapotranspiration (ET) and retention depth from the historic (pre-drainage) and modern landscapes. For scenarios 1, 2, and 3 wetlands were assumed to have a maximum ET of 600, 700, and 800 mm, respectively. For all simulations, cropland was assumed to have an ET of 550 mm.

Simulation Set	**Scenario**	**Historic depressions**		**Modern wetlands**		**Modern cropland**		**Difference (Historic – Modern)**		
		Retention Depth	ET	Retention Depth	ET	Retention Depth	ET	Retention Depth	ET	Total Change
1		---mm---								
	1	152	129	56	45	-	77	96	7	103
	2	152	150	56	53	-	77	96	20	116
	3	152	172	56	60	-	77	96	35	131
2*	1	152	93	56	23	-	77	96	-7	89
	2	152	102	56	26	-	77	96	-1	95
	3	152	109	56	29	-	77	96	3	99

For both set of simulations, ET losses from historic depressions (Lidar data) varied from 93 to 172 mm, while ET losses from modern wetlands (NWI data base) varied from 23 to 60 mm (Table 17). On the other hand, ET from croplands within depressions remained the same (77 mm) for all simulations because of the assumption of a constant ET (550 mm) from row crops. This translates to a net decrease in ET of 7 mm to 35 mm from replacement of wetlands with croplands (Table 17). Relative to annual precipitation, this decrease in annual ET from wetland drainage is minor. For example, a marginal difference of 250 mm yr^{-1} ET between row crops (550 mm) and wetland ET (800 mm) resulted in a maximum decrease of 35 mm (Historic ET-Modern Wetland ET-Modern Cropland ET) in annual ET from wetland drainage. This translates to a maximum change of 7% and 3% of annual precipitation ranging from 500 mm and 1200 mm, respectively. If the marginal difference in ET between row crops (550 mm) and wetlands (600 mm) was 50 mm yr^{-1}, surficial water retention in all depressions would only change by a maximum of 1% for annual precipitation of 500 mm and 0.5% when annual precipitation is 1200 mm. This suggests that the impact of wetland conversion to cropland on annual ET was minimal in the GBERB. The marginal change of 250 mm yr^{-1} in ET between row crops (550 mm) and wetlands (800 mm) for the Blue Earth River, Le Sueur River and Watonwan River watersheds corresponded to 4%, 4%, and 5% of 30 year (1981-2010) average annual precipitation of 807mm, 817 mm, and 751 mm, respectively. While ET differences between wetlands and the row crops that replaced them may be up to 250 mm yr^{-1} at individual sites, the maximum impact on the surficial water retention capacity and ET at a watershed (GBERB) scale is rather small.

The second set of simulations, where wetland ET was restricted to the average depth of a depression (i.e. the wetland dries out), showed the modern landscape would provide an additional 7 mm of ET relative to the historic landscape if maximum wetland ET was 600 mm and row crop ET was 550 mm (Table 17). Comparatively, there would be a decrease of 3 mm in ET in the modern landscape if the maximum wetland ET was 800 mm and row crop ET was 550 mm. This indicates that if shallow wetlands dry out, the row crops that replaced them caused only a minor loss in annual ET for the GBERB. The results of both simulations indicate that the impact of wetland drainage on annual basin ET was relatively small.

Considering drainage and associated reduced ET impacts, the loss in surficial water retention capacity varied from 103 to 131 mm for simulation set 1 (maximum ET losses possible) and 89 mm to 99 mm for simulation set 2 (ET losses limited to depression's average depth) (Table 17). Accounting for change in storage from drainage and the difference in annual ET between wetlands and the croplands that replaced them, restoration of all depressions would provide a maximum of 131 mm additional capacity over and above the modern day capacity of 193 mm (Table 17). This analysis did not account for ET from wetland plants that may have been present in depression as they dried. It is possible that wetland restoration along with establishment of perennial crops such as grasses could further increase the retention capacity of the GBERB.

CONCLUSIONS

The historic maximum water retention capacity of depressions in the GBERB was relatively small (152 mm) due to the flat nature of the landscape. However, there

was a large spatial variation in water retention among individual depressions both at HUC 12 and HUC 8 watersheds levels. Our analysis further showed that the majority of the landscape has little capacity to retain water and most of this capacity is concentrated in large depressions > 40 ha in area. Compared with the RWI and NWI, Lidar estimated retention depth appeared to be an over estimate, thus confirming that 152 mm of storage was likely the maximum historic retention capacity of the landscape. The loss in water retention capacity from drainage and associated reduced ET varied from 89 to 131 mm. This storage loss translates to 7% and 26% of the annual precipitation in GBERB during wet (1200 mm) and dry (500 mm) years, respectively. Based on depressional morphology, it appears that GBERB volume-area relationships are on the lower end of the range found in other parts of the PPR. If wetland restoration is implemented to manage river flows and associated NSP in the GBERB then a targeted approach using depression (>40 ha) that had high historic retention capacities (53%) would be advantageous. Further inclusion of medium size (10 to 40 ha) depressions could provide an additional 24% retention capacity. Selection of >10 ha depressional areas for wetland restoration is based on the observation that depressional depths in smaller areas were within the range of uncertainty of the Lidar DEMs.

REFERENCES

Allred, E.R., P.W. Manson, G.M. Schwartz, P. Golany, and J.M.W. Reinke. 1971. Continuation of studies on the hydrology of ponds and small lakes. University of Minnesota Agricultural Experiment Station, Technical Bulletin 274. pp 62.

Babbar-Sebens, M., R.C. Barr, L.P. Tedesco, and M. Anderson. 2013. Spatial identification and optimization of upland wetlands in agricultural watersheds. Ecological Engineering. 52:130-142.

Bauder, J.W. and M.J. Ennen. 1981. Water use of field crops in eastern North Dakota. Farm Research. 38:3-5.

Clayton, L. and S.R. Moran. 1982. Chronology of late-Wisconsin glaciations in middle North America. Quaternary Science Reviews. 1:55-82.

Cowardin, L.M., V. Carter, F.C. Golet, and E.T. Laroe. 1979. Classification of wetlands and deepwater habitats of the United States. U.S. Fish and Wildlife Service FWS/OBS 79/31, Washington, DC.

Crumpton, W.G.. 2001. Using wetlands for water quality improvement in agricultural watersheds: the importance of a watershed scale approach. Water Science Technology. 44:559-564.

Dahl, T.E. 2006. Status and trends of wetlands in the conterminous United States 1998 to 2004. U.S. Department of the Interior, Fish and Wildlife Service, Washington, D.C.

David, M.B., J.E. Drinkwater, and G.F. McIsaac. 2010. Sources of nitrate yields in the Mississippi River Basin. Journal of Environmental Quality. 39:1657-1667.

Davis, J.C.., 1973. Statistics and data analysis in geology. John Wiley & Sons, New York, NY. pp 550.

Delgado, J.A., and J.K. Berry. 2008. Advances in precision conservation. Advances in Agronomy. 98:1-44.

Gleason, R.A., Tangen, B.A., Laughan, M.K., Kermes, K.E., Euliss, and N.H., Jr. 2007. Estimating water storage capacity of existing and potentially restorable wetland depression in a subbasin of the Red River of the North. US Geological Survey Scientific Investigations Report 2007-1159, p. 36. http://pubs.er.usgs.gov/publication/ofr20071159.

Gran, K.B., P. Belmont, S.S. Day, C. Jennings, A. Johnson, L. Perg, and P.R. Wilcock. 2009. Geomorphic evolution of the Le Sueur River, Minnesota, USA, and implications for current sediment loading. The Geological Society of America Special Paper. 451:119-130.

Haan, C.T., and H.P. Johnson. 1967. Geometrical properties of depressions in North-Central Iowa. Iowa State Journal of Science. 42:149-160.

Haan, C.T., and H.P. Johnson. 1968a. Hydraulic model of runoff from depressional areas part I. General considerations. Transactions of the ASAE. 11:364-367.

Haan, C.T., and H.P. Johnson. 1968b. Hydraulic model of runoff from depressional areas part II. Development of the model. Transactions of the ASAE. 11:368-373.

Harrold, L.L. and F.R. Dreibelbis. 1953. Water use by crops as determined by weighing monolith lysimeters. Soil Science Society of America Journal. 17:72-74.

Hattendorf, M.J., M.S. Redelfs, B. Amos, L.R. Stone, and R. E. Gwin. 1988. Comparative water use characteristics of six row crops. Agronomy Journal. 80:80-85.

Huang, S., C. Young, M. Feng, K. Heidemann, M. Cushing, D.M. Mushet, and S. Liu, 2011. Demonstration of a conceptual model for using Lidar to improve the

estimation of floodwater mitigation potential of Prairie Pothole Region wetlands. Journal of Hydrology. 405:417-426.

Johnson, H.O., S.C. Gupta, A.V. Vecchia, and F. Zvomuya. 2009. Assessment of water quality in the Minnesota River using non-parametric and parametric methods. Journal of Environmental Quality. 38:1018-1030.

Keckler, D., 1994. Surfer for windows, version 7.0. Golden Software, Golden, CO.

Lindsay, J.B. and I.F. Creed. 2005. Sensitivity of digital landscapes to artifact depression in remotely-sensed DEMs. Photogrammetric Engineering & Remote Sensing. 71:1029-1036.

Liu, H. and L. Wang, 2008. Mapping detention basins and deriving their spatial attributes from airborne Lidar data for hydrological applications. Hydrological Processes 22:2358-2369.

Ludden, A.P., D.L. Frink, and D.H. Johnson. 1983. Water storage capacity of natural wetland depressions in the Devils Lake Basin of North Dakota. Journal of Soil and Water Conservation. 38:45-48.

Matsch, C.L. 1983. River Warren, the southern outlet of Lake Agassiz. In: Teller, J.T., and Clayton, L., (Eds.)., Glacial Lake Agassiz. Geological Association of Canada Special Paper 26, pp. 232-244.

Miller, J.E. and D.L. Frink. 1984. Changes in flood response of the Red River of the North Basin, North Dakota-Minnesota. Water-Supply Paper 2243, U.S. Geological Survey, Alexandria, Virginia. http://pubs.er.usgs.gov/publication/ofr82774.

Miller, R. 1999. Hydrologic effects of wetland drainage and land use change in a tributary watershed of the Minnesota River Basin: A modeling approach. Master's Thesis, University of Minnesota, St. Paul, Minnesota.

Minke, A.G., C.J. Wetbrook, and G. van der Kamp. 2010. Simplified volume-area-depth method for estimating water storage of prairie potholes. Wetlands. 30:541-551.

Mitsch, W.J., J.W. Jr. Day, J. W. Gilliam, P.M. Groffman, D.L. Hey, G.W. Randall, and N. Wang. 2001. Reducing nitrogen loading to the Gulf of Mexico from the Mississippi River Basin: strategies to counter a persistent ecological problem. BioOne. 51:373-388.

Mitsch, W.J., L. Zhang, C.J. Anderson, A.E. Altor, and M.E. Hernandez. 2005a. Creating riverine wetlands: ecological succession, nutrient retention, and pulsing effects. Ecological Engineering. 25:510-527.

Mitsch, W.J., J.W. Day, L. Zhang, and R.R. Lane. 2005b. Nitrate-nitrogen retention in wetlands in the Mississippi River Basin. Ecological Engineering. 24:267-278.

Mitsch, W.J. and J.W. Day. 2006. Restoration of wetlands in the Mississippi-Ohio-Missouri (MOM) River Basin: experience and needed research. Ecological Engineering. 26:55-69.

Moore, I.D. and C.L. Larson. 1979. Effects of drainage projects on surface runoff from small depressional watersheds in north central region. Water Resources Research Center Bulletin 99. University of Minnesota, Minneapolis, MN.

Ozesmi S.L. and M.E. Bauer. 2002. Satellite remote sensing of wetlands. Wetlands Ecology and Management. 10:381-402.

Rabalais, N.N, R.E. Turner, and D. Scavia. 2002. Beyond science into policy: Gulf of Mexico hypoxia and the Mississippi River. BioOne 52:129-142.

Richardson, C.J., 1985. Mechanisms controlling phosphorus retention capacity in freshwater wetlands. Science. 228:1424-1427.

Schilling, K.E. and M. Helmers. 2008. Effects of subsurface drainage tiles on streamflow in Iowa agricultural watersheds: Exploratory hydrograph analysis. Hydrological Processes. 22:4497-4506.

Shaw, D.A., G. Vanderkamp, F.M. Conly, A. P. Pietroniro, and L. Martz. 2011. The fill-spill hydrology of prairie wetland complexes during drought and deluge. Hydrological Processes. DOI: 10.1002/hyp.8390.

Shejflow, J.B. 1968. Evapotranspiration and the water budget of prairie potholes in North Dakota. US Geological Survey Scientific Investigations Report 585-B, http://pubs.er.usgs.gov/publication/pp585B.

Shook, K.R. and J.W. Pomeroy 2011. Memory effects of depression storage in Northern Prairie hydrology. Hydrological Processes. 25:3890-3898.

Skaggs, R.W., M.A. Brevè, and J.W. Gilliam. 1994. Hydrologic and water quality impacts of agricultural drainage. Critical Reviews in Environmental Science and Technology. 24:1-32.

Strock, J.S., P.J.A. Kleinman, K.W. King, and J.A. Delgado. 2010. Drainage water management for water quality protection. Journal of Soil and Water Conservation. 65:131-136.

Suyker, A.E. and S.B. Verma. 2009. Evapotranspiration of irrigated and rainfed maize-soybean cropping systems. Agricultural and Forest Meteorology. 149:443-452.

Tomer, M.D., W.G. Crompton, R.L. Bingner, J.A. Kostel, and D.E. James, 2013. Estimating nitrate load reductions from placing constructed wetlands in a HUC-12 watershed using Lidar data. Ecological Engineering. 56:69-78.

U.S. Bureau of the Census. 1940. Census of agriculture. Vol. 3, Special reports Part 06. Drainage of agricultural lands. Washington, D.C.: U.S. Government Printing Office.

U.S. Department of Agriculture, Natural Resources Conservation Service, 1994. State Soil Geographic Database (STATSGO), data use information. Miscellaneous Publication Number 1492 U.S. Department of Agriculture, Natural Resources Conservation Service.

U.S. Department of Agriculture, Soil Conservation Service, 1978. Soil Survey of Blue Earth County, Minnesota. USDA, SCS, Washington, DC.

U.S. Fish and Wildlife Service, 2011. Habitat and Population Evaluation Team, Restorable Wetlands Inventory, Washington DC. http://www.fws.gov/midwest/hapet/RWI.html (accessed January, 2014).

van der Kamp, G. and M. Hayashi. 2009. Groundwater-wetland ecosystem interaction in the semiarid glaciated plans of North America. Hydrogeology Journal. 17:203-214.

Wilson, B. 1997. Return periods corresponding to the storage capacity of surface depressions. Internal Report.

Winter. 1989. Hydrologic studies of wetlands in the northern prairie. *In* Van Der Valk, A. Northern Prairie Wetlands.

Woltemade, C.J.. 2000. Ability of restored wetlands to reduce nitrogen and phosphorus concentrations in agricultural drainage water. Journal of Soil and Water Conservation 55:303-309.

CHAPTER 6: CONCLUSIONS

The research reported in this dissertation covered four topics: (1) assessment of river bank erosion using Lidar technology, (2) degree of bank erosion since post-European settlement, (3) quantifying seepage induced river bank erosion using Lidar, and (4) potential loss of upland water retention capacity from land drainage and adoption of row crops. The focus of this research was the Greater Blue Earth River Basin, a major contributor of sediments and water to the Minnesota River at Mankato and then to Lake Pepin.

The results of the assessment showed that bank erosion/sloughing in Blue Earth County is the primary source of sediments to rivers in the GBERB, accounting for as much as 63% to 79% of the total suspended loads at the outlets of the Blue Earth and Le Sueur Rivers, respectively. The majority of this sediment came from large river banks (>3 m high), making up 75% of the estimated erosion from river banks. The total phosphorus associated with eroded bank materials also made up a substantial portion of the load transported by rivers of the GBERB. The Le Sueur River estimates showed as much as 49% of the TP load was coming from river bank materials.

Rates of river bank retreat between early European settlement periods (1855 to 1938) were statistically similar to those of modern periods (1971 to 2009) suggesting that river banks have remained a major source of sediment to waterways in the GBERB since European settlement in Minnesota. Also, the annual volume loss rates measured from aerial photographs decreased with an increase in time interval between observation periods suggesting that bank erosion in the GBERB was episodic and thus comparisons based on dissimilar time scale (as has been done in the literature) can lead to mis-

interpretation. The results also showed that because of different mechanism controlling bank failure at different times, one cannot estimate bank erosion rates using relationships based on simple bank physical features like area, length, orientation, or its aspect as has been done in recent studies in the Minnesota River Basin.

Terrestrial Lidar scans on Carver Creek and the Blue Earth River provided evidence that Lidar return intensity can be used to delineate seep locations along the face of river banks as an alternative to thermal imaging. Although there was a significant relationship between Lidar return intensity and the soil moisture, these relationships were highly dependent on soil color with darker colors masking the wetness differences. Overlaying Lidar delineated seep locations with Geomorphic Change Detection from Lidar measurements provided a qualitative indication that mass wasting was occurring in proximity to the location of active seeps along the Blue Earth River.

An analysis of elevation data from airborne Lidar scans showed that the historic surface retention capacity of GBERB was relatively small (152 mm) and was mostly concentrated (53%) in large historic depressions > 40 ha. Furthermore, after accounting for differences in ET between wetlands and crops lands that replaced them, restoration of all depressions will provide only 131 mm of additional capacity over and above the modern day capacity. However, this capacity is not uniformly distributed in the basin and water will have to be conveyed to these depressions. Furthermore, this capacity is only available first year when the depressions are empty and for subsequent years this capacity will decrease unless these depressions are emptied each year.

In brief, we conclude that (1) river banks in the GBERB have historically been and continue to be a major source of sediment to the Minnesota River and Lake Pepin,

(2) for comparable time intervals average river bank retreat rates were statistically similar but there are a greater number of banks slumping in recent years than in the past, (3) Lidar return intensity could be used to identify seepage (a major mechanism for bank failures) on river banks and this in combination with elevation change from Lidar can characterize extent of seepage induced bank erosion, and (4) relative to annual precipitation the decrease in surficial water retention from land drainage and adoption of row crops is very minimal.

BIBLIOGRAPHY

Altman, D.G., and J.M. Bland. 1983. Measurement in medicine: the analysis of method comparison studies. The Statistician. 32:307-317.

Allred, E.R., P.W. Manson, G.M. Schwartz, P. Golany, and J.M.W. Reinke. 1971. Continuation of studies on the hydrology of ponds and small lakes. University of Minnesota Agricultural Experiment Station, Technical Bulletin 274. pp 62.

Babbar-Sebens, M., R.C. Barr, L.P. Tedesco, and M. Anderson. 2013. Spatial identification and optimization of upland wetlands in agricultural watersheds. Ecological Engineering. 52:130-142.

Bartier, P. M. and C. P. Keller. 1996. Multivariate interpolation to incorporate thematic surface data using inverse distance weighting (IDW). Computers & Geosciences. 22:795-799.

Bater, C.W. and N.C. Coops. 2009. Evaluating error associated with Lidar-derived DEM interpolation. Computers & Geosciences. 35:289-300.

Bauder, J.W. and M.J. Ennen. 1981. Water use of field crops in eastern North Dakota. Farm Research. 38:3-5.

Belmont, P., K.B. Gran, S.P. Schottler, P.R. Wilcock, S.S. Day, C. Jennings, J.W. Lauer, E. Viparelli, J.K. Willenbring, D.R. Engstrom, and G. Parker. 2011. Large shift in source of fine sediment in the Upper Mississippi River. Environmental Science and Technology. 45:8804-8810.

Bennett, H.H. and L. A. Hurst.1907. Soil survey of Blue Earth County, Minnesota. U.S. Department of Agriculture, Bureau of Soils, Government Printing Office, Washington, DC. pp 55.

Black, E., C.E. Renshaw, F.J. Magilligan, J.M. Kaste, W.B. Dade, and J.D. Landis. 2010. Determining lateral migration rates of meandering rivers using fallout radionuclides. Geomorphology. 123:364-369.

Bohling, S., 2012. Turbidity total maximum daily load study: Greater Blue Earth River Basin. Draft report submitted to the Minnesota Pollution Control Agency. Available online: http://www.pca.state.mn.us/index.php/view-document.html?gid=17673, *(accessed on March 18, 2013).*

Bowen, Z.H. and R.G. Waltermire. 2002. Evaluation of light detection and ranging (Lidar) for measuring river corridor topography. Journal of the American Water Resources Association. 38:33-41.

Brennan, R., and T.L. Webster. 2006. Object-oriented land cover classification of Lidar-derived surfaces. Canadian Journal of Remote Sensing. 32:162-172.

Brennan, R., and T. L. Webster. 2006. Object-oriented land cover classification of Lidar-derived surfaces. Canadian Journal of Remote Sensing. 32:162-172.

Cancienne, R., G.A. Fox, and A. Simon. 2008. Influence of seepage undercutting on the root reinforcement of river banks. Earth Surface Processes and Landforms. 33:1769-1786.

Chu-Agor, M.L., G.A. Fox, and G.V. Wilson. 2009. Empirical sediment transport function predicting seepage erosion undercutting for cohesive bank failure prediction. Journal of Hydrology. 377:155-164.

Chu-Agor, M.L., G.A. Fox, R.M. Cancienee, and G.V. Wilson. 2008. Seepage caused tension failures and erosion undercutting of hillslopes. Journal of Hydrology. 359:247-259. DOI: 10.1016/j.jhydrol.2008.07.005.

Clayton, L., and S.R. Moran. 1982. Chronology of late-Wisconsin glaciations in middle North America. Quaternary Science Reviews. 1:55-82.

Couper, P., T. Scott, and I. Maddock. 2002. Insights into river bank erosion processes derived from analysis of negative erosion pin recordings: observations from three recent UK studies. Earth Surface Processes and Landforms 27, 59-79.

Couper, P. 2003. Effects of silt-clay content on the susceptibility of river banks to subaerial erosion. Geomorphology. 56:95-108.

Cowardin, L.M., V. Carter, F.C. Golet, and E.T. Laroe. 1979. Classification of wetlands and deepwater habitats of the United States. U.S. Fish and Wildlife Service FWS/OBS 79/31, Washington, DC.

Cressie, N. 1990. The origins of kriging. Mathematical Geology. 22:239-252.

Crumpton, W.G.. 2001. Using wetlands for water quality improvement in agricultural watersheds: the importance of a watershed scale approach. Water Science Technology. 44:559-564.

Dahl, T.E. 2006. Status and trends of wetlands in the conterminous United States 1998 to 2004. U.S. Department of the Interior, Fish and Wildlife Service, Washington, D.C.

David, M.B., J.E. Drinkwater, and G.F. McIsaac. 2010. Sources of nitrate yields in the Mississippi River Basin. Journal of Environmental Quality. 39:1657-1667.

Davis, J.C.., 1973. Statistics and data analysis in geology. John Wiley & Sons, New York, NY. pp 550.

Day, S.S., K.B. Gran, P. Belmont, and T. Wawrzyniec. 2013a. Measuring bluff erosion part 2: pairing aerial photographs and terrestrial laser scanning to create a

watershed scale sediment budget. Earth Surface Processes and Landforms. DOI:10.1002/esp.3359.

Day, S.S., K.B. Gran, P. Belmont, and T. Wawrzyniec. 2013b. Measuring bluff erosion Part 1: Terrestrial laser scanning methods for change detection. Earth Surface Processes and Landforms. DOI:10.1002/esp.3353.

Delgado, J.A., and J.K. Berry. 2008. Advances in precision conservation. Advances in Agronomy. 98:1-44.

De Rose, R.C., and L.R. Basher. 2011. Measurement of river bank and cliff erosion from sequential Lidar and historical aerial photography. Geomorphology. 126:132-147.

Deitchman, R.S., and S.P. Loheide II. 2009. Ground-based thermal imaging of groundwater flow processes at the seepage face. Geophysical Research Letters. 36:L14401, DOI: 10.1029/2009GL038103.

Devauchelle, O., A.P. Petroff, H.F. Seybold, and D.H. Rotherman. 2012. Ramification of stream networks. Proceedings of the National Academy of Sciences. 109:20832-30836.

Engstrom, D.R., J.E. Almendinger, and J.A. Wolin. 2009. Historical changes in sediment and phosphorus loading to the upper Mississippi River: mass-balance reconstructions from the sediments of Lake Pepin. Journal of Paleolimnology. 41:563-588.

Evans, D.J., C.E. Bison, and R.S. Rossell. 2006. Sediment loads and sources in heavily modified Irish catchments: a move towards informed management strategies. Geomorphology. 79:93-113.

Flood, M. 2004. American Society for Photogrammetry and Remote Sensing guidelines: Vertical accuracy reporting for Lidar data. Available online: http://www.asprs.org/a/society/committees/Lidar/Downloads/Vertical_Accuracy_Reporting_for_Lidar_Data.pdf (*accessed on March 18, 2013*). ASPRS, Bethesda, MD.

Flood, M. 2004. American Society for Photogrammetry and Remote Sensing Guidelines – Vertical Accuracy Reporting for Lidar Data, ASPRS, Bethesda, Maryland, 15 p. http://www.asprs.org/society/committees/Lidar/downloads/vertical_accuracy_reporting_for_Lidar_data.pdf (retrieved February 18, 2011)

Fox, G.A., and G.V. Wilson. 2010. The role of subsurface flow in hillslope and stream bank erosion: a review. Soil Science Society of America Journal. 74:717-733.

Fox, G.A., G.V. Wilson, A. Simon, E.J. Langendoen, O. Akay, and J.W. Fuchs. 2007. Measuring streambank erosion due to ground water seepage: correlation to bank pore water pressure, precipitation and stream stage. Earth Surface Processes and Landforms. 32:1558-1573, DOI: 10.1002/esp.1490.

Fuller, I.C., A.R.G. Large, M.E. Charlton, G.L. Heritage, and D.J. Milan. 2003. Reach-scale sediment transfers: An evaluation of two morphological budgeting approaches. Earth Surface Processes and Landforms. 28:889-903.

Galatowitsch, S.M. 1990. Using the original land survey notes to reconstruct presettlement landscapes in the American West. Great Basin Naturalist. 50:181-191.

Gee, G.W., and D. Or. (2002) Particle size analysis. p 255-293. In Dane and Topp (Eds.), *Methods of soil analysis: Part 4, Physical methods*, Soil Science Society of America, Madison, WI.

Ginting, D., J.F. Moncrief, and S.C. Gupta. 2000. Runoff, solids, and contaminant losses into surface tile inlets draining lacustrine depressions. J. Environ. Qual. 29:551–560.

Gleason, R.A., Tangen, B.A., Laughan, M.K., Kermes, K.E., Euliss, and N.H., Jr. 2007. Estimating water storage capacity of existing and potentially restorable wetland depression in a subbasin of the Red River of the North. US Geological Survey Scientific Investigations Report 2007-1159, p. 36. http://pubs.er.usgs.gov/publication/ofr20071159.

Gran, K., P. Belmont, S. Day, C. Jennings, A. Johnson, L. Perg, and P. Wilcox. 2009. Geomorphic evolution of the Le Sueur River, Minnesota, USA, and implications for current sediment loading. The Geological Society of America. Special Paper 451.

Grossman, R.B. and T.G. Reinsch. 2002. Bulk density and linear extensibility. p 201-228. In Dane and Topp (Eds.), *Methods of soil analysis: Part 4, Physical methods*, Soil Science Society of America, Madison, WI.

Grundtner, A.L., S.C. Gupta, P.R. Bloom. 2014. River bank materials as a source and as carriers of phosphorus to Lake Pepin. Journal of Environmental Quality 43:1991-2001.

Guo, Q., W. Li, H. Yu, and O. Alvarez. 2010. Effects of topographic variability and Lidar sampling density on several dem interpolation methods. Photogrammetric Engineering and Remote Sensing. 76:1-12.

Gupta, S.C., and U.B. Singh, 1996. A review of non-point source pollution models: Implications for the Minnesota River Basin. A report submitted to the Minnesota Department of Agriculture. p77.

Gupta, S.C., A.C. Kessler, M.K. Brown, and F. Zvomuya. 2015. Climate and agricultural land use change impacts on streamflow in the upper Midwestern United States. Water Resources Research. DOI:10.1002/2015WRO17323.

Haan, C.T., and H.P. Johnson. 1967. Geometrical properties of depressions in North-Central Iowa. Iowa State Journal of Science. 42:149-160.

Haan, C.T., and H.P. Johnson. 1968a. Hydraulic model of runoff from depressional areas part I. General considerations. Transactions of the ASAE. 11:364-367.

Haan, C.T., and H.P. Johnson. 1968b. Hydraulic model of runoff from depressional areas part II. Development of the model. Transactions of the ASAE. 11:368-373.

Hagerty, D.J. 1991a. Piping/sapping erosion. I: Basic considerations. Journal of Hydraulic Engineering. 117:991-1008.

Hagerty, D.J. 1991b. Piping/sapping erosion. II: Identification-diagnosis. Journal of Hydraulic Engineering. 117:1009-1025.

Harrold, L.L. and F.R. Dreibelbis. 1953. Water use by crops as determined by weighing monolith lysimeters. Soil Science Society of America Journal. 17:72-74.

Hattendorf, M.J., M.S. Redelfs, B. Amos, L.R. Stone, and R. E. Gwin. 1988. Comparative water use characteristics of six row crops. Agronomy Journal. 80:80-85.

Huang, S., C. Young, M. Feng, K. Heidemann, M. Cushing, D.M. Mushet, and S. Liu, 2011. Demonstration of a conceptual model for using Lidar to improve the

estimation of floodwater mitigation potential of Prairie Pothole Region wetlands. Journal of Hydrology. 405:417-426.

Hayashi, M., G. van der Kamp, and D.L. Rudolph. 1998. Water and solute transfer between a prairie wetland and adjacent uplands, International Water Balance. Journal of Hydrology. 207:42-55.

Hodgson, M.E. and P. Bresnahan. 2004. Accuracy of airborne Lidar-derived elevation: empirical assessment and error budget. Photogrammetric Engineering and Remote Sensing. 70:331-339.

Hooke, J.M. 1979. An analysis of the processes of river bank erosion. Journal of Hydrology. 42:39–62.

Hooke, J.M. 2007. Spatial variability, mechanism and propagation of change in an active meandering river. Geomorphology. 84:277-296.

Huang, S., C. Young, M. Feng, K. Heidemann, M. Cushing, D.M. Mushet, and S. Liu, 2011. Demonstration of a conceptual model for using Lidar to improve the estimation of floodwater mitigation potential of Prairie Pothole Region wetlands. Journal of Hydrology. 405:417-426.

Hughes, M.L., P.F. McDowell, and W.A. Marcus, 2006. Accuracy assessment of georectified aerial photographs: implications for measuring lateral channel movement in GIS. Geomorphology. 74:1-16.

IBM Corp. 2010. IBM SPSS Statistics for Windows, Version 19.0. Armonk, NY.

Johnson, H.O., S.C. Gupta, A.V. Vecchia, and F. Zvomuya. 2009. Assessment of water quality in the Minnesota River using non-parametric and parametric methods. Journal of Environmental Quality. 38:1018-1030.

Keckler, D., 1994. Surfer for windows, version 7.0. Golden Software, Golden, CO.

Kelley, D.W., and E.A. Nater. 2000. Historical sediment flux from three watersheds into Lake Pepin, Minnesota, USA. Journal of Environmental Quality. 29:561-568.

Kessler, A.C., S.C. Gupta, H.A.S. Dolliver, and D.P. Thoma. 2012. Lidar quantification of bank erosion in Blue Earth County, Minnesota. Journal of Environmental Quality. 41:197-207.

Kronvang, B, J. Aude, A. Baattrup-Pedersen, H.S. Jensen, and S.E. Larsen. 2011. Phosphorus load to surface water from bank erosion in a Danish lowland river basin. Journal of Environmental Quality. 41: 304-313.

Kuo, S. 1986. Phosphorus, extraction with water or dilute salt solution. In A. Klute (Ed.), *Methods of soil analysis: Part 1. Physical and mineralogical methods*, Soil Science Society of America, Madison, WI.

Lane, S.N., R.M. Westaway, and D.B. Hicks. 2003. Estimation of erosion and deposition volumes in a large, gravel-bed, braided river using synoptic remote sensing. Earth Surface Processes and Landforms. 28:249-271.

Lawler, D.M. 1995. The impact of scale on the processes of channel-side sediment supply: a conceptual model. In: Osterkamp W.R. (Ed.), Effects of Scale on Interpretation and Management of Sediment and Water Quality. IAHS Publ. no. 226, pp. 175-184.

Lenhart, C.F., M.L. Titov, J.S. Ulrich, J.L. Nieber, and B.J. Suppes. 2013 The role of hydrologic alteration and riparian vegetation dynamics in channel evolution along the lower Minnesota River. Transactions of the ASABE. 56:549-561.

Leys, K.F., and A. Werritty. 1999. River channel planform change: software for historical analysis. Geomorphology. 29:107-120.

Lindow, N., G.A. Fox, and R.O. Evans. 2009. Seepage erosion in layered stream bank material. Earth Surface Processes and Landforms. 34:1693-1701, DOI: 10.1002/esp.1974.

Lindsay, J.B. and I.F. Creed. 2005. Sensitivity of digital landscapes to artifact depression in remotely-sensed DEMs. Photogrammetric Engineering & Remote Sensing. 71:1029-1036.

Liu, H. and L. Wang, 2008. Mapping detention basins and deriving their spatial attributes from airborne Lidar data for hydrological applications. Hydrological Processes. 22:2358-2369.

Lloyd, C.D. and P.M. Atkinson. 2002. Deriving DSMs from Lidar data with kriging. In. J. Remote Sensing. 23:2519-2524.

Ludden, A.P., D.L. Frink, and D.H. Johnson. 1983. Water storage capacity of natural wetland depressions in the Devils Lake Basin of North Dakota. Journal of Soil and Water Conservation. 38:45-48.

Matsch, C.L. 1983. River Warren, the southern outlet of Lake Agassiz. In: Teller, J.T., and Clayton, L., (Eds.)., Glacial Lake Agassiz. Geological Association of Canada Special Paper 26, pp. 232-244.

Meyer, M.L., and S.M. Schellhaass. 2002. Sources of phosphorus, chlorophyll, and sediment to the Mississippi River upstream of Lake Pepin: 1976-1996. A report for environmental studies of phosphorus. Metropolitan Council Environmental Services, St. Paul, MN.

Microsoft Office. 20009. Microsoft Excel (computer software), Microsoft, Redmond, Washington.

Midgley, T.L., G.A. Fox, G.V. Wilson, D.M. Heeren, E.J. Langendoen, and A. Simon. 2013. Seepage-induced streambank erosion and instability: in situ constant-head experiments. Journal of Hydrologic Engineering. 18:1200-1210, DOI: 10.1061/(ASCE)He.1943-5584.0000685.

Milan, D.J., G.L. Heritage, A.R.G. Large, and I. C. Fuller. 2011. Filtering spatial error from DEMs: implications for morphological change estimation. Geomorphology. 125:160-171, DOI: 10.1016/j.geomorph.2010.09.012.

Miller, J.E. and D.L. Frink. 1984. Changes in flood response of the Red River of the North Basin, North Dakota-Minnesota. Water-Supply Paper 2243, U.S. Geological Survey, Alexandria, Virginia. http://pubs.er.usgs.gov/publication/ofr82774.

Miller, R. 1999. Hydrologic effects of wetland drainage and land use change in a tributary watershed of the Minnesota River Basin: A modeling approach. Master's Thesis, University of Minnesota, St. Paul, Minnesota.

Minke, A.G., C.J. Wetbrook, and G. van der Kamp. 2010. Simplified volume-area-depth method for estimating water storage of prairie potholes. Wetlands. 30:541-551.

Minnesota Pollution Control Agency (MPCA). 1994. Minnesota River Assessment Project report. Vol. II Physical and Chemical assessment, and Vol. III. Biological and Toxicological Assessment. Report to the legislative Commission on Minnesota Resources. January 1994.

Mitasova, H. and J. Hofierka. 1993 Interpolation by regularized spline with tension: II. Application to terrain modeling and surface geometry analysis. Mathematical Geology 25:657-669.

Mitsch, W.J., J.W. Jr. Day, J. W. Gilliam, P.M. Groffman, D.L. Hey, G.W. Randall, and N. Wang. 2001. Reducing nitrogen loading to the Gulf of Mexico from the Mississippi River Basin: strategies to counter a persistent ecological problem. BioOne. 51:373-388.

Mitsch, W.J., L. Zhang, C.J. Anderson, A.E. Altor, and M.E. Hernandez. 2005a. Creating riverine wetlands: ecological succession, nutrient retention, and pulsing effects. Ecological Engineering. 25:510-527.

Mitsch, W.J., J.W. Day, L. Zhang, and R.R. Lane. 2005b. Nitrate-nitrogen retention in wetlands in the Mississippi River Basin. Ecological Engineering. 24:267-278.

Mitsch, W.J. and J.W. Day. 2006. Restoration of wetlands in the Mississippi-Ohio-Missouri (MOM) River Basin: experience and needed research. Ecological Engineering. 26:55-69.

Moore, I.D. and C.L. Larson. 1979. Effects of drainage projects on surface runoff from small depressional watersheds in north central region. Water Resources Research Center Bulletin 99. University of Minnesota, Minneapolis, MN.

Moran, M.S., C.D. Peters-Lidard, J.M. Watts, and S. McElroy. 2004. Estimating soil moisture at the watershed scale with satellite-based radar and land surface models. Canadian Journal Remote Sensing. 30:805-826.

Moran, M.S., D.C. Hymer, J. Qi, and E.E. Sano. 2000. Soil moisture evaluation using multi-temporal synthetic aperture radar (SAR) in semiarid rangeland. Agricultural and Forest Meteorology. 105:69-80.

Muller E. and H. Decamps. Modeling soil moisture-reflectance. Remote Sensing of the Environment. 76:173-180.

Narayanan, R.M., S.E. Gree, and D.R. Alexander. 1993. Mid-infrared laser reflectance of moist soils. Applied Optics. 32:6043-6052.

Newcombe, C.P., and J.O.T. Jensen. 1996. Channel suspended sediment and fisheries: a synthesis for quantitative assessment of risk and impact. North American Journal of Fisheries Management. 16:693-727.

Nicoll, T.J., and E.J. Hickin,. 2010. Planform geometry and channel migration of confined meandering river on the Canadian prairies. Geomorphology. 116, 37-47.

Notebaert, B., G. Verstraeten, G. Govers, and J. Poesen. 2009. Qualitative and quantitative applications of Lidar imagery in fluvial geomorphology. Earth Surface Processes and Landforms. 34:217-231.

Ozesmi S.L. and M.E. Bauer. 2002. Satellite remote sensing of wetlands. Wetlands Ecology and Management. 10:381-402.

Payne, G.A. 1994. Sources and transport of sediment, nutrients and oxygen demanding substances in the Minnesota River Basin, 1989-92. USGS Water Resources Investigations Report 93-4232.

Perroy, R.L., B. Bookhagen, G.P. Asner, and O.A. Chadwick. 2010. Comparison of gully erosion estimates using airborne and ground-based Lidar on Santa Cruz Island, Californian. Geomorphology. 118:288-300.

Pfister, L., J.J. McDonnell, C. Hissler, and L. Hoffmann 2010. Ground-based thermal imagery as a simple, practical tool for mapping saturate area connectivity and dynamics. Hydrological Processes. 24:3123-3132, DOI: 10.1002/hyp.7840.

Pollen, N., and A. Simon. 2005. Estimating the mechanical effects of riparian vegetation on stream bank stability using a fiber bundle model. Water Resources Research. 41:W07025. doi:10.1029/2004WR003801.

Rabalais, N.N, R.E. Turner, and D. Scavia. 2002. Beyond science into policy: Gulf of Mexico hypoxia and the Mississippi River. BioOne 52:129-142.

Richardson, C.J., 1985. Mechanisms controlling phosphorus retention capacity in freshwater wetlands. Science. 228:1424-1427.

Rinaldi, M., and N. Casagli. 1999. Stability of river banks formed in partially saturated soils and effects of negative pore water pressures: the Sieve River (Italy). Geomorphology. 26:253-277.

Sadler, P.M. 1981. Sediment accumulation rates and the completeness of stratigraphic sections. The Journal of Geology. 89:569-584.

Sekely, A.C., D.J. Mulla and D.W. Bauer. 2002. Streambank slumping and its contribution to the phosphorus and suspended sediment load of the Blue Earth River, Minnesota. Journal of Soil and Water Conservation. 57:243-250.

Schilling, K.E. and M. Helmers. 2008. Effects of subsurface drainage tiles on streamflow in Iowa agricultural watersheds: Exploratory hydrograph analysis. Hydrological Processes. 22:4497-4506.

Schottler, S.P., J. Ulrich, P. Belmont, R. Moore, J.W. Lauer, D.R. Engstrom, and J.E. Almendinger. 2014. Twentieth century agricultural drainage creates more erosive rivers. Hydrological Process. 28:1951-1961, DOI: 10.1002/hyp.9738.

Schurch, P., A.L. Densmore, N. J. Rosser, M. Lim, and B. W. McArdell. 2011. Detection of surface change in complex topography using terrestrial laser scanning: application to the Illgraben debris-flow channel. Earth Surface Processes and Landforms. 36:1847-1859, DOI: 10.1002/esp.2206.

Sekely, A.C., D.J. Mulla and D.W. Bauer. 2002. Streambank slumping and its contribution to the phosphorus and suspended sediment load of the Blue Earth River, Minnesota. Journal of Soil and Water Conservation. 57:243-250.

Shaw, D.A., G. Vanderkamp, F.M. Conly, A. P. Pietroniro, and L. Martz. 2011. The fill-spill hydrology of prairie wetland complexes during drought and deluge. Hydrological Processes. DOI: 10.1002/hyp.8390.

Shejflow, J.B. 1968. Evapotranspiration and the water budget of prairie potholes in North Dakota. US Geological Survey Scientific Investigations Report 585-B, http://pubs.er.usgs.gov/publication/pp585B.

Shields, F.D. Jr., A. Simon, and L.J. Steffen. 2000. Reservoir effects on downstream river channel migration. Environmental Conservation. 27 54-66.

Shook, K.R. and J.W. Pomeroy. 2011. Memory effects of depression storage in Northern Prairie hydrology. Hydrological Processes. 25:3890-3898.

Sibson, R. 1981. A brief description of natural neighbor interpolation. Interpolating Multivariate Data. New York, John Wiley & Sons. pp. 21-36.

Simon, A., A. Curini, S.E. Darby, and E.J. Langendoen, E.J. 2000. Bank and near-bank processes in an incised channel. Geomorphology. 35:193-217.

Skaggs, R.W., M.A. Brevè, and J.W. Gilliam. 1994. Hydrologic and water quality impacts of agricultural drainage. Critical Reviews in Environmental Science and Technology. 24:1-32.

Strock, J.S., P.J.A. Kleinman, K.W. King, and J.A. Delgado. 2010. Drainage water management for water quality protection. Journal of Soil and Water Conservation. 65:131-136.

Suyker, A.E. and S.B. Verma. 2009. Evapotranspiration of irrigated and rainfed maize-soybean cropping systems. Agricultural and Forest Meteorology. 149:443-452.

Tomer, M.D., W.G. Crompton, R.L. Bingner, J.A. Kostel, and D.E. James, 2013. Estimating nitrate load reductions from placing constructed wetlands in a HUC-12 watershed using Lidar data. Ecological Engineering. 56:69-78.

Thoma, D.P., S.C. Gupta, J.S. Strock, and J.F. Moncrief. 2005a. Tillage and nutrient source effects on water quality and corn yield from a flat landscape. Journal of Environmental Quality 34:1102-1111.

Thoma, D. P., S. C. Gupta, M. E. Bauer, and C. E. Kirchoff. 2005b. Airborne laser scanning for riverbank erosion assessment. Remote Sensing Environ. 95:943-501.

Topp, G.C., and P.A. Ferré. 2002. Water Content. In Dane and Topp (eds.) Methods of Soil Analysis, Part 4, Physical Methods. Soil Science Society of America, Madison, WI.

U.S. Bureau of the Census. 1940. Census of agriculture. Vol. 3, Special reports Part 06. Drainage of agricultural lands. Washington, D.C.: U.S. Government Printing Office.

U.S. Department of Agriculture, Natural Resources Conservation Service, 1994. State Soil Geographic Database (STATSGO), data use information. Miscellaneous Publication Number 1492 U.S. Department of Agriculture, Natural Resources Conservation Service.

U.S. Department of Agriculture, Soil Conservation Service, 1978. Soil Survey of Blue Earth County, Minnesota. USDA, SCS, Washington, DC.

U.S. Fish and Wildlife Service, 2011. Habitat and Population Evaluation Team, Restorable Wetlands Inventory, Washington DC. http://www.fws.gov/midwest/hapet/RWI.html (accessed January, 2014).

USDA SCS (U.S. Department of Agriculture Soil Conservation Service), 1978. Soil Survey of Blue Earth County, Minnesota. USDA, SCS, Washington, DC.

van der Kamp, G. and M. Hayashi. 2009. Groundwater-wetland ecosystem interaction in the semiarid glaciated plans of North America. Hydrogeology Journal. 17:203-214.

Walling, D. E. 2005. Tracing suspended sediment sources in catchments and river systems. Science of the Total Environment. 344.159-184.

Weidong, L., F. Baret, G. Xingfa, T. Qingxi, Z. Lanfen, and Z. Bing. 2002. Relating soil surface moisture to reflectance. Remote Sensing of the Environment. 81:238-246.

Wheaton, J.M., J. Brasington, S.E. Darby, and D.A. Sear. 2010. Accounting for uncertainty in DEMs from repeat topographic surveys: improved sediment budgets. Earth Surface Processes and Landforms. 35:136-156.

Wheaton, J.M., J. Brasington, S.E. Darby, A. Kasprak, D. Sear, and D. Vericat. 2013. Morphodynamic signatures of braiding mechanisms as expressed through change in sediment storage in a gravel-bed river, Journal of Geophysical Research: Earth Surface. 118:759-779, DOI: 10.1002/jgrf.20060.

Wilcox, P. 2009. Identifying sediment sources in the Minnesota River Basin: Minnesota River Sediment Colloquium. Minnesota Pollution Control Agency. http://www.lakepepinlegacyalliance.org/SedSynth_FinalDraft-formatted.pdf (retrieved February 18, 2011).

Willet, C.D., R.N. Lerch, R.C. Schultz, S.A. Berges, R.D. Peacher, and T.M. Isenhart. 2012. River bank erosion in two watersheds of the Central Claypan Region of Missouri, United States. Journal of Soil and Water Conservation. doi:10.2489/jswc.67.4.249.

Wilson, G.V., R. Periketi, G.A. Fox, S. Dabney, D. Shields, R.F. Cullum. 2007. Soil properties controlling seepage erosion contributions to river bank failure. Earth Surface Processes and Landforms. 32:447–459.

Wilson, B. 1997. Return periods corresponding to the storage capacity of surface depressions. Internal Report.

Winter. 1989. Hydrologic studies of wetlands in the northern prairie. *In* Van Der Valk, A. Northern Prairie Wetlands.

Woltemade, C.J.. 2000. Ability of restored wetlands to reduce nitrogen and phosphorus concentrations in agricultural drainage water. Journal of Soil and Water Conservation 55:303-309.

Wright Jr., H.E. 1972a. Quaternary history of Minnesota. p 515-547. *In* Sims and Morey (eds.) *Geology of Minnesota: A Centennial Volume*. Minnesota Geological Survey, Univ. of Minnesota, St. Paul, MN.

Wright Jr., H.E. 1972b. Physiography of Minnesota. p 561-578. *In* Sims and Morey (eds.) *Geology of Minnesota: A Centennial Volume*. Minnesota Geological Survey, Univ. of Minnesota, St. Paul, MN.

Zaimes, G.N., R.C. Schultz, and T.M. Isenhart. 2004. Stream bank erosion adjacent to riparian forest buffers, row-crop fields, and continuously-grazed pastures along Bear Creek in central Iowa. Journal of Soil and Water Conservation. 59:19-27.

Zinger, J.A., B.L. Rhoads, and J.L. Best. 2011. Extreme sediment pulses generated by bend cutoffs along a large meandering river. Nature Geoscience. 4:675-678.